B E R I C H T E

aus dem

I N S T I T U T F Ü R M E E R E S K U N D E

an der

Christian-Albrechts-Universität Kiel

Nr. 165

1 9 8 7

I S O P Y C N I C P O T E N T I A L V O R T I C I T Y A T L A S O F T H E N O R T H A T L A N T I C O C E A N

- m o n t h l y m e a n m a p s -

by

D. Stammer and J.D. Woods

DOI 10.3289/IFM_BER_165

Copies are available from

Institut für Meereskunde an der Universität Kiel
Abteilung Regionale Ozeanographie
Düsternbrooker Weg 20
D-2300 Kiel 1, FRG

ISSN 0431 - 8561

Contents

LIST OF FIGURES (1-6) AND TABLES (1-3)

1 INTRODUCTION

This atlas describes the annual cycle of the isopycnic potential vorticity in the permanent thermocline and the seasonal boundary layer as computed from the Robinson, Bauer and Schroeder numerical atlas (1979), which comprises monthly mean temperature and annual mean salinity values on standard depth levels on a one-degree longitude and latitude grid. The distribution of pressure, temperature and salinity on isopycnal surfaces is given in the atlas of Bauer and Woods (1984), based on the same data set.

In the absence of diabatic processes, the stable stratification of the ocean constrains fluid motion to be nearly along surfaces of constant potential density which, according to Montgomery (1938), approximately coincide with isentropic surfaces. A further constraint acting on the motion of a fluid element bounded by two isopycnal surfaces arises from Ertel's theorem of potential vorticity conservation which states that for adiabatic and frictionless motion the potential vorticity defined as

$$Q = (2\vec{\Omega} + \nabla \times \vec{u}) \cdot \nabla\rho/\rho$$

is, like the potential density, a conservative quantity in the sense that Q remains constant for each fluid element following its motion. Here Ω denotes the angular velocity of the earth's rotation, $2\vec{\Omega}$ the planetary vorticity, $\nabla \times \vec{u}$ the relative vorticity field. $\vec{u}$ and ρ denote the three-dimensional velocity and density fields, respectively. The definition of Q is valid in the statically stable interior of the ocean. It is not valid in statically unstable locations such as the surface convection layer at the top of the ocean (Woods, 1985). For the study of potential vorticity the ocean has three regimes. Regime one comprises convection layers which are the sources and sinks of Q, notably the mixed layer at the top of the ocean; regime two and three are the statically stable seasonal thermocline and the permanent thermocline, respectively, in which potential vorticity circulates quasi-geostrophically. Q is created as water is released from regime one into regime two, it is destroyed as water returns from regime two into regime one. The potential vorticity distribution in the permanent thermocline (regime three) is determined by geostrophic flow from the seasonal thermocline (regime two). In the literature this process is frequently called "ventilation" (e.g. Luyten et al., 1983; Woods, 1985).

For quasi-geostrophic baroclinic dynamics with lateral scales much larger than the Rossby radius of deformation (~ 50 km) the relative vorticity is very much less than the planetary vorticity. Therefore for large-scale geostrophic flow the synoptic potential vorticity can be approximated by the Sverdrupian (large-scale) potential vorticity $Q_S = \frac{f}{\rho} \cdot \frac{\partial \rho}{\partial z}$, which can be evaluated from hydrographic measurements of ρ alone. Relative vorticity comparable with f only occurs at small scale (less than the Rossby radius) in association with transient motions. Climatological values of absolute vorticity computed from a sufficiently large number of independent samples are close to the planetary vorticity with a negligible residual relative vorticity. Thus relative vorticity is not a factor in mapping climatological potential vorticity from a large sample of independent hydrographic profiles. That is true regardless of the scale: all climatological potential vorticity maps are Sverdrupian.

A schematic diagram of large-scale potential vorticity generation and destruction is given in fig. 1; the depth of the same pair of isopycnals is shown during three successive summers along the track of a water column assumed to move barotropically across the ocean. The annual variation of the net daily surface buoyancy flux B is shown in the top panel. The water column suffers a small net annual buoyancy flux gain giving rise to a weak downstream decrease in depth D of the top of the permanent thermocline. The lowest H_S of the water column subducted from the mixed layer into the seasonal thermocline "ventilates" into the permanent thermocline, the remainder is reentrained into the mixed layer. The diagram represents a region with downwelling into the seasonal thermocline due to Ekman pumping.

The magnitude of Q of a water parcel circulating within the seasonal boundary layer and permanent thermocline can be changed by diabatic processes, including solar heating (Woods et al., 1984), molecular diffusion, double diffusive convection and turbulent fluxes. A discussion of the effects of those processes is given in Woods (1985). Mixing of potential vorticity occurs along density surfaces leading to homogenization within closed contours of Q (Rhines and Young, 1982a).

The application of Ertel's concept of potential vorticity conservation to dynamical oceanography provides the basis for understanding baroclinic circulation. During the past few years several new theories have been developed predicting the structure of the horizontal and vertical structure

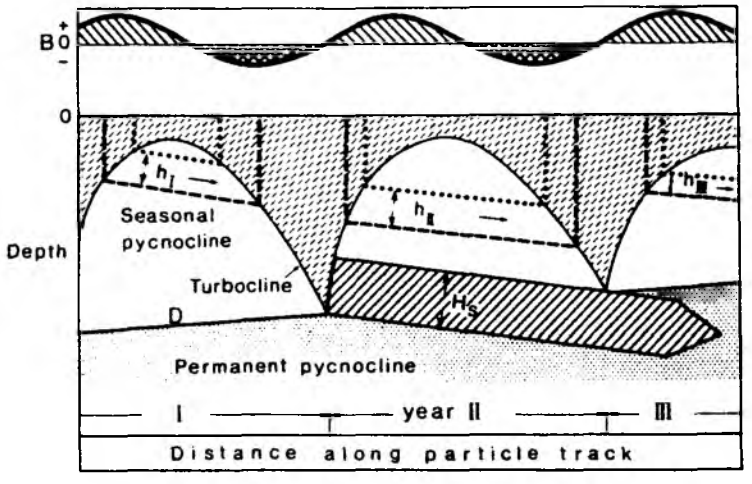

Fig. 1:

Schematic diagram of isopycnic potential vorticity generation.
The depth of the same pair of isopycnals is shown during three successive summers along a track of a water column assumed to move barotropically across the ocean. The diagram represents a region with small annual buoyancy flux gain (top panel), which gives a decrease in D, the line of annual maximum depth of the mixed layer, and with downwelling in the seasonal thermocline due to Ekman pumping, which gives a downward tilt of the isopycnals. The lowest H_s of the water column subducted from the mixed layer into the seasonal thermocline flows geostrophically into the permanent thermocline, the remainder is re-entrained into the mixed layer.

of the thermocline. (Rhines and Young, 1982b; Luyten et al., 1983; Pedlosky, 1983; Woods, 1985, Woods and Barkmann, 1986). The isopycnic gradient of Q is a dynamical variable (unlike the isopycnic gradient of a passive scalar such as temperature or salinity); changing it leads to acceleration of the mass field and to the creation of mesoscale jets (Bleck, Onken and Woods, 1987). The importance of the isopycnic potential vorticity is summarized in the invertibility principle of Hoskins et al. (1985), which states that the full dynamical state of the ocean is known if the spatial distribution of Q is known everywhere and there exists knowledge of a conservative scalar like density at a reference level (e.g. the sea surface) and a suitable balance condition.

In this analysis we calculated the finite difference form of the large-scale isopycnal potential vorticity $Q_S = \frac{f}{\rho} \cdot \frac{\Delta\rho}{\Delta z}$ from hydrographic data of the Robinson, Bauer and Schroeder atlas. A detailed description of the data processing method is given in paragraph 2.3.

This is the first atlas to show the monthly mean distribution of Q_S. It provides information about the seasonal cycle which is lacking in maps of the climatological mean distribution of the isopycnic potential vorticity published by Sarmiento, Rooth and Roether (1982), McDowell, Rhines and Keffer (1982) and Keffer (1985). Synoptic isopycnic maps of thickness and potential vorticity have been published by McWilliams (1976), Minnett and Woods (1984), Harvey and Glynn (1985), Fischer (1986), Hua et al. (1986) and Fischer, Leach and Woods (1987).

2 DATA AND METHOD

2.1 The Robinson, Bauer and Schroeder Numerical Atlas

The starting point for this work was the numerical version of the atlas produced by Robinson, Bauer and Schroeder (1979) (henceforth abbreviated as RBS). The description of the archive data used in the compilation of the atlas and the processing method are given in Robinson et al. (1979). The RBS Atlas is primarily based on bathythermograph (BT) measurements and data from hydrographic stations collected during the period between 1900 and 1967. It has been supplemented in 1975 with expendable bathythermograph and BT-data measured between 1967 and 1973 in the tropical Atlantic between 5° S and 35° N.

The special feature of the RBS atlas is the extensive use of BT measurements to supplement hydrocast data. This yields a data density sufficient to justify the calculation of monthly mean temperature at intervals of 1° in longitude and latitude in the top 150 m. The high spatial resolution has been retained for temperature at depths greater than 150 m and for salinity at all depths, although the data base is then too small to justify monthly mean values. The monthly mean temperatures at depths down to 150 m and the high spatial resolution provide more detailed information about the seasonal cycle than is available in other atlases (e.g. Levitus, 1982).

The RBS-atlas contains hydrographic data for the major ocean basins on a 1° x 1° geographical grid on the following 33 standard depths between the sea surface and 7000 m: 0, 30, 60, 90, 125, 150, 183, 200, 244, 250, 300, 305, 366, 400, 500, 600, 700, 800, 900, 1000, 1100, 1200, 1300, 1400, 1500, 1750, 2000, 2500, 3000, 4000, 5000, 6000, 7000 m. The mean value of temperature and salinity calculated by averaging the sample values lying in a 1° x 1° grid square refer to the centre of the square and the monthly mean value for temperature within the top 150 m refer to the middle of the month.

Despite the high concentration of data in the top 150 m it was not possible to obtain a uniform coverage of temperature data over the whole North Atlantic. There are areas with few (1 - 10 measurements) or no data at all. To obtain an even distribution on a geographical grid, missing data have been interpolated two-dimensionally and subsequently smoothed with a least squares fit first meridionally and then zonally. In the surface layer (the top 150 m) the 12 monthly values for temperature at each position have been smoothed in time by fitting a 3rd harmonic Fourier curve to the data.

This analysis of the isopycnic potential vorticity (IPV) is based on the part of the whole atlas which covers the North Atlantic Ocean between 90° W and 0° W in longitude and 5° S and 60° N in latitude. It is the same selection of the RBS data set which Bauer and Woods (1984) used for their isopycnic analysis of the seasonal variability of pressure, temperature and salinity. The data set contains 4266 profiles in 112074 data cycles with 12 variables each: longitude, latitude, depth, annual mean temperature, annual mean salinity and 12 monthly mean temperature values, starting with January.

Here the annual mean temperature and salinity are the "all data" means, which are simply the unweighted average of all data present in a 1°-quadrangle. They can differ substantially from the true annual mean value for the observation period because of the concentration of data in summer.

2.2 Seasonal variation

The RBS-atlas offers the possibility of a climatological isopycnic analysis of the seasonally varying parameters in the upper ocean. However, the limitation of the atlas (no monthly temperatures below 150 m or salinity at any depth) forced us to base this analysis of the seasonal distribution of isopycnic potential vorticity on a pseudo monthly-mean density designed to approximate the true monthly mean density. The latter would be calculated from monthly mean temperature and salinity at all depths. Our assumption is that the difference between the pseudo- and ideal monthly-mean density distribution is not so serious as to invalidate the distribution of IPV presented below. Differences can be due to a variety of sources. Bauer and Woods (1984) discussed three of them, the seasonal variation of temperature below 150 m, the seasonal variation of salinity in the top 150 m and secular changes of temperature and salinity.

(1) Seasonal variation of temperature below 150 m

The numerical atlas data exhibit significant variation of temperature at 150 m (the maximum depth of monthly mean temperature data). Robinson et al. (1979) used a temperature criterion to estimate the mean depth of the monthly mean mixed layer by determining the depth at which the surface temperature minus 2° F (≈ 1.2 K) occurs. A similar method can be used to determine the maximum depth of seasonal variation by determining the depth for which the

temperature has the value of the annual minimum surface temperature minus 2° F. Levitus (1982) used a modified method by applying a density criterion of $\Delta\sigma_t = 0.125$ kg m^{-3}. (Fig. 2 shows the result of applying that criterion to the RBS data set.) Both methods show that only in or near the tropics the annual maximum depth of the mixed layer is less than 150 m. Seasonal variation extends deeper than 150 m in higher latitudes.

(2) Seasonal variation of salinity

Levitus (1986) discussed the influence of the seasonal variation of surface salinity on density. He showed that the influence is significant only in areas with a large annual cycle in freshwater supply (river run-off, ice melting/freezing). In all other regions the influence of the seasonal salinity variation on density is small ($\Delta\sigma \leq 0.2$ kg m^{-3}) compared to that of temperature variations with maximum amplitude near the surface. The analysis of OWS "C" data (35°5' W, 52°7' N) showed that at this location the difference between pseudo- and ideal monthly-mean density is less than 0.05 kg m^{-3} with maximum differences in the top 100 m (Reikowski, 1987). However, quantities depending on the gradient of the density profile (e.g. the mixed layer depth) turn out to be very sensitive to the averaging procedure. The same might be true a priori for the potential vorticity, but inspections of our maps and analysis of the limited available synoptic data (Stammer, 1984) shows that it is not the case.

These results support our assumption that the neglect of seasonal variation of salinity and the data bias towards summer samples are not serious enough to invalidate this analysis. A comparison of the pseudo monthly mean density distribution at the sea surface with those of the "Meteor"-Expedition 1924 - 27 (Böhnecke, 1936) gives further support to our assumption.

(3) Secular changes of temperature and salinity

There is evidence of interannual and decadal variation of temperature and salinity in the North Atlantic (Rodewald, 1972; Folland et al., 1984; Pollard and Pu, 1985). The archive data set used in the numerical atlas sampled this secular variation unevenly over the period 1900 to 1975 with different profiles for temperature and salinity sampling in the top 150 m. There are presumably local trends in temperature and salinity to higher or lower values depending on the period in which the data has been collected. Barkmann (1986) showed that at OWS "C" the seasonal variability of monthly-mean

temperature at 150 m from the RBS-atlas data is far larger than in data from the period 1957 - 1974 which might be due to the secular variation in temperature but it may also be due to the smoothing and interpolation method of RBS. Our knowledge concerning interannual and decadal variation is not sufficient to justify attempting to correct the sampling biases.

The pseudo-monthly density profile

The use of pseudo-monthly mean density produces a discontinuity in the density profile between 150 m and 183 m. The different averaging intervals for temperature and salinity data create density inversions within the top 150 m and between 150 m and 183 m in winter time. In the real ocean inversions would be removed by convection and therefore it is physically reasonable to monotonize the density profile. However this implicitly creates a seasonal variation of density below 150 m with maximum depth D determined by the maximum surface density in winter. On the other hand it does not seem plausible to connect the monthly and annual mean density profile when the density at 150 m depth is less than the density at 183 m. This would create a high density gradient in this depth range. To avoid an artificially high density gradient it seems physically reasonable to connect the density profile between 150 m and the maximum depth D of winter convection, rejecting any data point in between.

Thus we end up with a seasonally varying layer which can reach to depths greater than 800 m despite the fact that the monthly-mean density profile derived from the atlas data explicitly documents the seasonal variation only in the top 150 m. The depth of the seasonally varying layer is determined by D which was calculated with a density criterion $\Delta\sigma_\theta = 0.125$ kg m^{-3} (fig. 2). It is less than 150 m in the tropics and the region of the western boundary current and exceeds 150 elsewhere with the maximum depth larger than 800 m in the European Basin and east of Cape Farewell.

2.3 Data processing

The RBS-atlas exhibits the highest vertical resolution in the top 150 m. However it is still inadequate to resolve the structure of the density profile which is expected to be most complicated near the sea surface. In summer the depth of the mixed layer can reduce to less than 30 m (the depth of the first atlas data point below the surface). Then a linear density

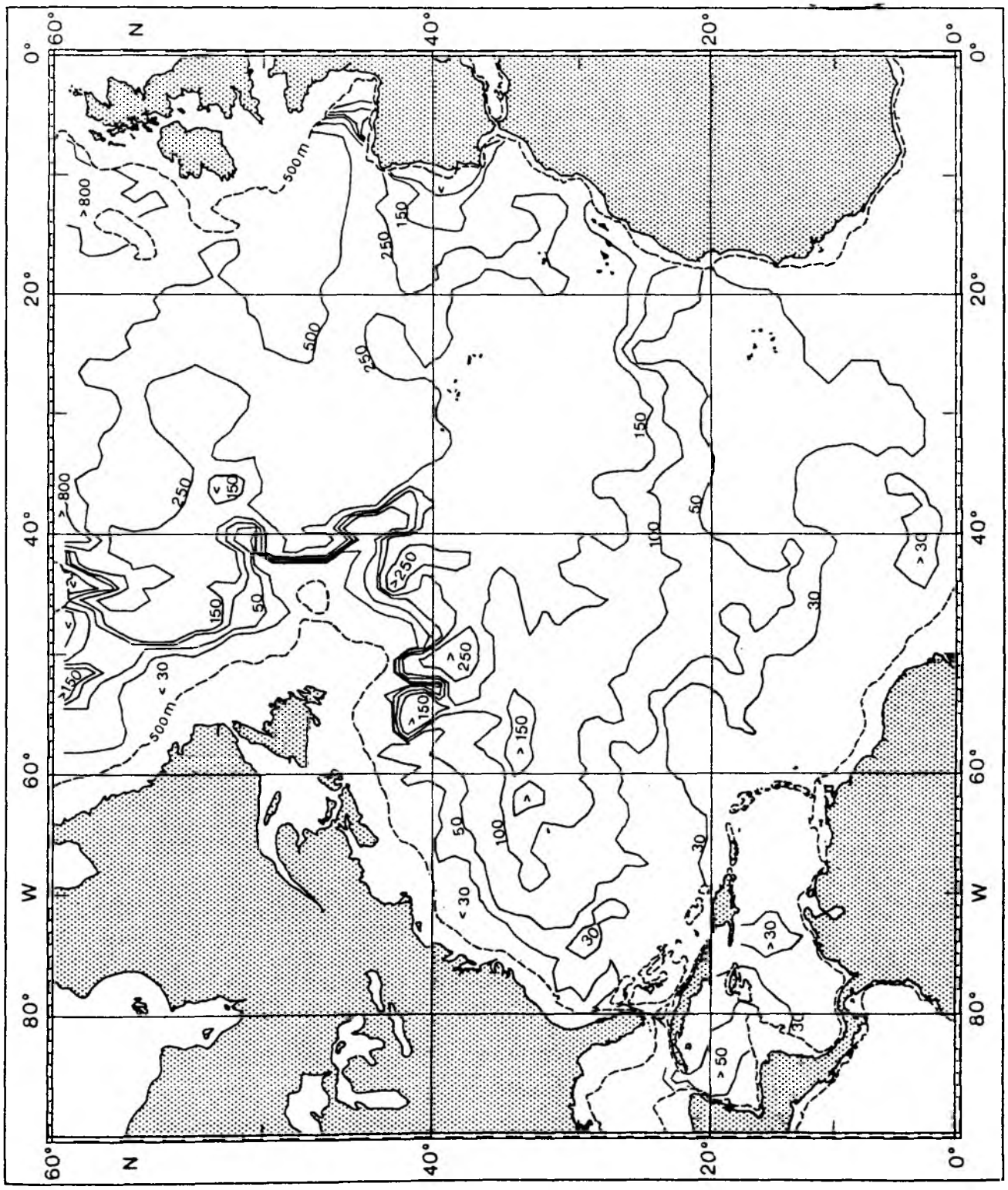

Fig. 2:

Maximum mean depth of the winter mixed layer from Robinson et al. (1979) atlas data, based on the criterion $\Delta\sigma_\theta$ = 0.125 kg m^{-3}.

profile between the surface and 30 m would be physically wrong. In order to get a more realistic profile a method frequently used of exponentially approximating hydrographic profiles (Warren, 1977) was applied to the density profiles to determine the mixed layer depth using the density criterion described above.

The derivation of IPV from the hydrographic RBS-atlas data was as follows and is given in Table 1. The monthly mean density profiles were calculated for the whole water column from the atlas temperature and salinity data. In order to correct for first order changes due to pressure changes we have based our analysis on potential density referred to the sea surface.

The maximum depth D of winter convection was calculated by determining the maximum depth in which the density takes the surface value plus $\Delta\sigma_\theta = 0.125$ kg m^{-3}. With the same density criterion the depth of the mixed layer was determined by using the exponential method mentioned above. When the mixed layer depth was shallower than 30 m an artificial data point was inserted into the density profile by extrapolating exponentially from the data points at 30 m and 60 m depth. This procedure is illustrated in fig. 3. Inversions in the density profile were eliminated by monotonization whenever they occurred within the top 150 m and below 150 m in winter time. When $\sigma_{\theta(150\ m)}$ was less than $\sigma_{\theta(183\ m)}$ (see left panel in fig. 4 for summer time) the data points between 150 m and the depth D were rejected. The finally obtained density profile was used to calculate the finite difference form on the large-scale potential vorticity

$$Q_S = \frac{f}{\rho_o} \cdot \frac{\Delta\sigma_\theta}{\Delta z}$$

by using the density difference $\Delta\sigma_\theta$ and depth difference Δz between adjacent data points and the planetary vorticity $f = 2\Omega \sin\phi$ at the latitude ϕ of the profile and the value of Q_S was positioned at the arithmetic mean of depth and density of the used data pair. Finally the Q_S-profile was interpolated onto potential density surfaces with a third order cubic spline function.

For illustration fig. 4 shows a density profile for summer time (left panel) and winter time (right panel) with data points on atlas depth levels (solid circles) and after IPV calculation (blank quadrangles). The two large circles show the artificial data points at the depth D and at the mixed

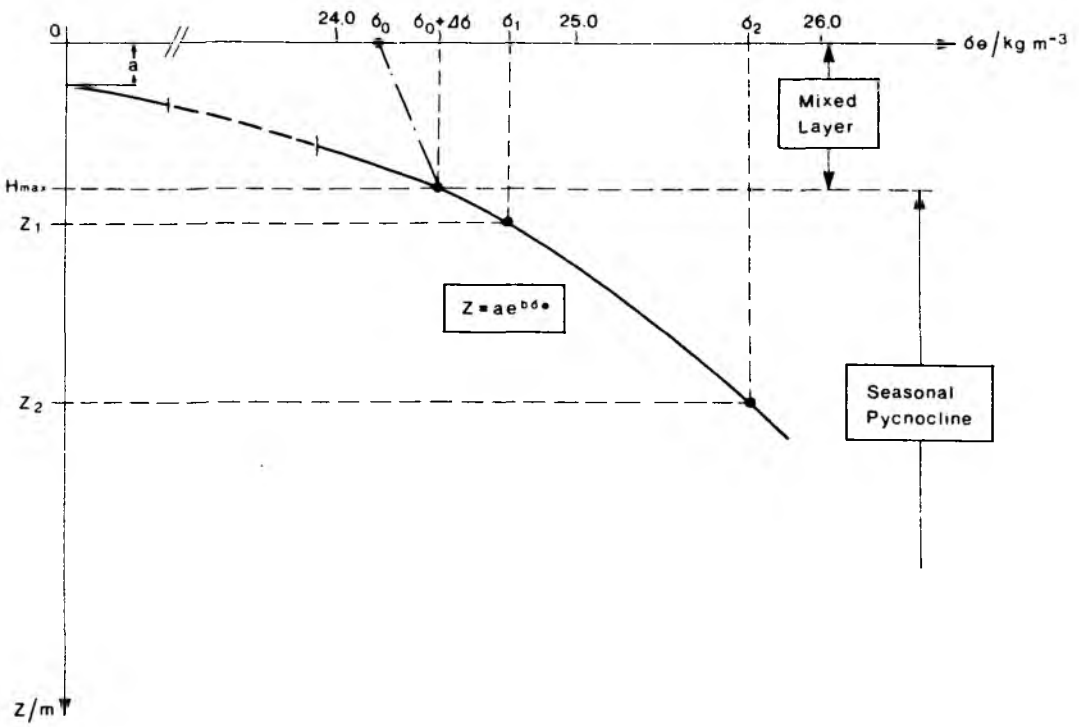

Fig. 3:

Schematic diagram illustrating the method of estimating the mixed layer depth H_{max} from the upper three atlas data points using a density criterion $\Delta\sigma_t$ = 0.125 kg m^{-3} and an exponential function $z = a \exp(\Delta\sigma_\theta)$. z_1 and z_2 are the depth levels of 30 m and 60 m, respectively, and σ_0 is the surface density. In case H_{max} was less than 30 m a new data point was introduced into the density profile.

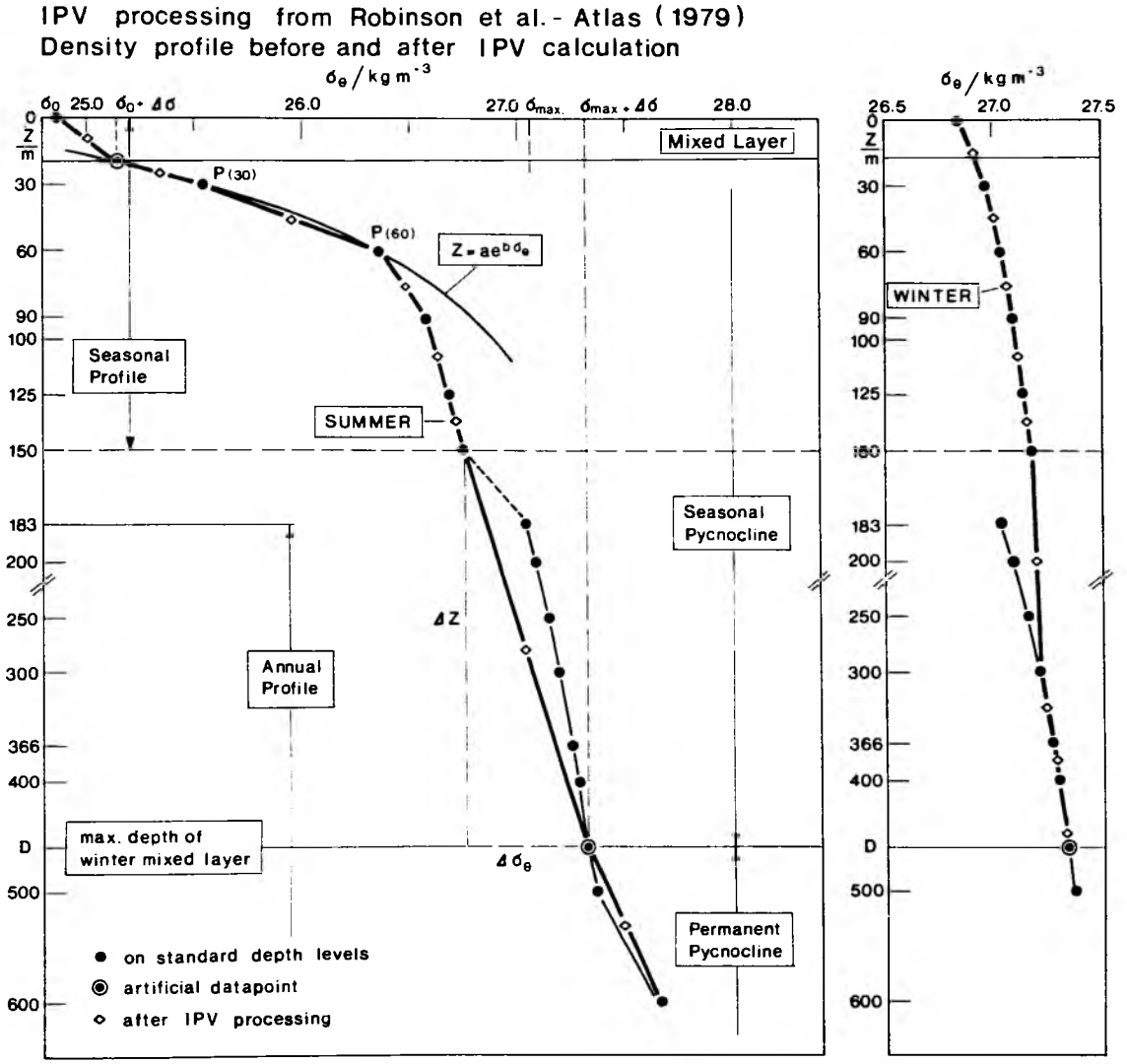

Fig. 4:

The manipulation of a density profile of the RBS atlas data during the derivation of the large-scale potential vorticity $Q_S = f \Delta\sigma_\theta / \rho_0 \Delta z$ is shown using the re-constructed profile for summer (left) and winter (right).

layer base which have been inserted into the profile before calculation of IPV.

Fig. 5 shows the top 300 m of a density- and IPV-profile at the position 27°30' W, 40°30' N in August during various stages of processing: (a) to (c) shows the density profile at atlas depth levels, after IPV-processing and after spline-interpolation onto isopycnals, respectively. In (d) and (e) the IPV-profile is given before and after spline interpolation.

Fig. 6 shows the IPV-profile after spline interpolation onto density surfaces with σ_θ as the vertical axis in place of z. The circled points indicate the basis for the spline interpolation.

Q_S was contoured in the horizontal by two-dimensional interpolation on the following selected isopycnals for the 12 months of the year and for annual mean values: σ_t = 25.0, 25.5, 26.0, 26.5, 27.0 and 27.5 kg m^{-3}.

The maps are arranged in order of increasing isopycnals with 12 monthly maps and one annual mean map each, starting with March, the beginning of the heating season. The units of Q_S are 10^{-9} rad/ms throughout this whole atlas. The annual mean values simply denote the IPV calculated from all the data mean values of temperature and salinity.

The IPV maps were not smoothed after calculation for two reasons. The history of the data comprised in the numerical atlas of Robinson et al. (1979) is quite complicated and includes horizontal and vertical interpolation as well as smoothing in time. An additional smoothing of the Q-contours in space would yield a further degradation of the results. Moreover a smoothing procedure in space would reduce dynamically interesting structures such as local maxima in the gradients of isopycnic potential vorticity.

The following notations are common to all maps.
The stippled regions show the land contours bounded by the 500 m isobath (dashed line). Between the coastlines and the 500 m isobath the IPV was not contoured since the conservation of the potential vorticity does not hold on the shallow shelf where the bottom boundary layer penetrates unevenly into the seasonal thermocline. The northernmost solid line indicates the outcrop of the isopycnals in each month surrounded by two dashed lines which indicate the outcrop of $\sigma_\theta \pm 0.1$ kg m^{-3}. The heavy line south of the monthly outcrop shows the surface position of the isopycnal in March with

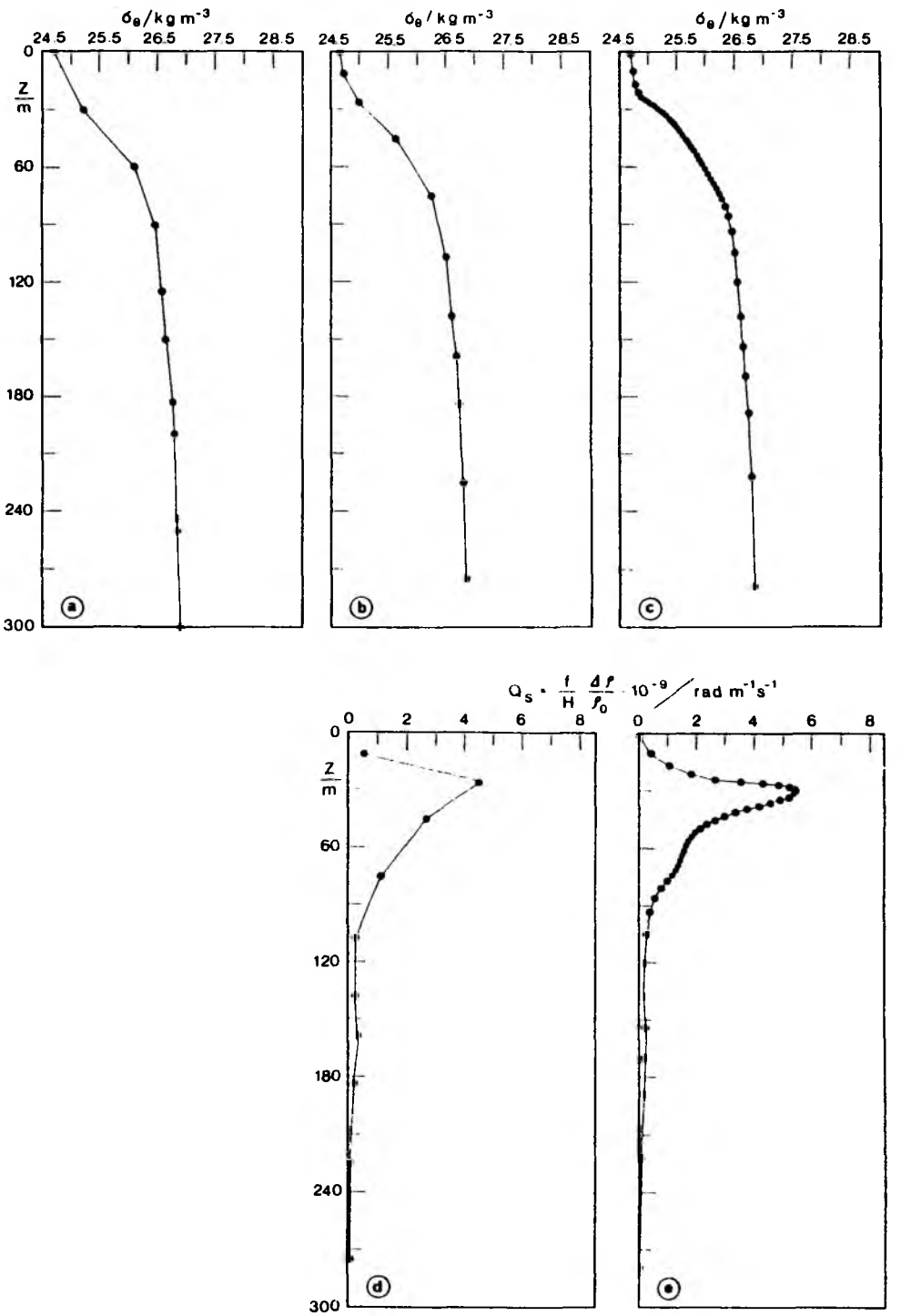

Fig. 5:

The top 300 m of a density and Q_s profile at the position 27°30' W, 40°30' N in August during various stages of data processing: (a) the density profile on atlas standard depth levels, (b) after IPV derivation and (c) after spline interpolation; (d) and (e) shows the Q_s profile before and after spline isopycnals, respectively.

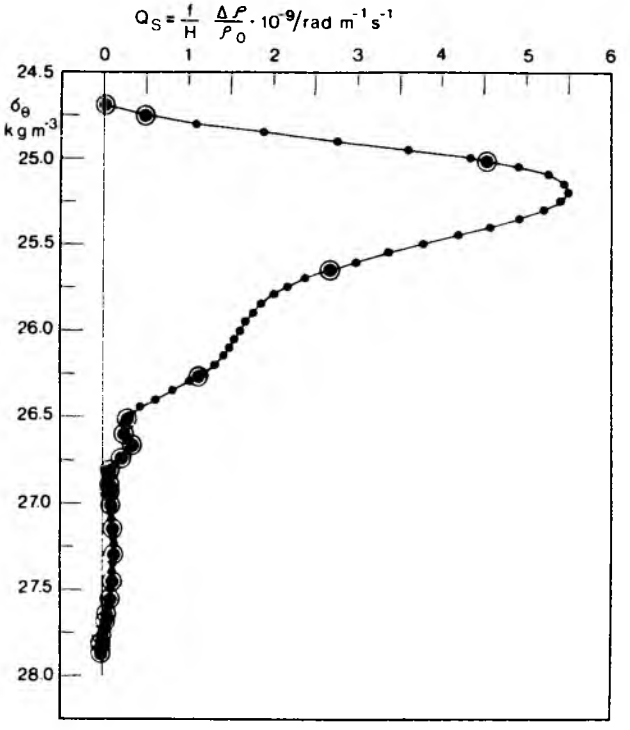

Fig. 6:

The Q_S profile after cubic spline interpolation with σ_θ as the vertical axis. The circled dots are the data base for the interpolation.

$\sigma_\theta \pm 0.1$ kg m^{-3} respectively. Since the isopycnals generally reach their equatorward extreme in March this outcrop divides the isopycnal surface into two parts; the part of the isopycnal south of the March outcrop lies in the permanent thermocline whereas the region north of it is part of the seasonal thermocline.

The potential vorticity can be defined in various ways. The definition used in this analysis is given over the vertical spacing between two isopycnals. Q cannot be specified whenever one of them reaches the mixed layer. We carried out a series of tests to investigate the sensitivity of the maps to the chosen range of density. They showed that the outcrop of the standard range ($\pm$ 0.1 kg m^{-3}) gave a good indication of where the layer was outcropping.

The values of Q on the different isopycnals covers several orders of magnitude. To resolve the major features on the different isopycnals the contour increment varies with the total IPV range and with isopycnals in the sense that deeper layers show additional contour lines. A list of contours used for the different isopycnals is given in Table 2.

Table 1: List of processing steps during IPV derivation from RBS data set

Processing	Procedure
1st	Calculation of the potential density from monthly mean temperature and mean salinity data referenced to the sea surface.
2nd	Determination of the maximum depth D of the winter mixed layer with a density criterion $\Delta\sigma_\theta = 0.125$ kg m^{-3} (Levitus, 1982) and insertion of a new data point at that depth whenever $D > 150$ m.
3rd	Determination of the monthly mixed layer depth with the density criterion $\Delta\sigma_\theta = 0.125$ kg m^{-3} by exponential extrapolation and insertion of a data point at that depth when the depth < 30 m.
4th	Monotonization of the density profile in the top 150 m
5th	a) $\sigma_\theta(150\ m) > \sigma_\theta(183\ m)$ (winter time) Monotonization of the density profile below 150 m b) $\sigma_\theta(150\ m) < \sigma_\theta(183\ m)$ (summer time) rejection of the data points between 150 m and D
6th	Calculation of $Q_S = f\,\Delta\sigma_\theta/\rho_o\Delta z$ by using the density difference $\Delta\sigma_\theta$ and depth difference Δz between adjacent data points and positioning Q_S at the arithmetic mean of σ_θ and z.
7th	Interpolation of the Q_S-profile onto isopycnal surfaces with interval $\Delta\sigma_\theta = 0.05$ kg m^{-3} by using a third order cubic spline function.
8th	Extraction of selected density surfaces (σ_θ = 25.0, 25.5, 26.0, 26.5, 27.0, 27.5 kg m^{-3}) and plotting of horizontally interpolated Q_S-contours.

Table 2: List of contours of IPV ($Q_S \cdot 10^{-9}$ rad m^{-1} s^{-1}) plotted on each isopycnic surface

Q_S	25.0	25.5	26.0	26.5	27.0	27.5	σ_θ /kg m^{-3}
0.02					x	x	
0.04					x	x	
0.06					x	x	
0.08					x	x	
0.10				x	x	x	
0.15					x	x	
0.2	x	x	x	x	x	x	
0.4	x	x	x	x	x	x	
0.5				x			
0.6	x	x	x	x	x	x	
0.8	x	x	x	x	x	x	
1.0	x	x	x	x	x	x	
1.5	x	x	x	x	x	x	
2.0	x	x	x	x	x	x	
2.5	x	x	x	x	x	x	
3.0	x	x	x	x	x	x	
4.0	x	x	x	x	x	x	
5.0	x	x	x	x	x	x	
6.0	x	x	x	x	x	x	
7.0	x	x	x	x	x	x	
8.0	x	x	x	x	x	x	
9.0	x	x	x	x	x	x	
10.0	x	x	x	x	x	x	

3 REFERENCES

Barkmann, W. (1986) Der Einfluß der Wärmebilanz auf die Struktur der saisonalen Grenzschicht.
Ph.D. Thesis, University of Kiel.

Bauer, J. & Woods, J.D. (1984) Isopycnic Atlas of the North Atlantic Ocean.
Ber. Inst. Meeresk., Kiel, 132.

Bleck, R., Onken, R. & Woods, J.D. (1987) A two-dimensional model of mesoscale frontogenesis in the ocean.
Quart. J. Roy. Met. Soc. (in press).

Böhnecke, G. (1986) Atlas: Temperatur, Salzgehalt und Dichte an der Oberfläche des Atlantischen Ozeans.
Wissenschaftl. Erg. der D. Atl. Expt. Meteor 1925-27, Vol. V.

Fischer, J. (1986) Struktur und Dynamik einer mesoskaligen Front im Wirbelfeld des Nordatlantischen Stromes.
Ph.D. Thesis, University of Kiel.

Fischer, J., Leach, H. & Woods, J.D. (1987) A synoptic map of isopycnic potential vorticity in the seasonal thermocline at the North Atlantic Polar Front (in preparation) .

Folland, C.K. Parker, D.E. & Kates, F.E. (1984) Worldwide marine temperature fluctuations 1856-1981.
Nature, 310, 670-673.

Harvey, J. & Glynn, S. (1985) Water mass structure and transport in the Tourbillon eddy.
Deep-Sea Res., 32(6), 675-695.

Hoskins, B.J., McIntyre, M.E. & Robertson, A.W. (1985) On the use and significance of isentropic potential vorticity maps.
Quart. J. Roy. Met. Soc., 111, 877-946.

Hua, B.L., McWilliams, J.C., Owens, W.B. (1986) An objective analysis of the POLYMODE Local Dynamics Experiment. Part II: Streamfunction and potential vorticity fields during the intensive period.
J. Phys. Oceanogr., 16, 506-522.

Keffer, T. (1985) The ventilation of the World's Ocean: Maps of the potential vorticity field.
J. Phys. Oceanogr., 15, 509-523.

Leach, H., Minnett, P.J. & Woods, J.D. (1985) The GATE Lagrangian Batfish Experiment.
Deep-Sea Res., 32, 575-597.

Levitus, S. (1982) Climatological Atlas of the World Ocean.
NOAA Prof. Paper 13, U.S. Dept. of Commerce, National Oceanic and Atmospheric Administration, 173 pp.

Levitus, S. (1986) Annual Cycle of Salinity in the World Ocean.
J. Phys. Oceanogr., 16, 322-343.

Luyten, J.R., Pedlosky, J. & Stommel, H. (1983) The ventilated thermocline.
J. Phys. Oceanogr., 13, 292-309.

McDowell, S., Rhines, P.B. & Keffer, T. (1982) North Atlantic potential vorticity and its relation to the general circulation.
J. Phys. Oceanogr., 12, 1417-1436.

McWilliams, J.C. (1976) Maps from the Mid-Ocean Dynamics Experiment. Part II. Potential Vorticity and its Conservation.
J. Phys. Oceanogr., 6, 828-846.

Montgomery, R.B. (1938) Circulation in upper layers of southern North Atlantic deduced with use of isentropic analysis.
Pap. Phys. Oceanogr. and Meteor., MIT and WHOI, 6(2), 55 pp.

Pedlosky, J. (1983) Eastern boundary ventilation and the structure of the thermocline.
J. Phys. Oceanogr., 13, 2038-2044.

Pollard, R.T. & Pu, S. (1985) Structure and circulation of the upper Atlantic Ocean northeast of the Azores.
Progr. Oceanogr., 14, 443-462.

Reikowski, A. (1987) Jahreszeitliche Veränderlichkeit hydrographischer Parameter an der Ozean Wetterstation "C".
Diplomarbeit, University of Kiel.

Rhines, P.B. & Young, W.R. (1982a) Homogenization of potential vorticity in planetary gyres.
J. Fluid Mech., 122, 347-368.

Rhines, P.B. & Young, W.R. (1982b) A theory of wind-driven ocean circulation. I. Mid-ocean gyres.
J. Mar. Res., 40 (Suppl.), 559-596.

Robinson, M., Bauer, R. & Schroeder, E. (1979) Atlas of North Atlantic - Indian Ocean Monthly Mean Temperatures and Mean Salinities of the Surface Layer.
Dept. of the Navy, Washington, D.C., USA.

Rodewald, M. (1972) Einige hydroklimatische Besonderheiten des Jahrzehnts 1961-1970 im Nordatlantik und im Nordpolarmeer.
Dt. hydrogr. Z., 25(3), 97-117.

Sarmiento, J.L., Rooth, C.G.H. & Roether, W. (1982) The North Atlantic tritium distribution in 1972.
J. Geophys. Res., 87(C10), 8047-8056.

Stammer, D. (1987) Die jahreszeitliche Veränderlichkeit der isopyknischen potentiellen Vorticity in der Warmwassersphäre des Nordatlantiks.
Diplomarbeit, University of Kiel.

Warren, A.B. (1977) Note on interpreting e-folding depth.
In: M. Angel (Ed.) A Voyage of Discovery. Pergamon Press.

Woods, J.D. (1985) The physics of thermocline ventilation.
In: J.C.J. Nihoul (Ed.) Coupled Ocean-Atmosphere Models. Elsevier, Amsterdam, 543-590.

Woods, J.D. & Barkmann, W. (1986) A Lagrangian mixed layer model of 18 °C water formation.
Nature, 319, 574-576.

Woods, J.D., Barkmann, W. & Horch, A. (1984) Solar heating of the oceans - diurnal, seasonal and meridional variation.
Quart. J. Roy. Met. Soc., 110, 633-656.

4 ACKNOWLEDGEMENTS

This work was undertaken as part of a long-term investigation of the warm water sphere of the North Atlantic Ocean. The work was supported by the Deutsche Forschungsgemeinschaft (German Research Society) under contract DFG-SFB-133 "Warm water sphere of the Atlantic" at the Institut für Meereskunde an der Christian-Albrechts-Universität, Kiel.

The data set used for this analysis is the numerical atlas produced by M. Robinson, R. Bauer and E. Schroeder (1979), purchased from Compass System Inc., 4640 Jewell Str. #204, San Diego, CA, 92109, USA and installed on the VAX 750/11 computer of the Institut für Meereskunde.

The authors wish to express their gratitude to their colleagues in the department of Regionale Ozeanographie (in particular Diplom-Oz. J. Bauer) for stimulating comments, and the head of the Regional Oceanographie cartography unit, Alfed Eisele, for the production of the atlas from computer plots.

5 MONTHLY MEAN IPV MAPS

Table 3: Index to page numbers of monthly mean IPV maps

Maps	25.0	25.5	26.0	26.5	27.0	27.5	σ_θ/kg m^{-3}
Seasonal migration	25	39	53	67	81	95	
March	26	40	54	68	82	96	
April	27	41	55	69	83	97	
May	28	42	56	70	84	98	
June	29	43	57	71	85	99	
July	30	44	58	72	86	100	
August	31	45	59	73	87	101	
September	32	46	60	74	88	102	
October	33	47	61	75	89	103	
November	34	48	62	76	90	104	
December	35	49	63	77	91	105	
January	36	50	64	78	92	106	
February	37	51	65	79	93	107	
Annual mean	38	52	66	80	94	108	

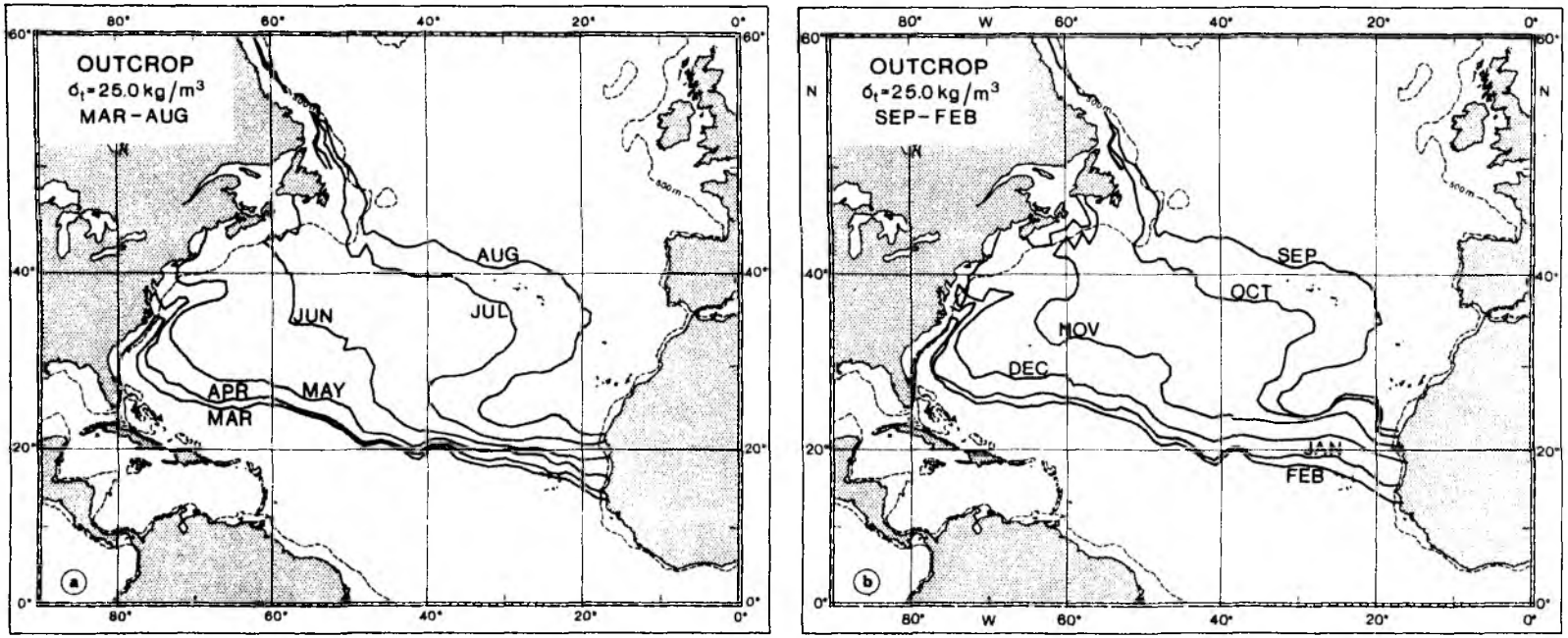

Seasonal migration of the outcrop of the isopycnal surface with σ_θ = 25.0 kg m^{-3};
(a) heating season, (b) cooling season.

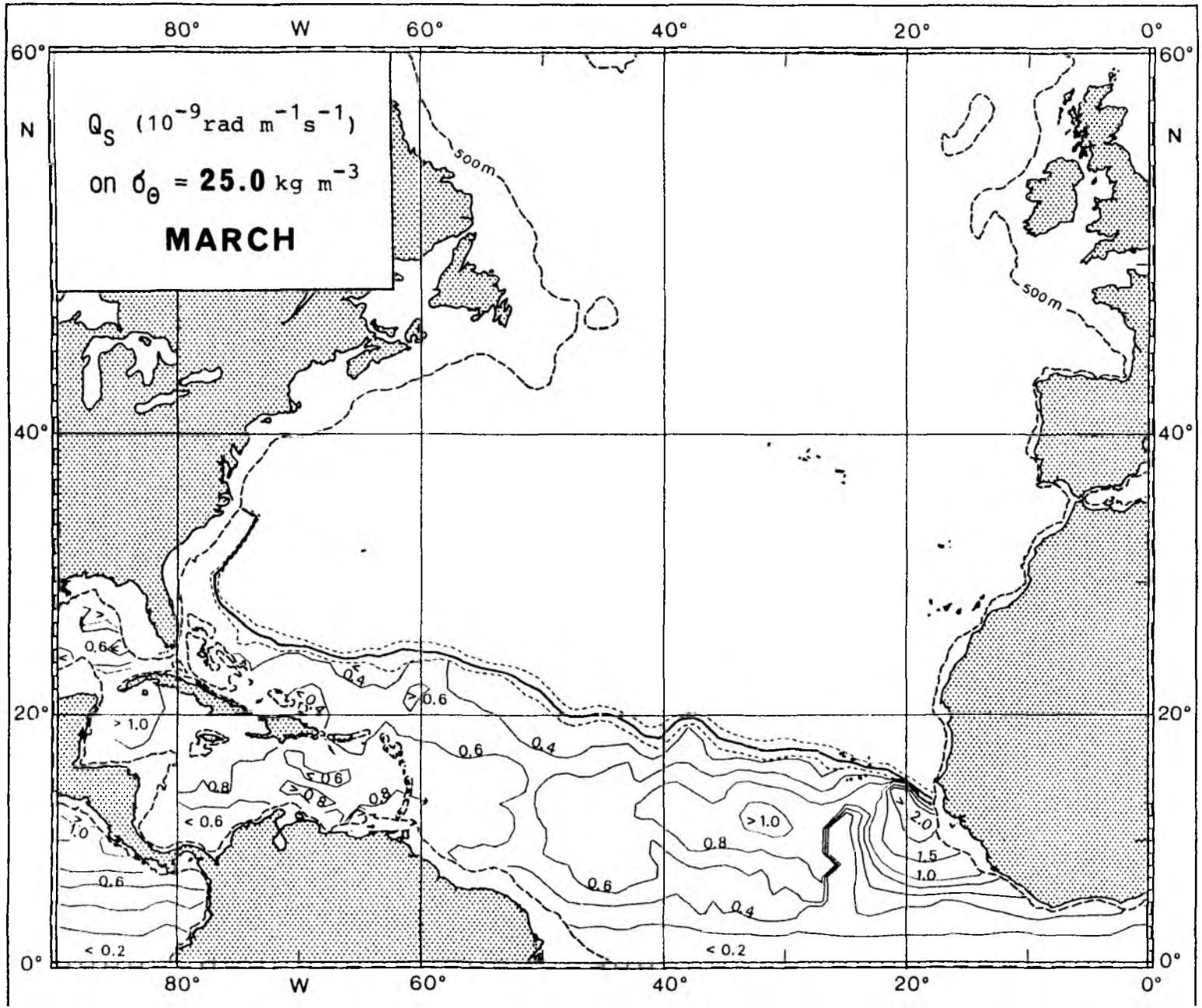
Q_S (10^{-9}rad $m^{-1}s^{-1}$)
on σ_θ = 25.0 kg m^{-3}
MARCH
80° W
60°
40°
20°
0°
60° N
40°
20°
0°
500m
500m
0.6
0.4
0.6
> 1.0
0.8
< 0.6
0.8
0.8
< 0.6
1.0
0.6
< 0.2
0.6
0.4
> 1.0
0.8
0.6
0.4
< 0.2
2.0
1.5
1.0

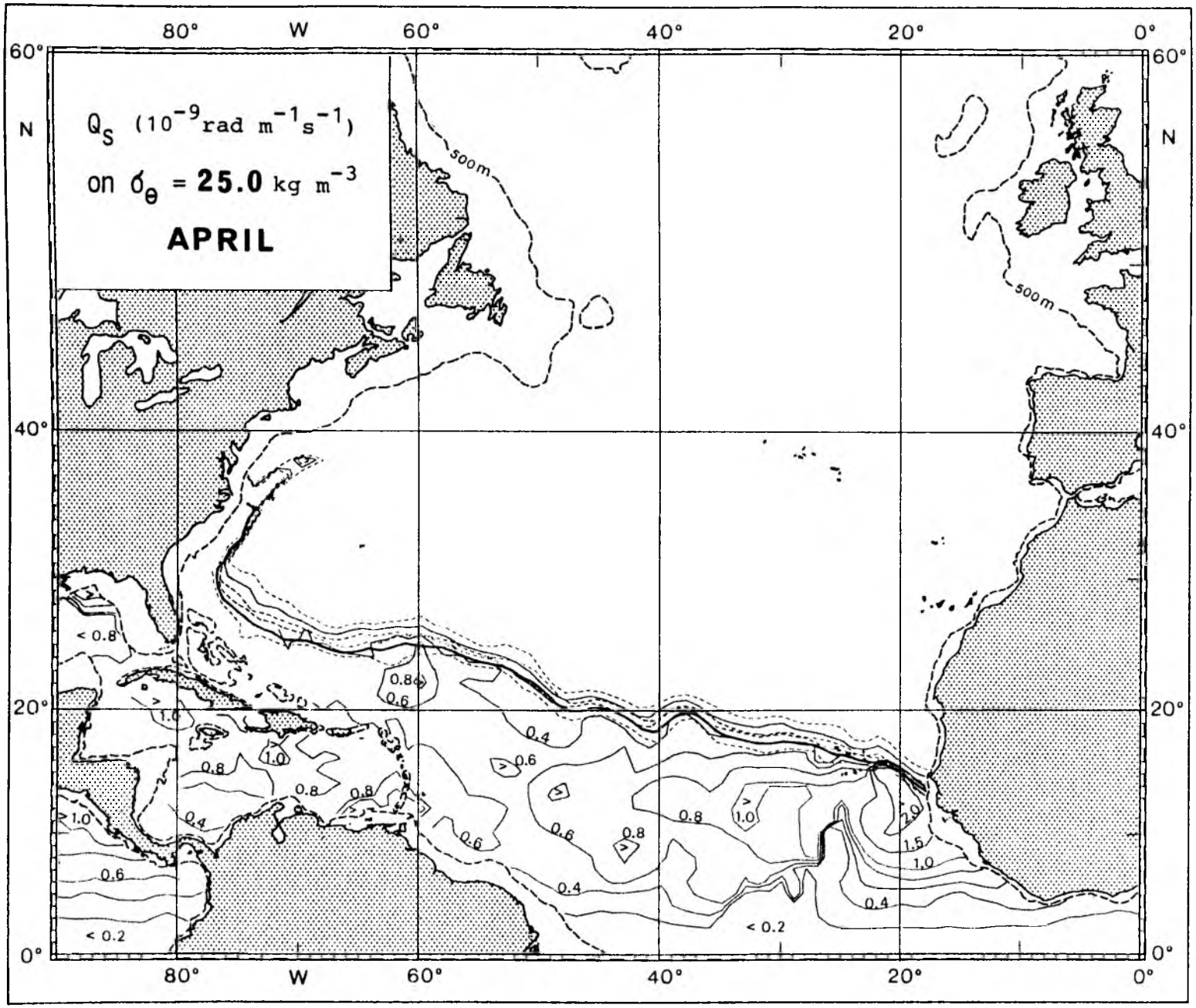
Q_S (10^{-9} rad $m^{-1}s^{-1}$)
on σ_θ = 25.0 kg m^{-3}
APRIL
80° W
60°
40°
20°
0°
60° N
40°
20°
0°
500m
500m
< 0.8
0.8
0.6
0.4
> 1.0
1.0
0.8
0.8
0.8
0.4
> 1.0
0.6
< 0.2
0.6
> 0.6
0.6
0.8
0.4
0.8
> 1.0
2.0
1.5
1.0
0.4
< 0.2

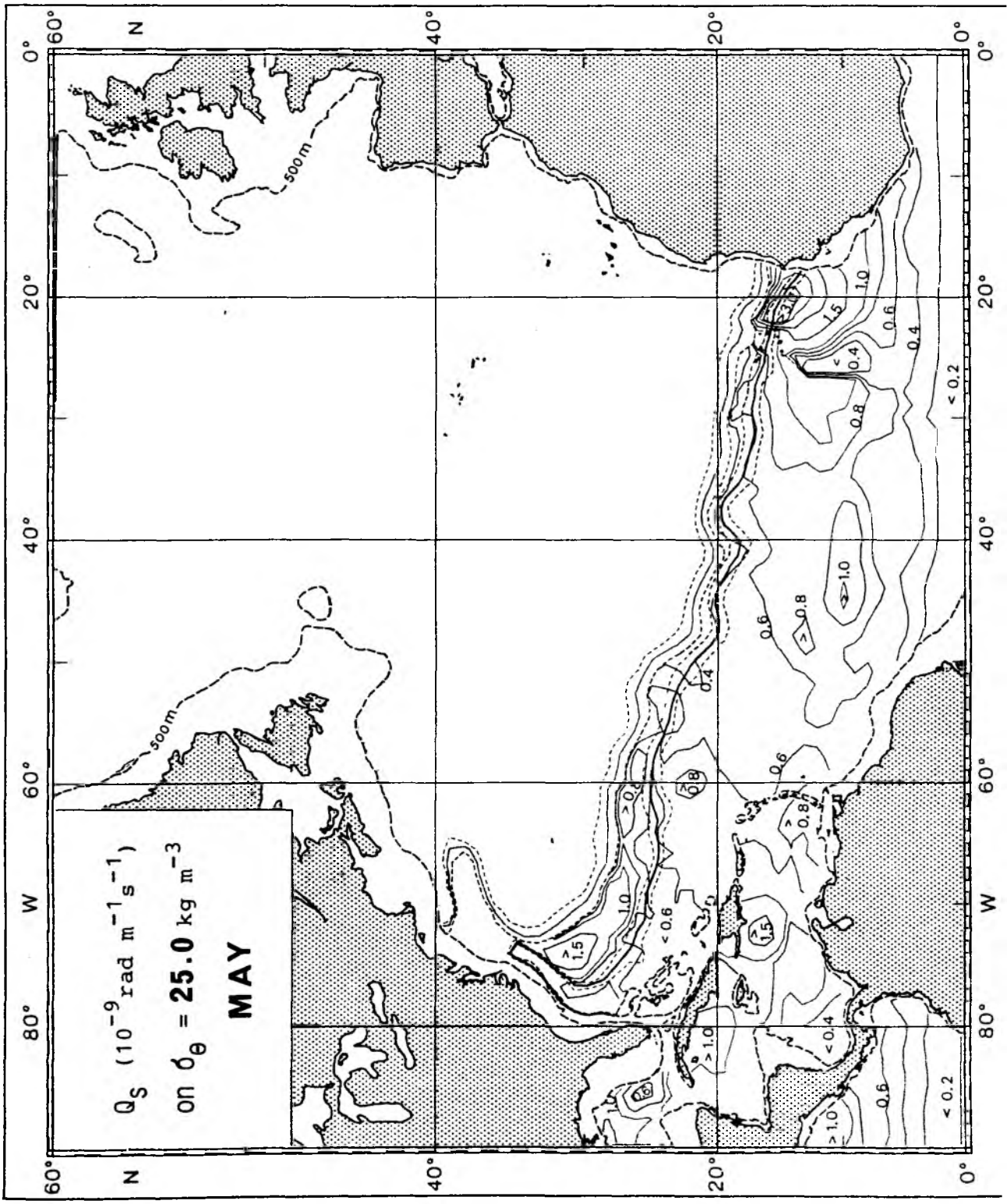
Q_S (10^{-9} rad $m^{-1}s^{-1}$)
on σ_θ = 25.0 kg m^{-3}
MAY
500m
500m
0°
20°
40°
60°
80° W
60° N

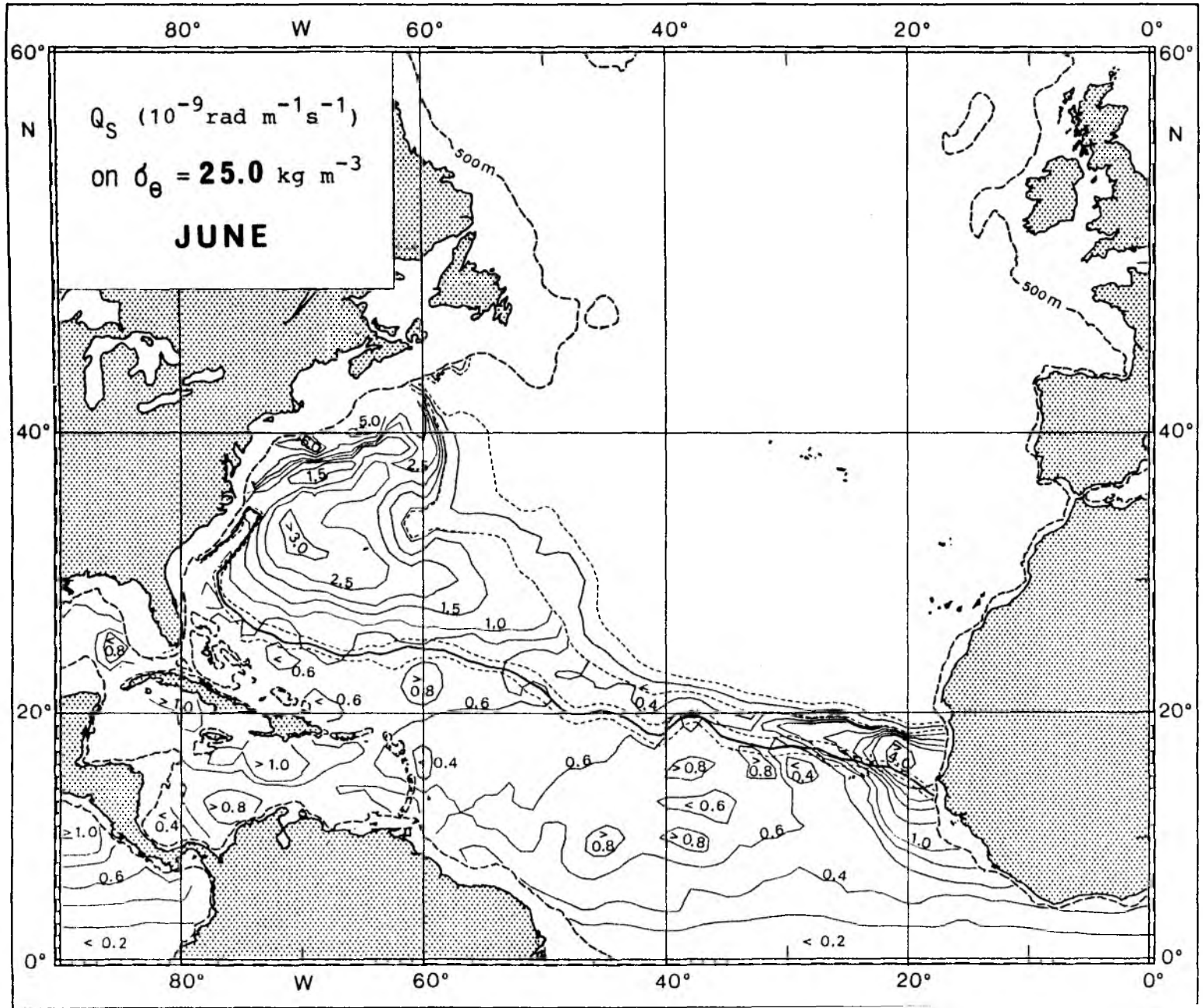
Q_S (10^{-9} rad $m^{-1}s^{-1}$)
on σ_θ = 25.0 kg m^{-3}
JUNE
80° W
60°
40°
20°
0°
60° N
40°
20°
0°
500m
5.0
3.0
2.5
2.0
1.5
1.0
0.8
0.6
0.4
0.2
< 0.2
> 1.0
> 0.8
< 0.6
< 0.4

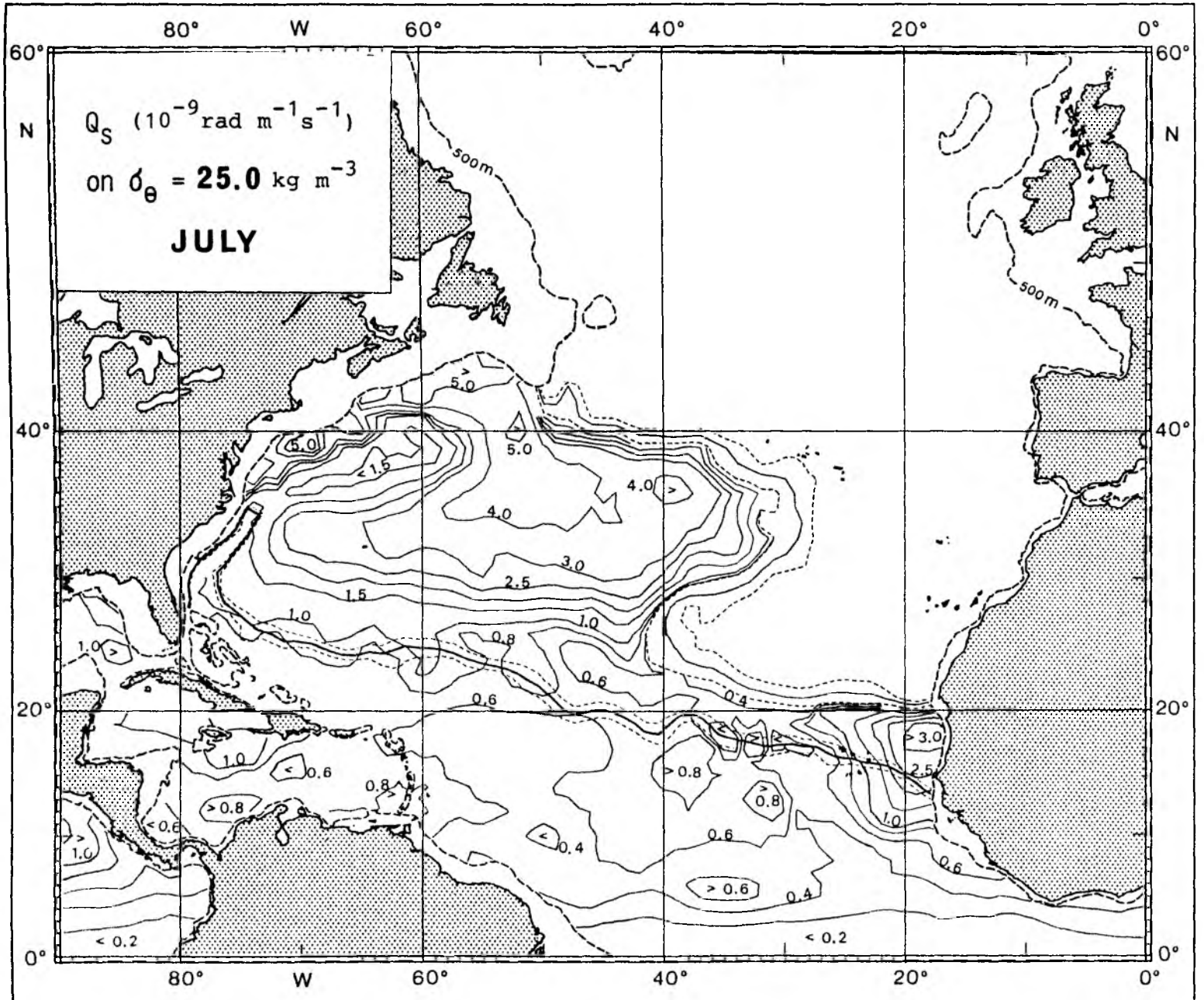
Q_S (10^{-9} rad $m^{-1}s^{-1}$)
on σ_θ = 25.0 kg m^{-3}
JULY
80° W
60°
40°
20°
0°
60° N
40°
20°
0°
500m
500m
5.0
4.0
3.0
2.5
1.5
1.0
0.8
0.6
0.4
< 0.2
> 0.8
> 0.6
< 0.6
< 0.4

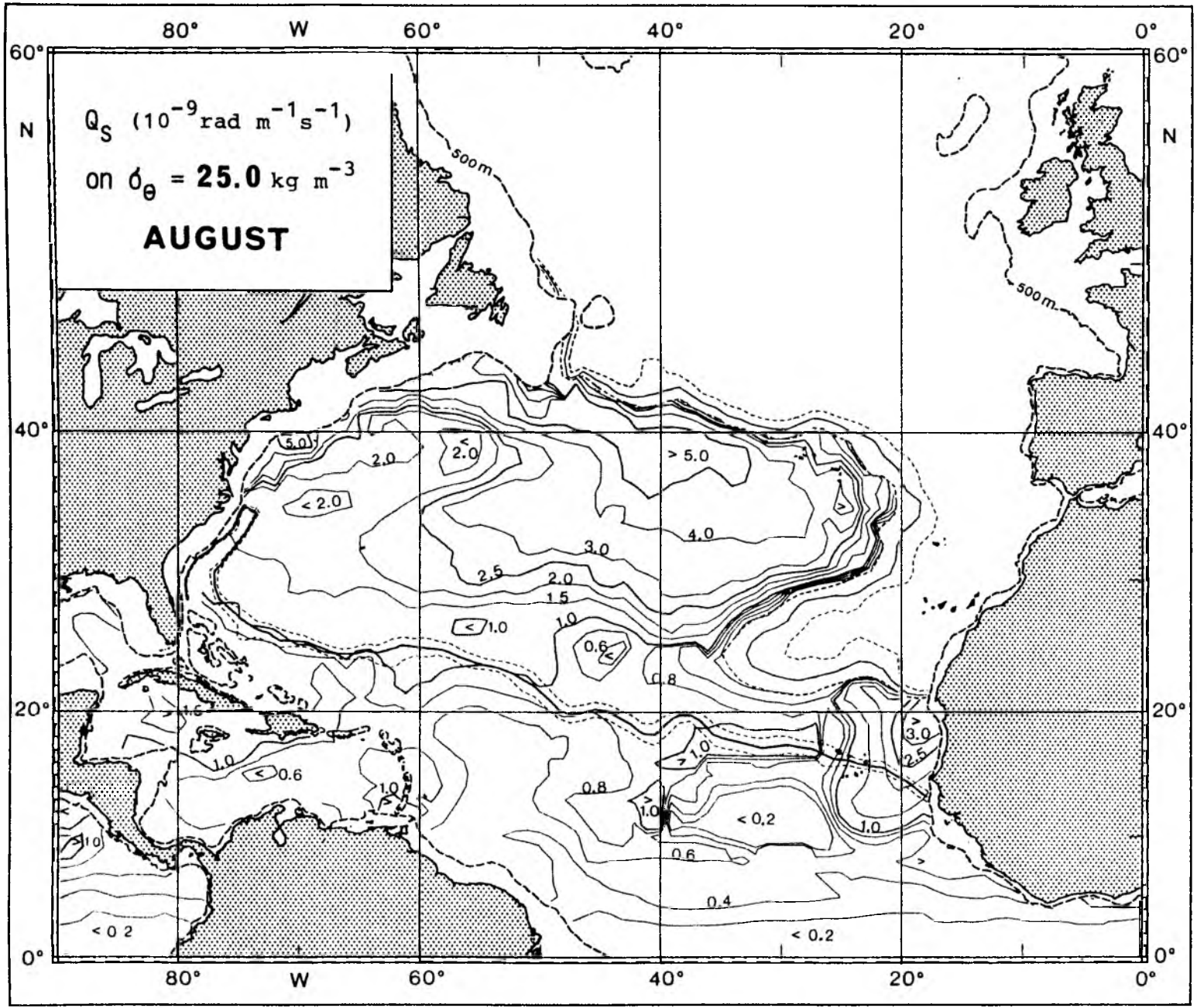
Q_S (10^{-9} rad $m^{-1}s^{-1}$)
on σ_θ = 25.0 kg m^{-3}
AUGUST
80° W
60°
40°
20°
0°
60° N
40°
20°
0°
500m
500m
5.0
2.0
< 2.0
2.0
> 5.0
4.0
3.0
2.5
2.0
1.5
1.0
< 1.0
0.6
0.8
1.0
< 0.6
1.0
1.0
0.8
> 1.0
< 0.2
1.0
0.6
0.4
< 0.2
< 0.2
3.0
2.5

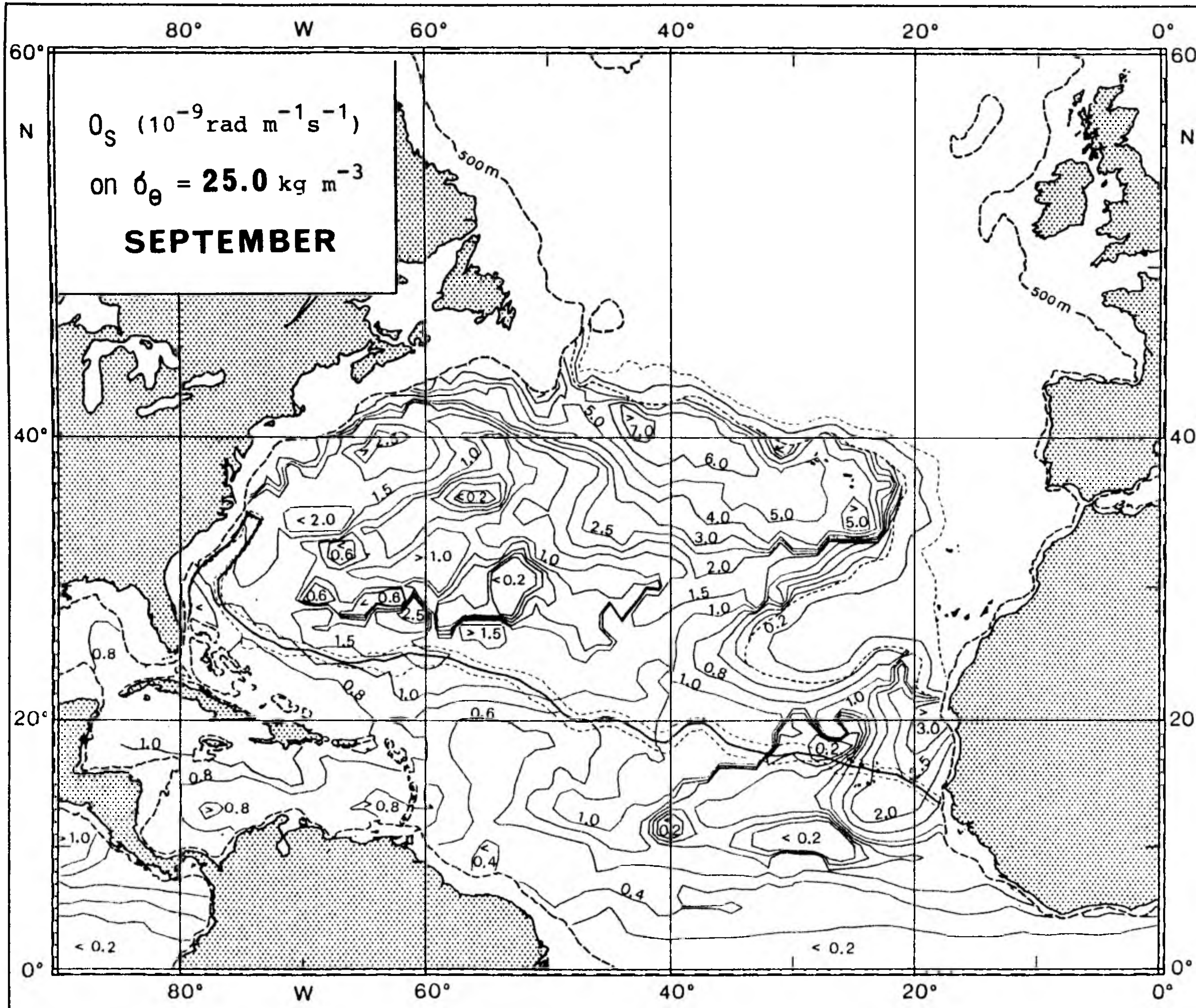

O_S (10^{-9}rad m^{-1}s^{-1})
on σ_θ = **25.0** kg m^{-3}
SEPTEMBER
80°
W
60°
40°
20°
0°
60°
N
40°
20°
0°
500m
500m
5.0
> 7.0
6.0
5.0
4.0
3.0
2.5
2.0
1.5
1.0
< 2.0
< 0.2
> 1.0
> 1.5
0.6
0.8
1.0
0.6
0.4
< 0.2
> 0.8
0.8
2.0
3.0
< 0.2

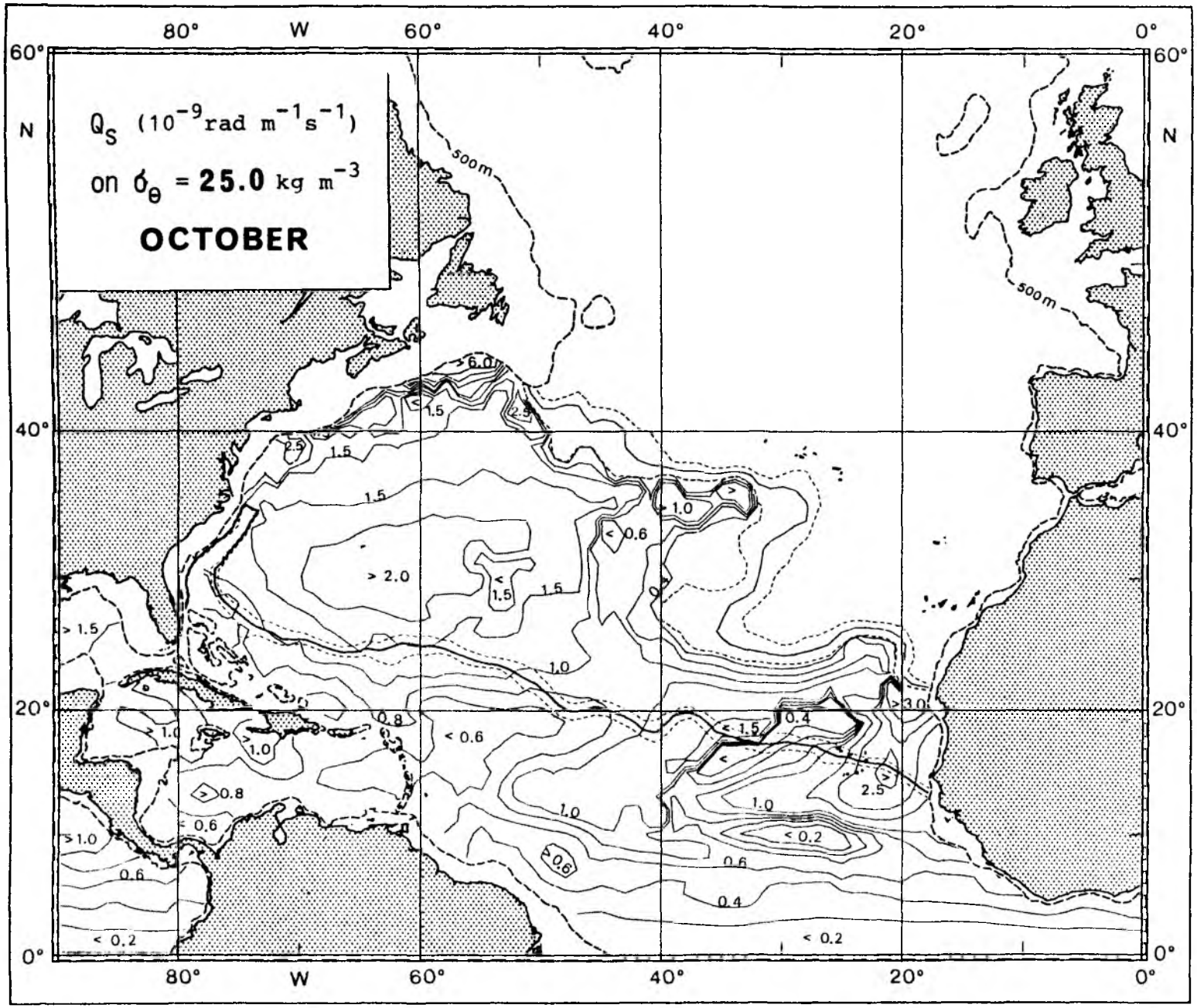
Q_S (10^{-9}rad $m^{-1}s^{-1}$)
on σ_θ = 25.0 kg m^{-3}
OCTOBER
80° W 60° 40° 20° 0°
60° N
40°
20°
0°
500m
500m
> 6.0
< 1.5
2.5
1.5
1.5
1.5
> 1.0
< 0.6
> 2.0
< 1.5
1.5
1.0
> 1.5
0.8
< 0.6
> 1.0
> 1.0
> 1.0
> 0.8
< 0.6
> 1.0
0.6
< 0.2
> 3.0
< 1.5
0.4
2.5
1.0
1.0
< 0.2
0.6
0.6
0.4
< 0.2

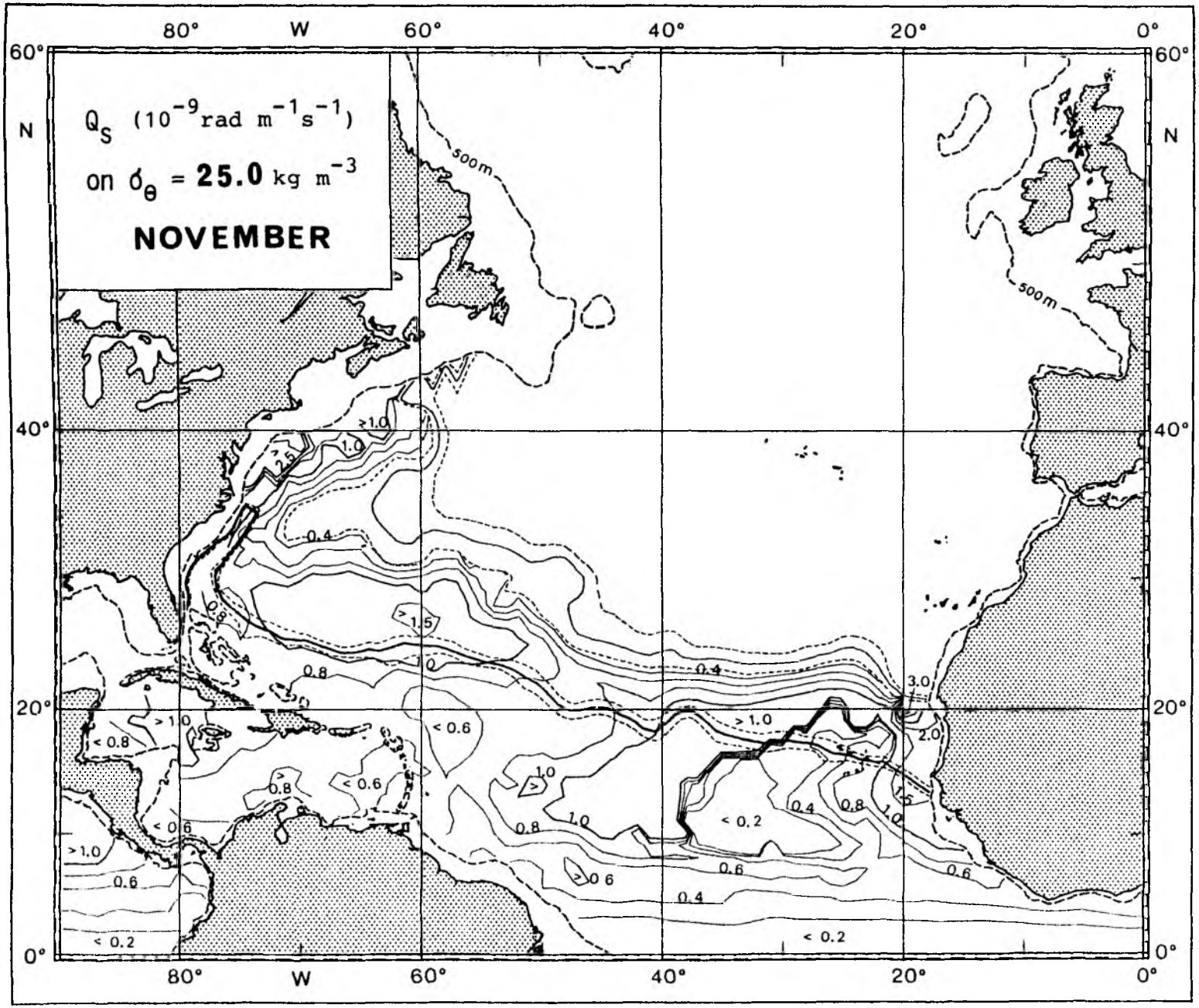
Q_S (10^{-9} rad $m^{-1}s^{-1}$)
on σ_θ = 25.0 kg m^{-3}
NOVEMBER
80° W
60°
40°
20°
0°
60° N
40°
20°
0°
500m
500m
>1.0
1.0
2.5
0.4
0.8
>1.5
1.0
0.8
0.4
3.0
2.0
>1.0
<0.8
<0.6
>1.0
0.8
<0.6
1.0
0.8
1.0
<0.2
0.4
0.8
1.0
1.5
<0.6
>1.0
0.6
>0.6
0.6
0.4
0.6
<0.2
<0.2

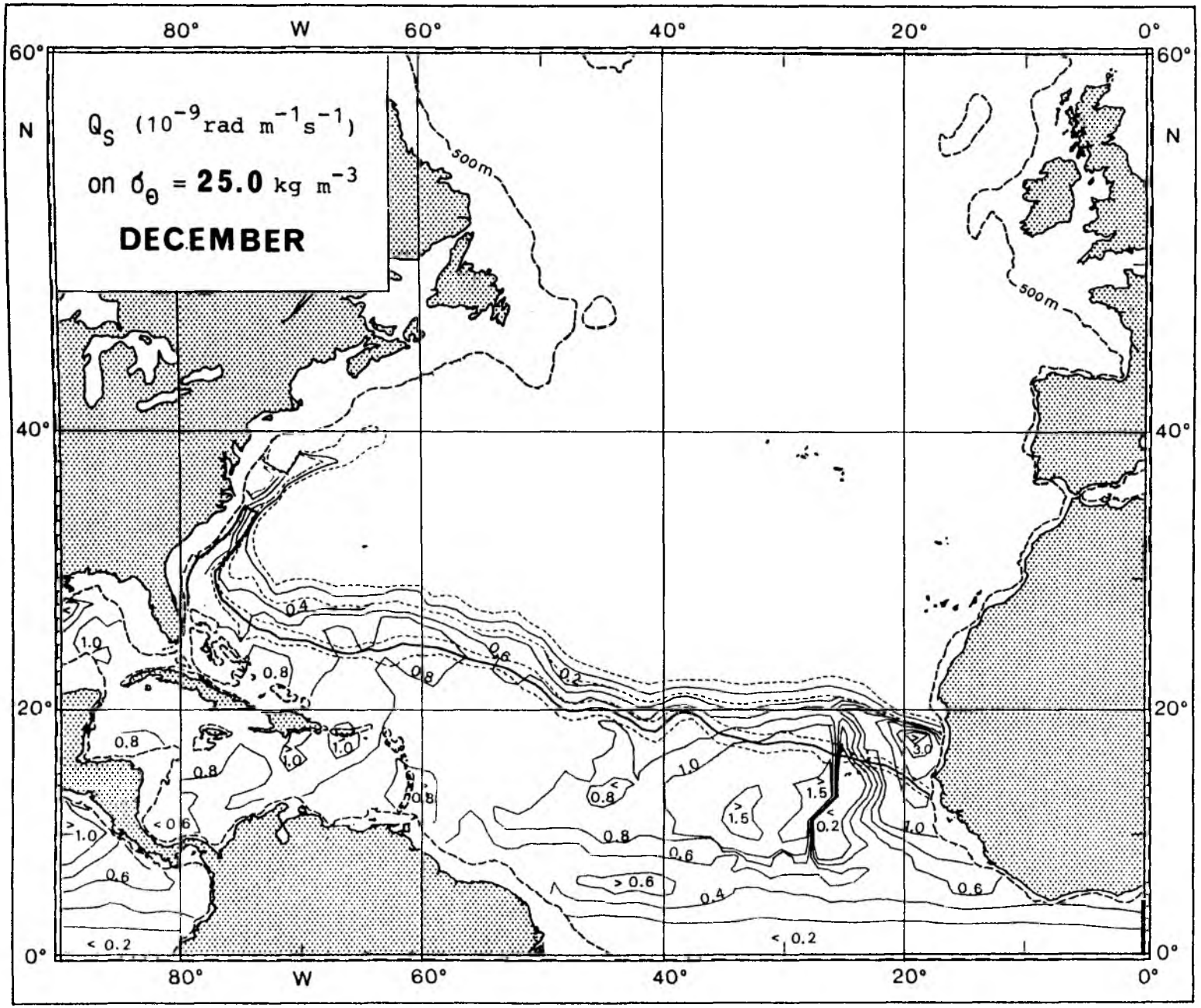
Q_S (10^{-9} rad $m^{-1}s^{-1}$)
on σ_θ = 25.0 kg m^{-3}
DECEMBER
80° W
60°
40°
20°
0°
60° N
40°
20°
0°
500m
500m
0.4
0.6
0.2
1.0
0.8
0.8
0.8
1.0
1.0
0.8
0.8
0.8
1.0
1.5
1.5
0.2
1.0
0.8
0.6
> 0.6
0.4
0.6
< 0.2
< 0.2

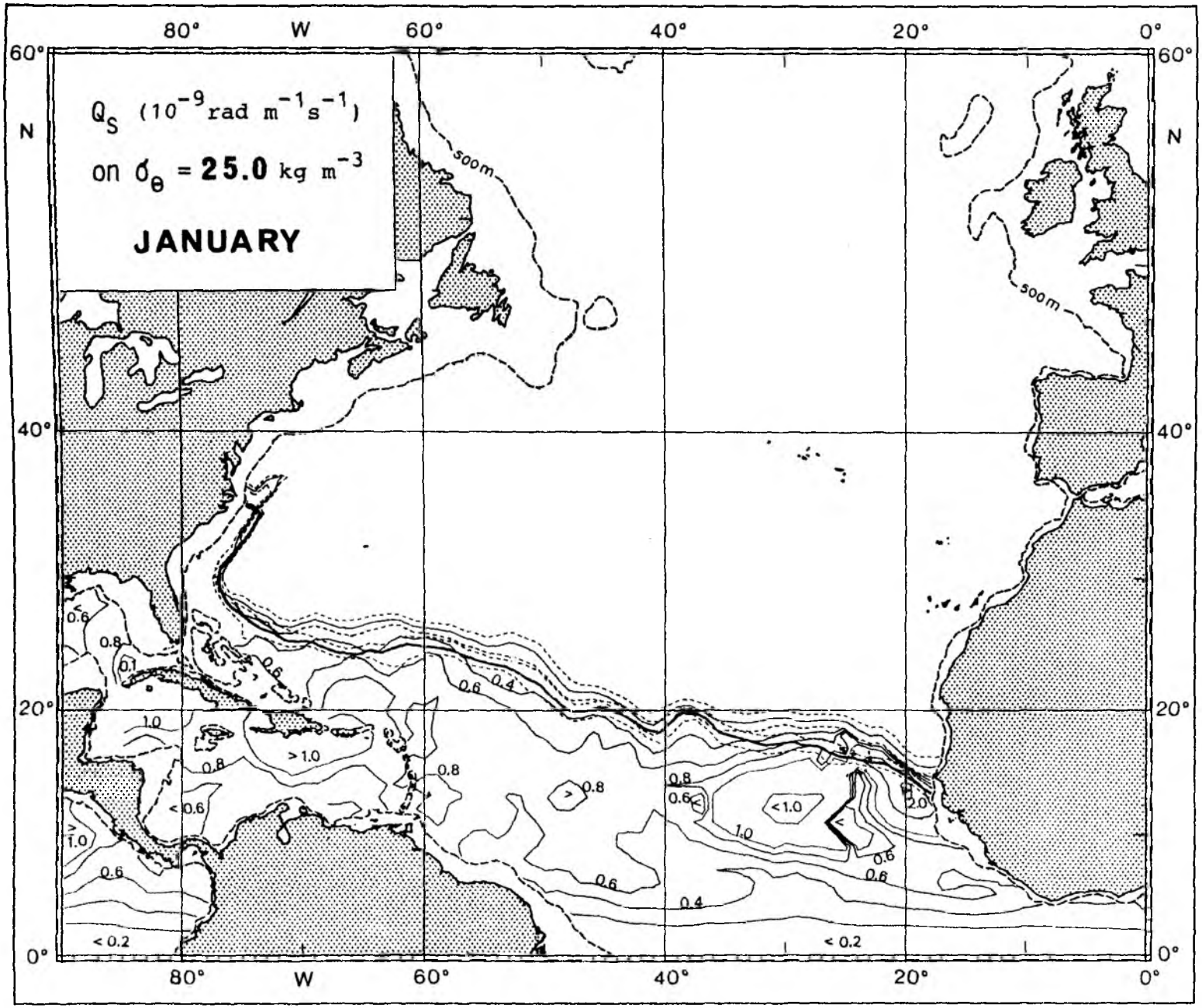
Q_S (10^{-9} rad $m^{-1}s^{-1}$)
on σ_θ = 25.0 kg m^{-3}
JANUARY
80° W
60°
40°
20°
0°
60° N
40°
20°
0°
500m
500m
0.6
0.8
0.1
0.6
0.4
0.6
1.0
0.8
> 1.0
0.8
0.8
< 0.6
> 1.0
0.6
0.8
0.6
< 1.0
2.0
1.0
0.6
0.6
0.6
0.4
< 0.2
< 0.2

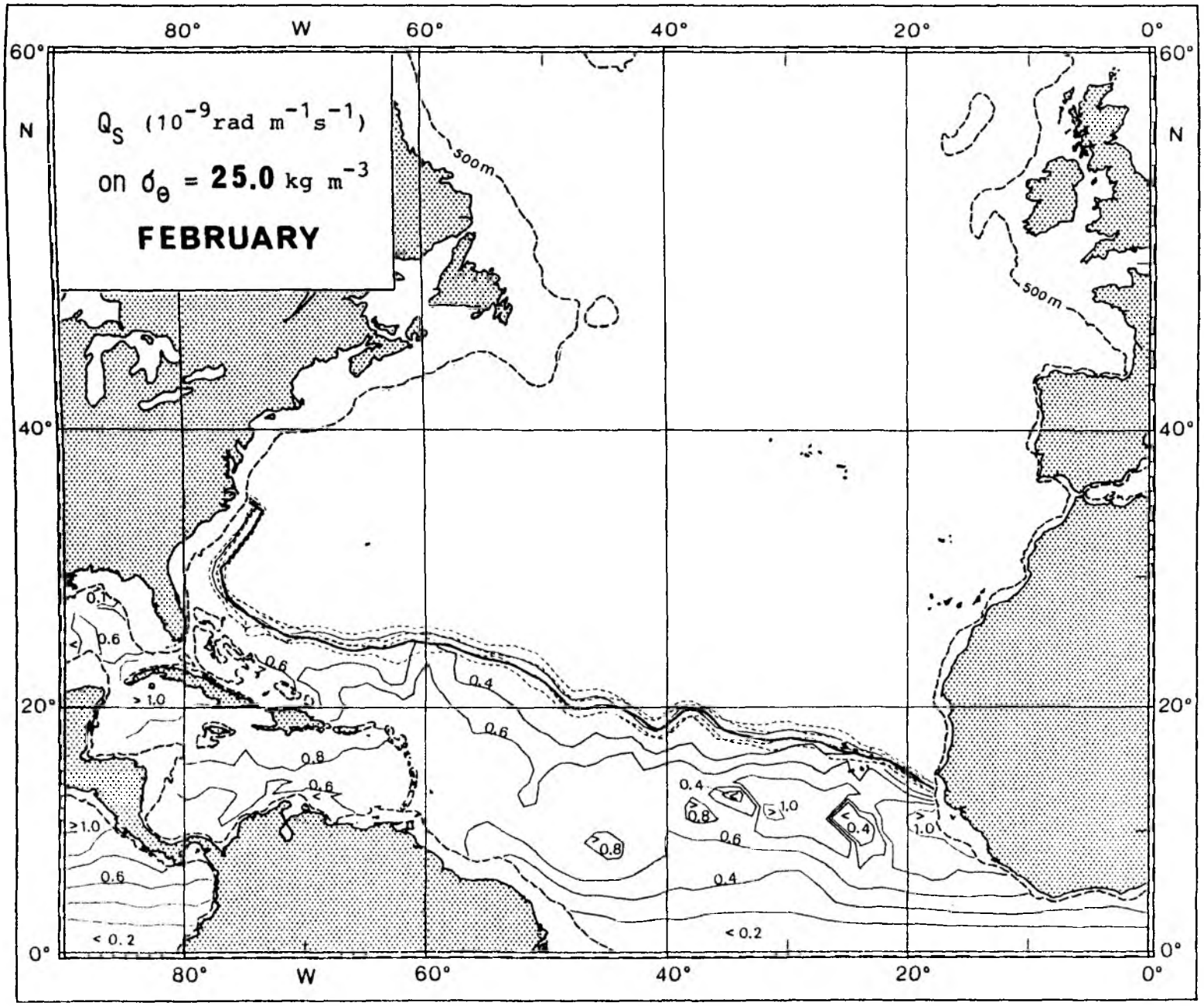
Q_S (10^{-9}rad $m^{-1}s^{-1}$)
on σ_θ = 25.0 kg m^{-3}
FEBRUARY
500m
500m
80° W
60°
40°
20°
0°
60° N
40°
20°
0°
0.1
0.6
0.6
0.4
> 1.0
0.6
0.8
0.6
≥1.0
0.6
< 0.2
0.4
< 0.8
≥ 1.0
< 0.4
≥ 1.0
0.6
0.4
< 0.2

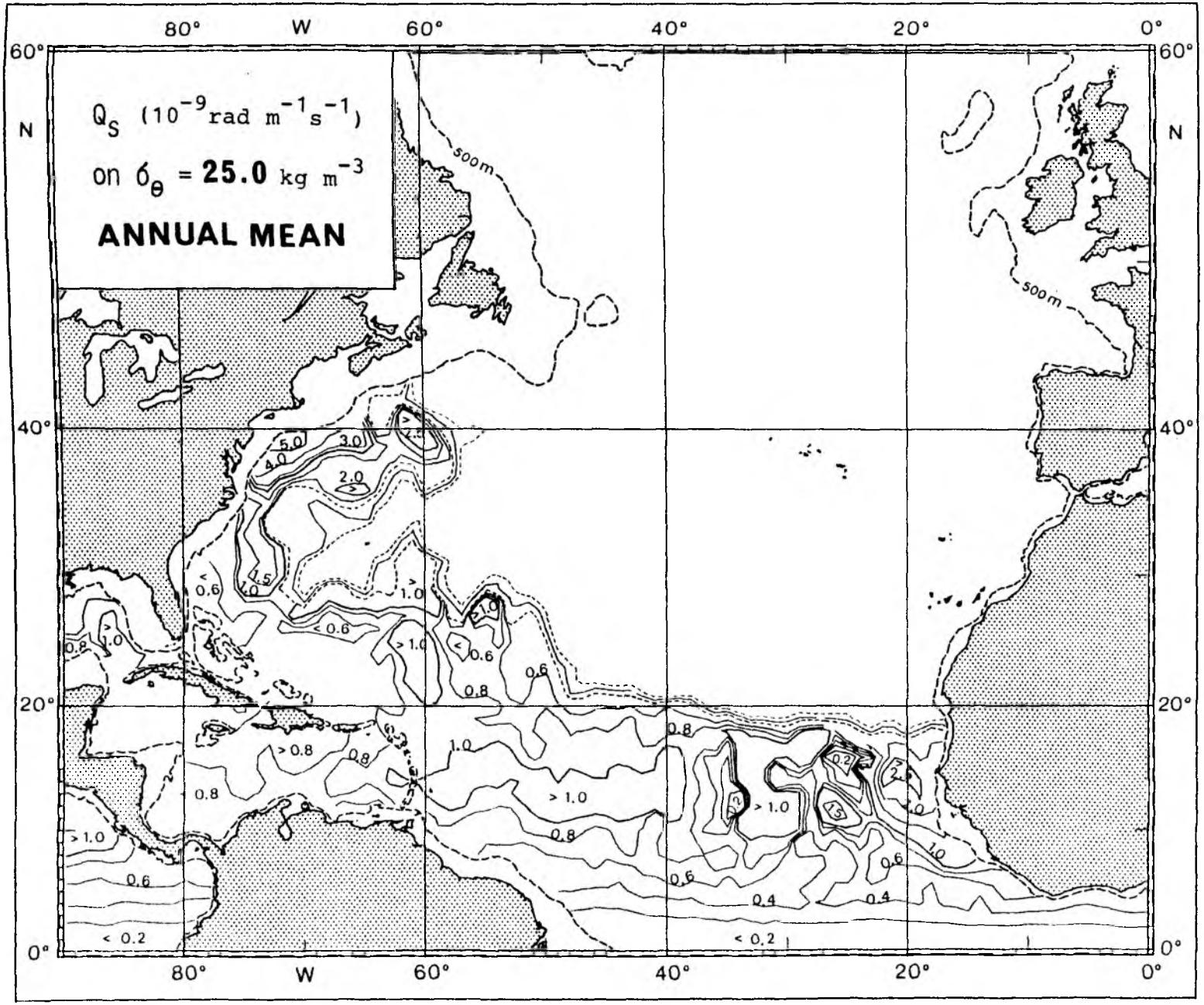
Q_S (10^{-9} rad m^{-1} s^{-1})
on σ_θ = 25.0 kg m^{-3}
ANNUAL MEAN
80° W
60°
40°
20°
0°
60° N
40°
20°
0°
500m
500m
5.0
4.0
3.0
2.0
1.5
1.0
0.8
0.6
0.4
0.2
< 0.6
> 1.0
> 0.8
< 0.2

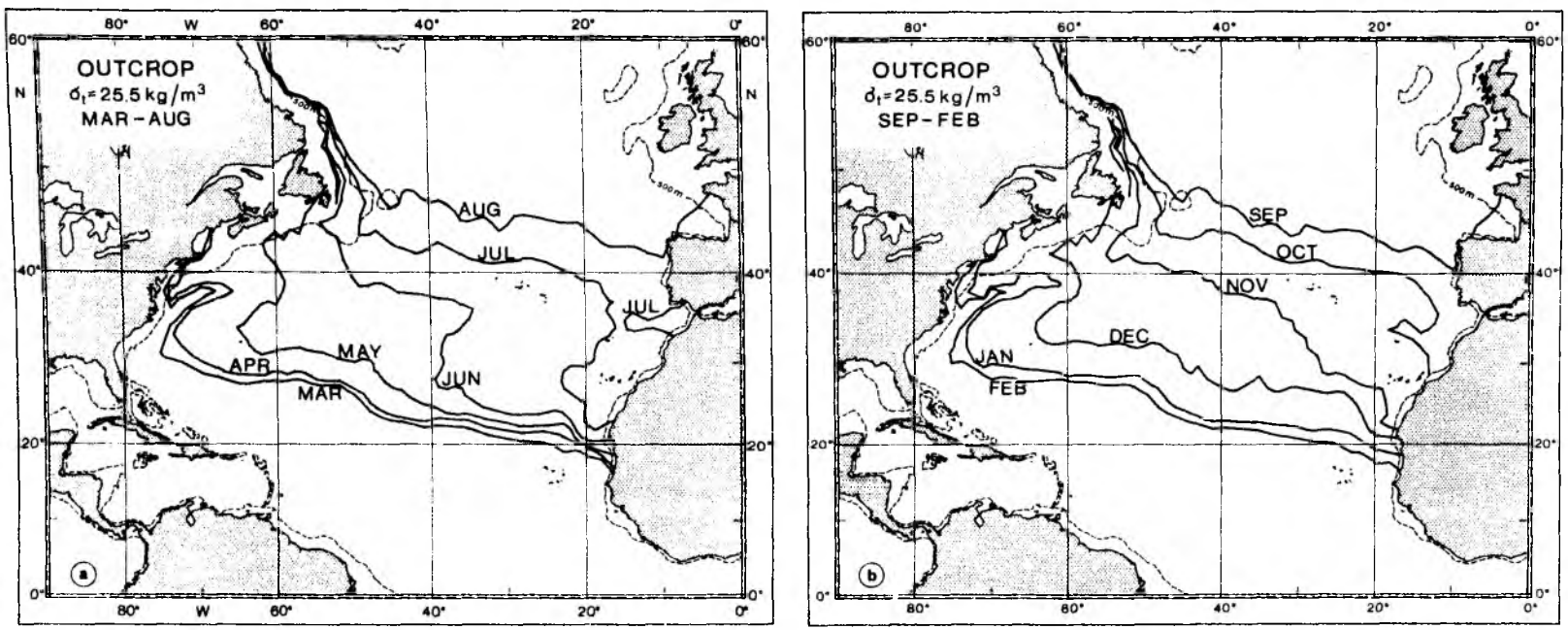

Seasonal migration of the outcrop of the isopycnal surface with σ_θ = 25.5 kg m^{-3}; (a) heating season, (b) cooling season.

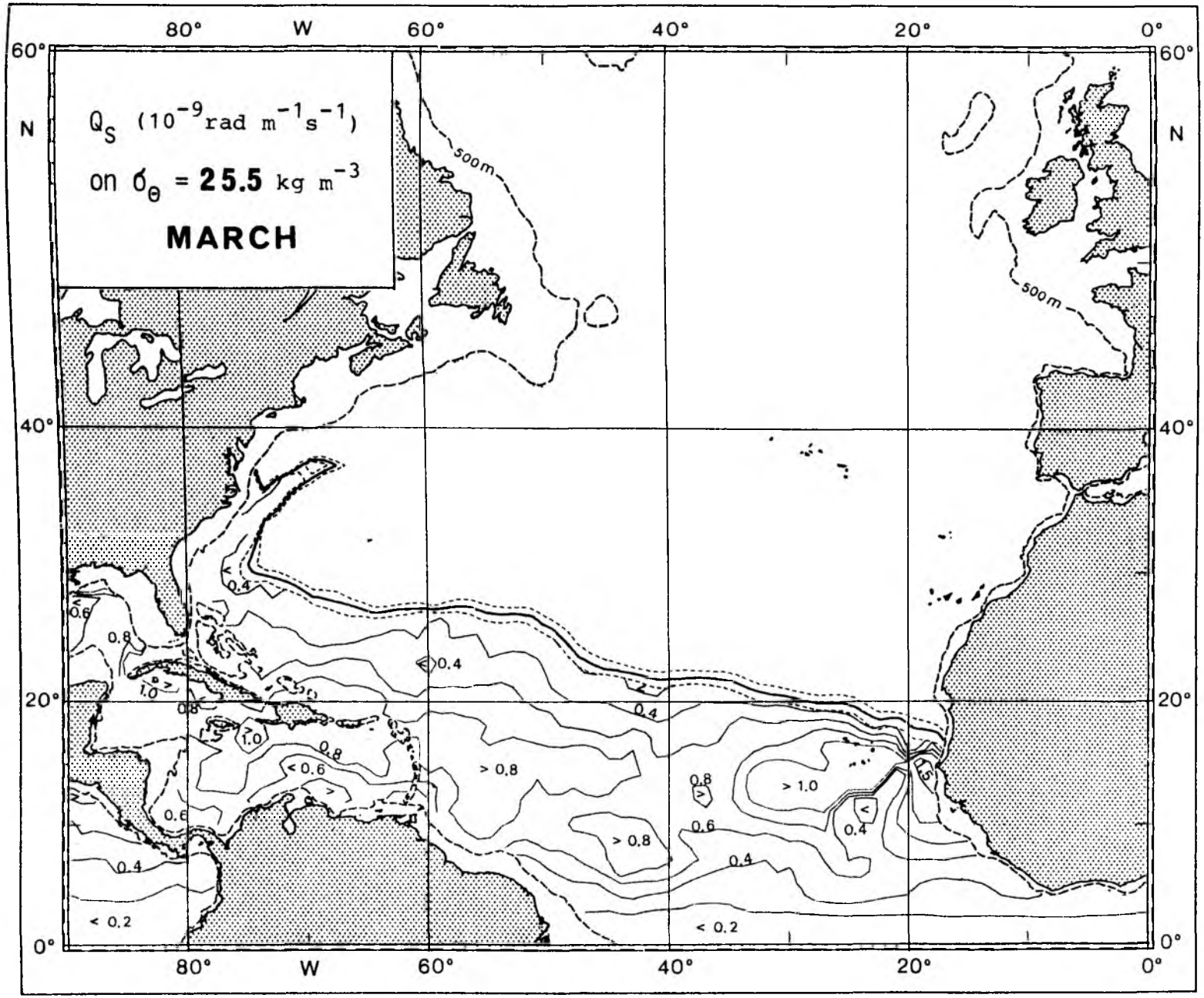
Q_S (10^{-9} rad $m^{-1}s^{-1}$)
on σ_θ = 25.5 kg m^{-3}
MARCH
80° W 60° 40° 20° 0°
60° N
40°
20°
0°
500m
500m
< 0.4
0.4
0.6
0.8
1.0
< 0.6
> 0.8
> 1.0
< 0.2

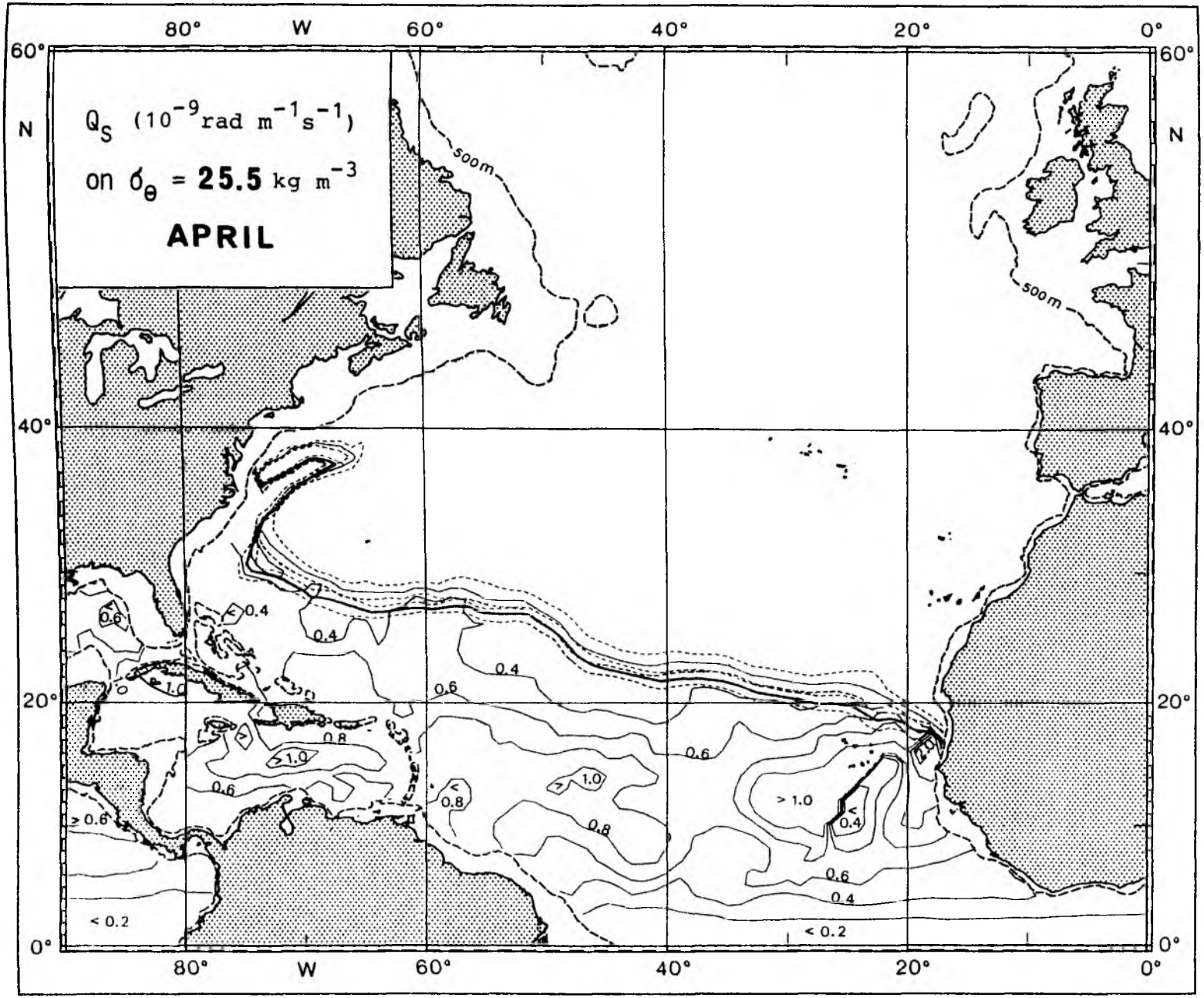
Q_S (10^{-9}rad $m^{-1}s^{-1}$)
on σ_θ = 25.5 kg m^{-3}
APRIL
80° W
60°
40°
20°
0°
60° N
40°
20°
0°
500m
500m
< 0.4
0.4
0.6
0.8
> 1.0
> 0.6
< 0.2

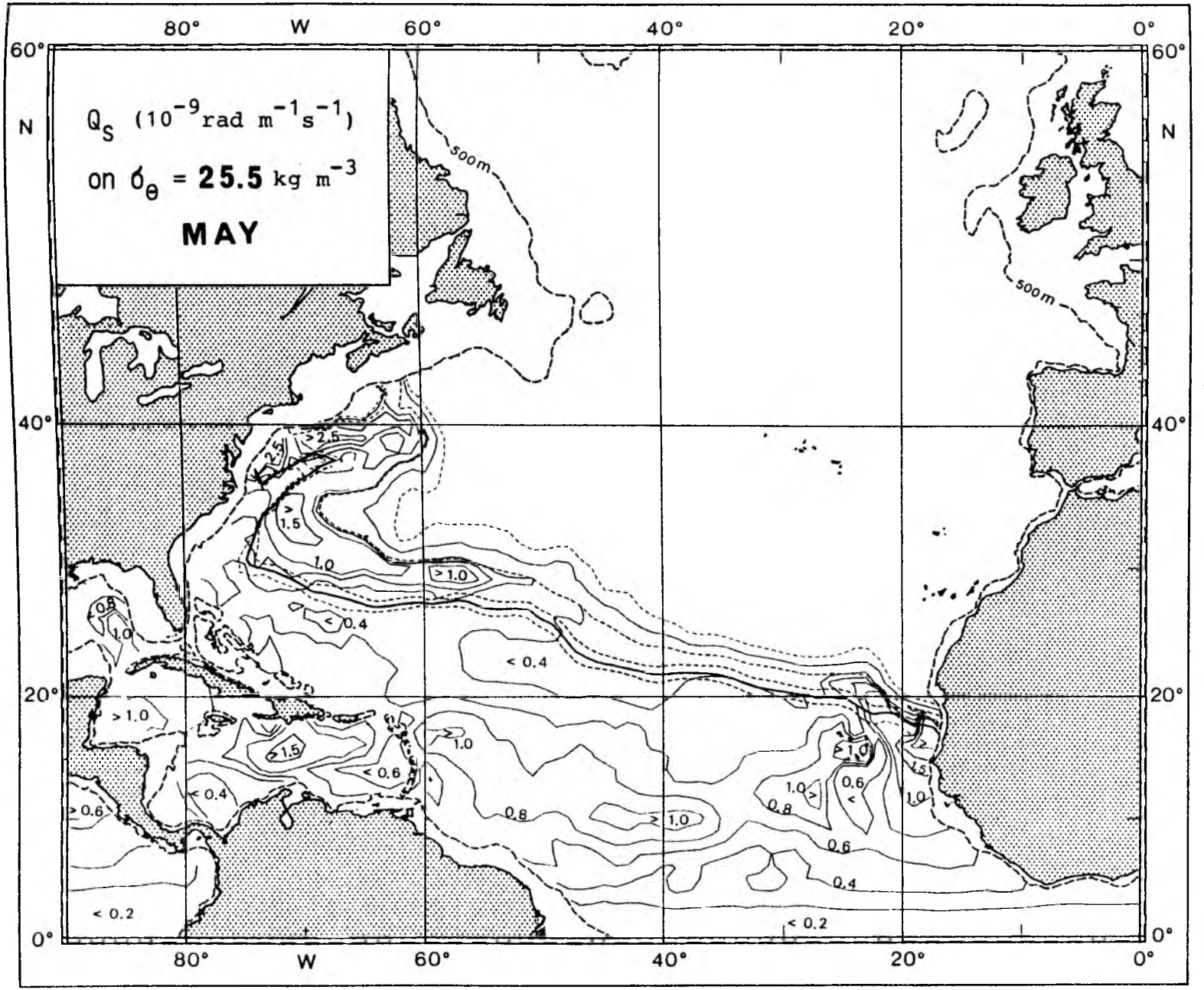
Q_S (10^{-9} rad $m^{-1}s^{-1}$)
on σ_θ = 25.5 kg m^{-3}
MAY
80° W
60°
40°
20°
0°
60° N
40°
20°
0°
500m
500m
> 2.5
2.5
> 1.5
1.5
1.0
> 1.0
< 0.4
< 0.4
0.8
1.0
> 1.0
> 1.5
1.0
< 0.6
< 0.4
> 0.6
0.8
> 1.0
1.0
> 1.0
1.5
0.6
1.0
0.8
0.6
0.4
< 0.2
< 0.2

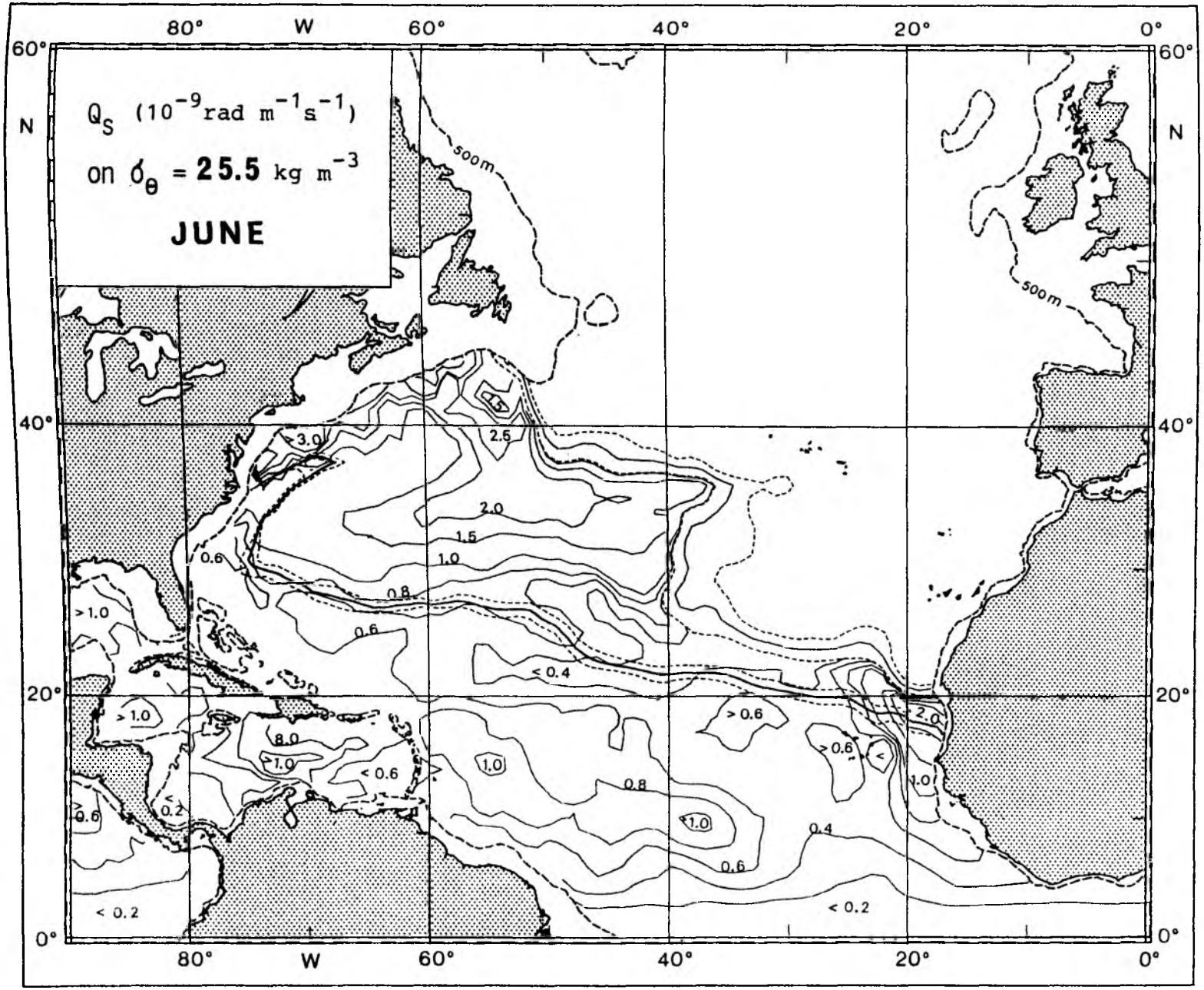
Q_S (10^{-9}rad $m^{-1}s^{-1}$)
on σ_θ = 25.5 kg m^{-3}
JUNE
80° W
60°
40°
20°
0°
60° N
40°
20°
0°
500m
500m
> 3.0
2.5
2.0
1.5
1.0
0.8
0.6
> 1.0
< 0.4
> 0.6
< 0.6
< 0.2

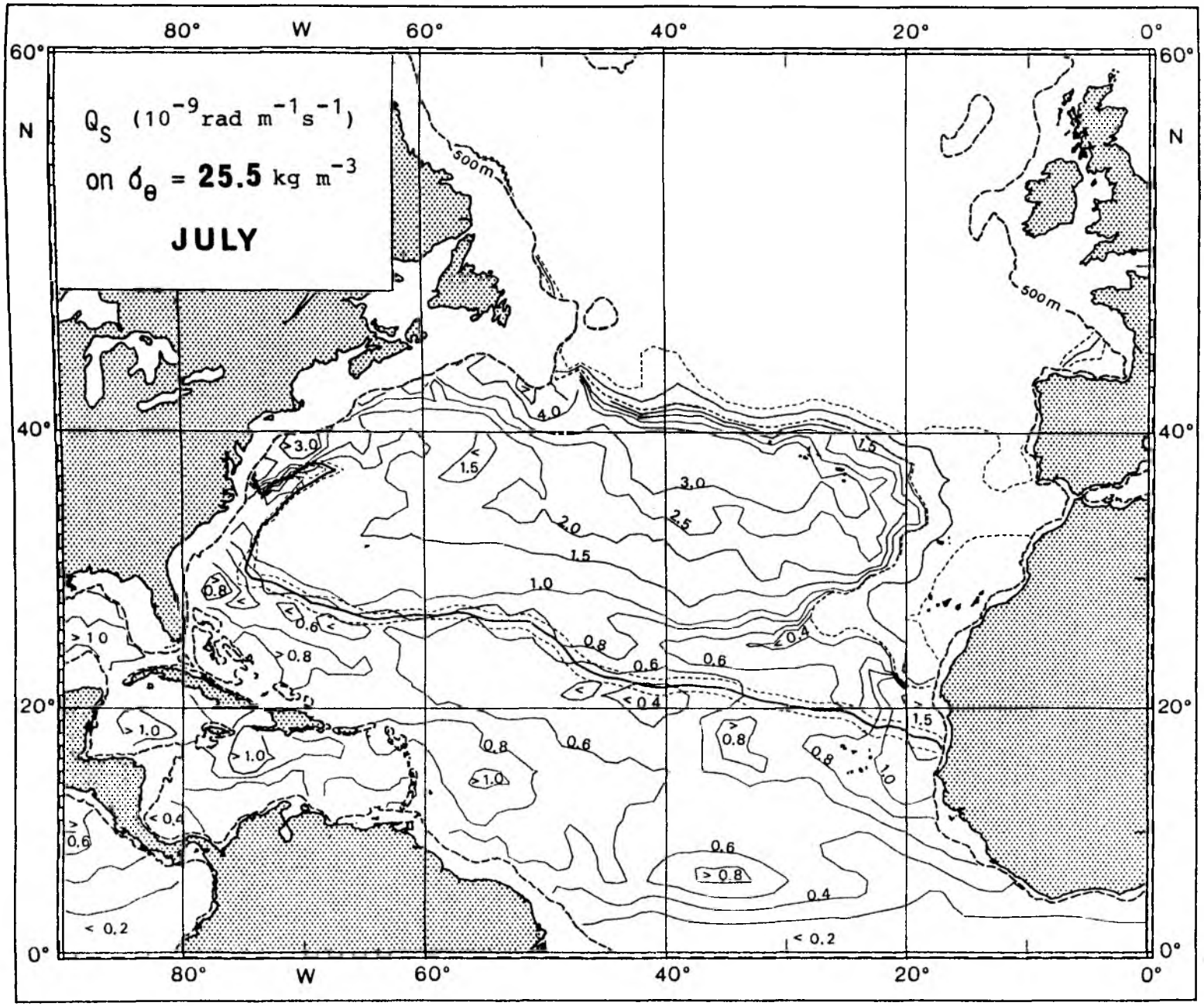
Q_S (10^{-9} rad $m^{-1}s^{-1}$)
on σ_θ = 25.5 kg m^{-3}
JULY
80° W
60°
40°
20°
0°
60° N
40°
20°
0°
500m
500m
4.0
3.0
2.5
2.0
1.5
1.0
0.8
0.6
0.4
0.2
< 1.5
< 0.8
< 0.6
< 0.4
> 1.0
> 0.8

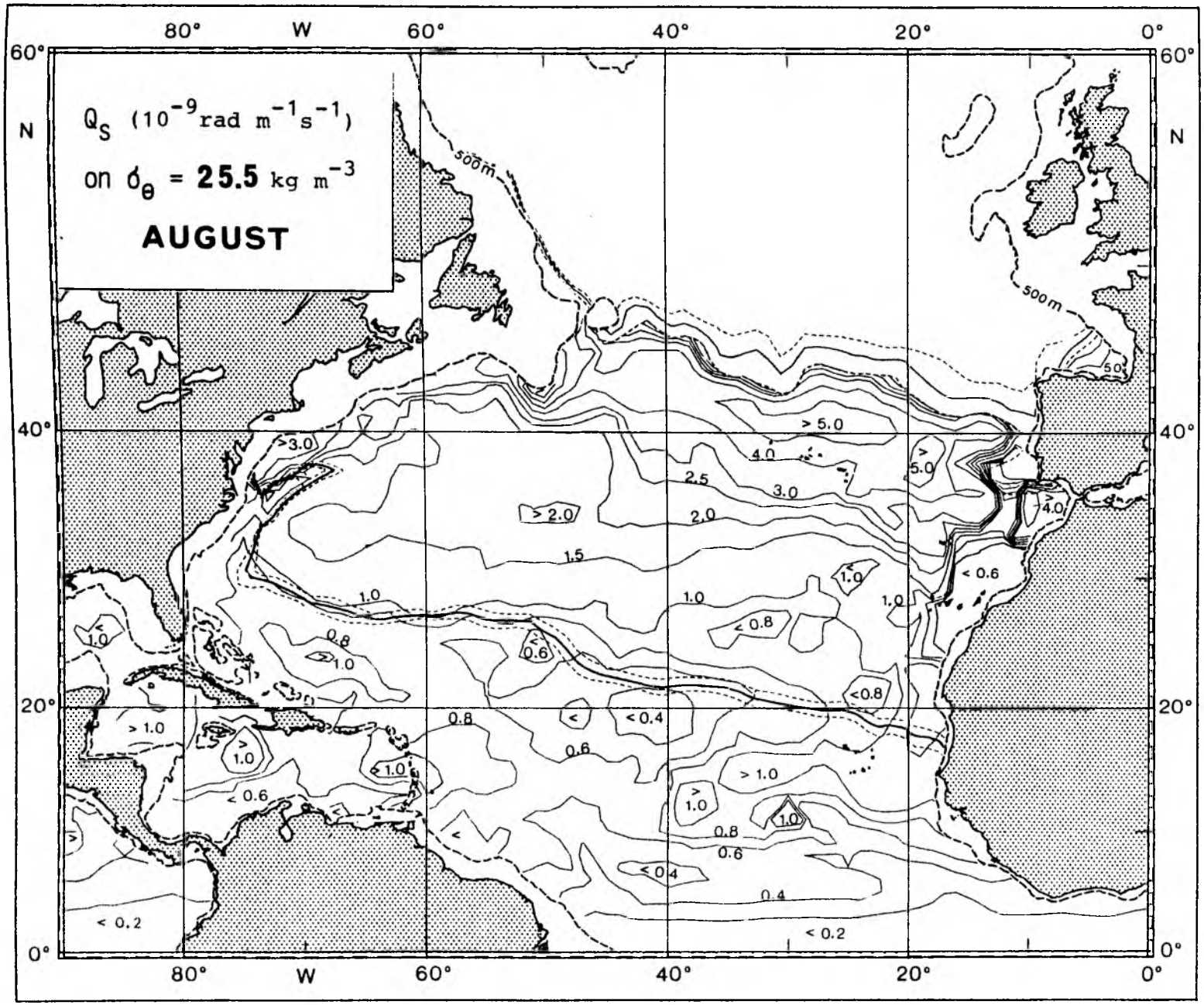
Q_S (10^{-9} rad $m^{-1}s^{-1}$)
on σ_θ = **25.5** kg m^{-3}
AUGUST
80° W
60°
40°
20°
0°
60° N
40°
20°
0°
500m
500m
50
> 5.0
4.0
2.5
3.0
2.0
1.5
1.0
0.8
0.6
0.4
0.2
> 3.0
> 2.0
> 1.0
< 1.0
< 0.8
< 0.6
< 0.4
< 0.2

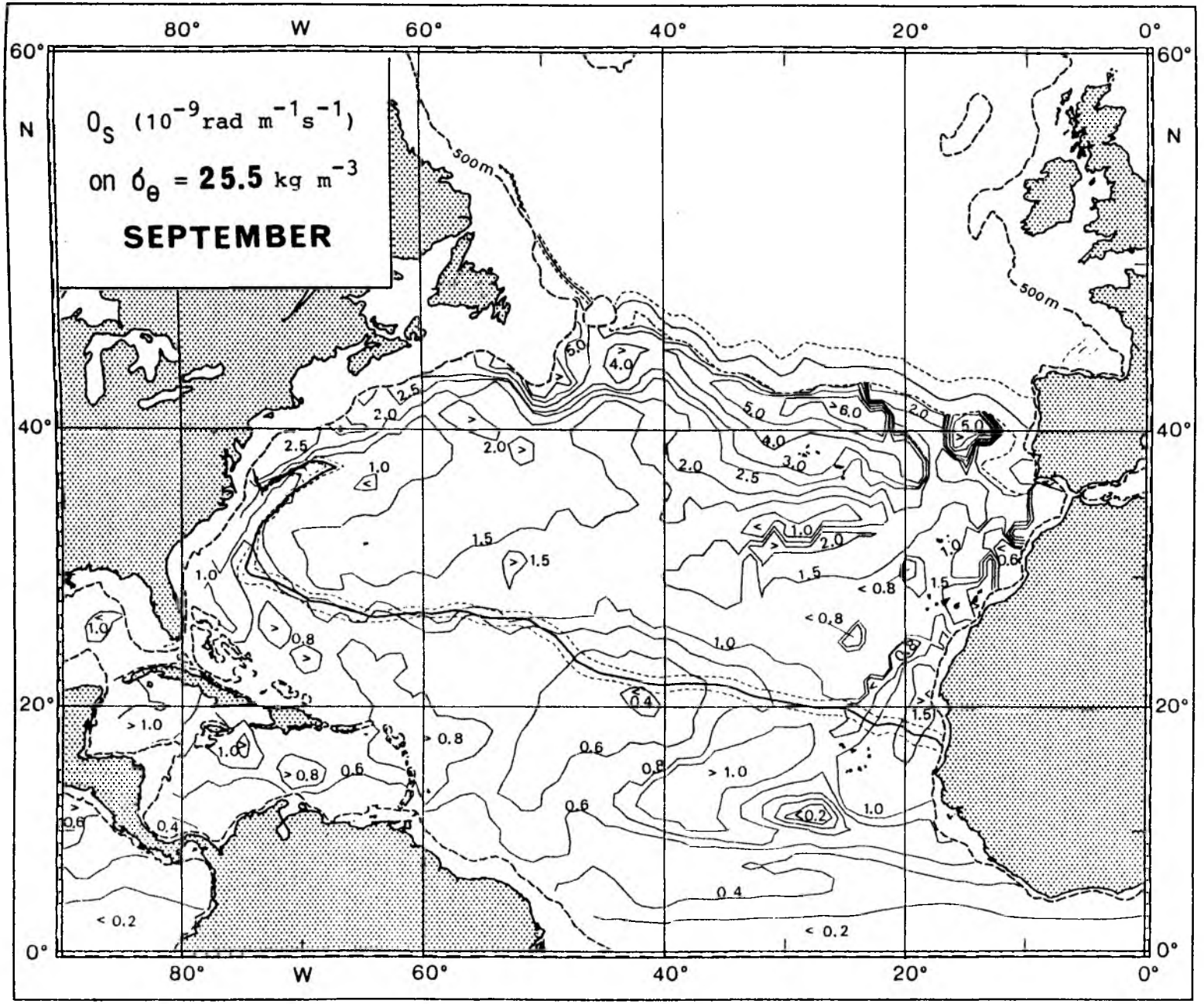
O_S (10^{-9}rad $m^{-1}s^{-1}$)
on σ_θ = 25.5 kg m^{-3}
SEPTEMBER
80° W
60°
40°
20°
0°
60° N
40°
20°
0°
500m
500m

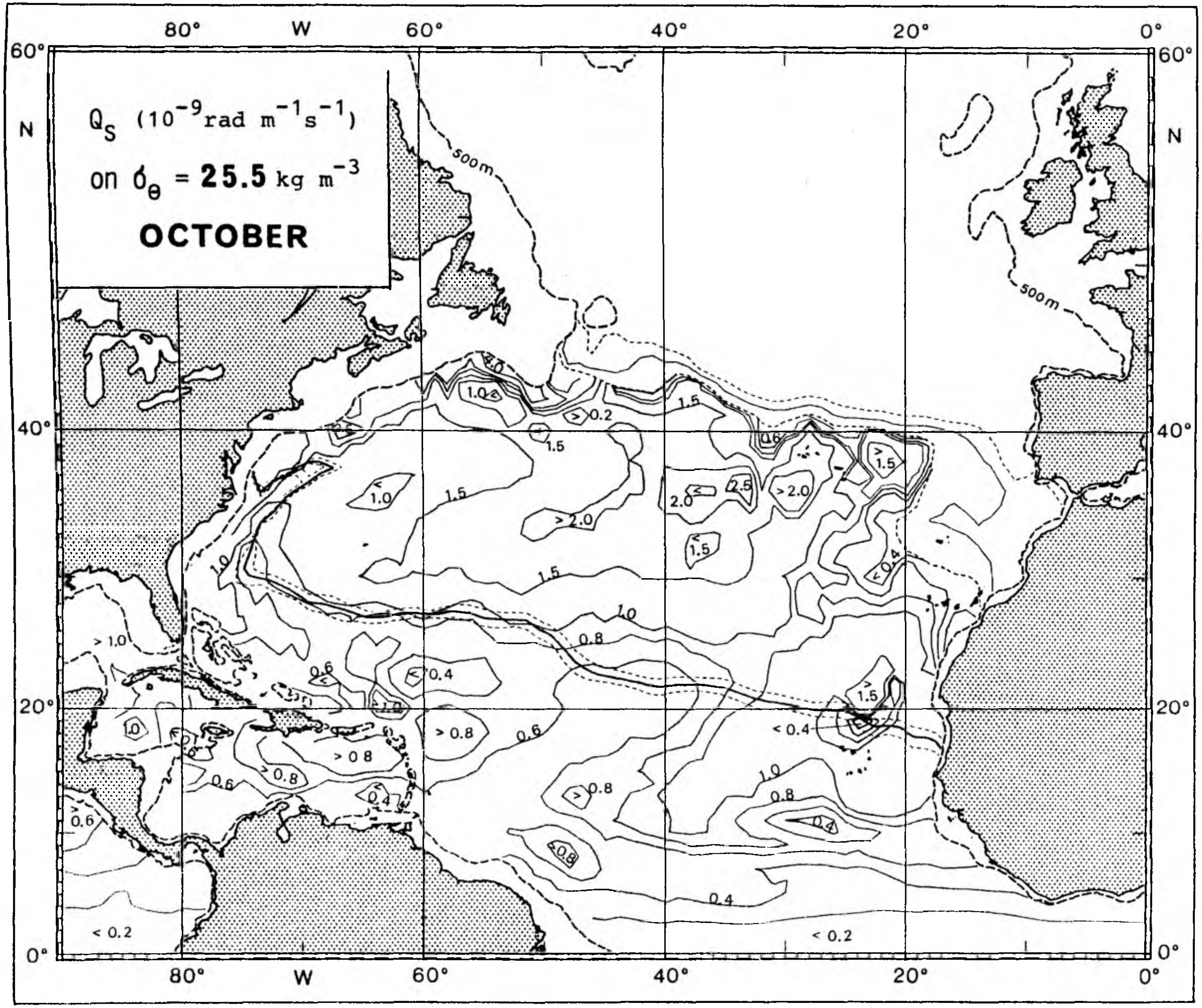
Q_S $(10^{-9}$ rad $m^{-1}s^{-1})$
on σ_θ = **25.5** kg m^{-3}
OCTOBER
80°
W
60°
40°
20°
0°
60°
40°
20°
N
500m
500m
2.0
1.0
1.5
0.2
0.6
2.5
> 2.0
> 2.0
1.0
1.5
0.4
1.0
0.8
> 1.0
0.6
< 0.4
1.0
> 0.8
0.6
> 0.8
0.8
< 0.4
0.6
0.4
0.8
0.8
0.4
0.6
0.4
< 0.2
< 0.2

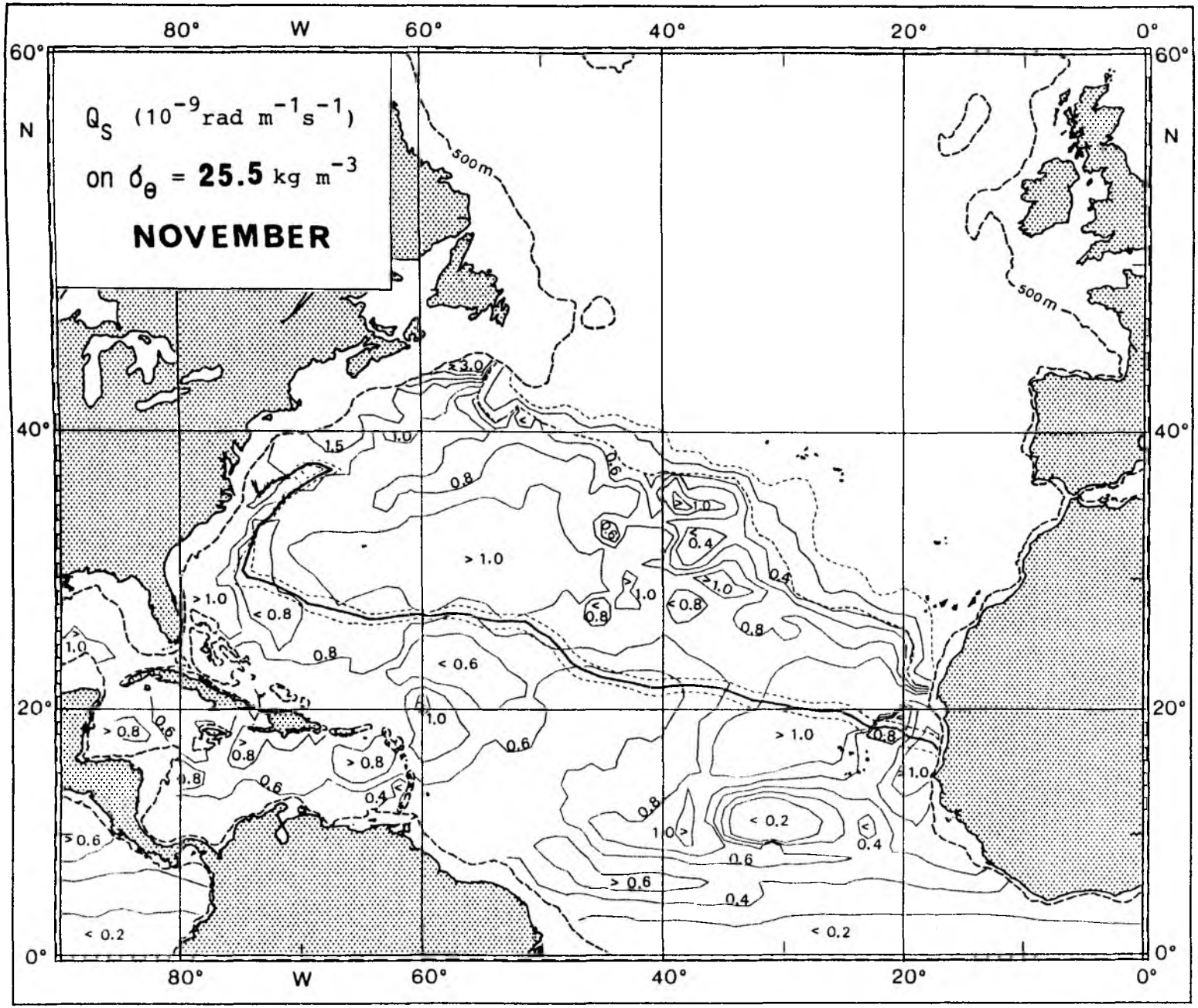
Q_S (10^{-9} rad $m^{-1}s^{-1}$)
on σ_θ = 25.5 kg m^{-3}
NOVEMBER
80° W
60°
40°
20°
0°
60° N
40°
20°
0°
500m
500m
> 3.0
1.5
1.0
0.8
0.6
0.4
> 1.0
< 0.8
< 0.6
> 0.8
> 0.6
< 0.2

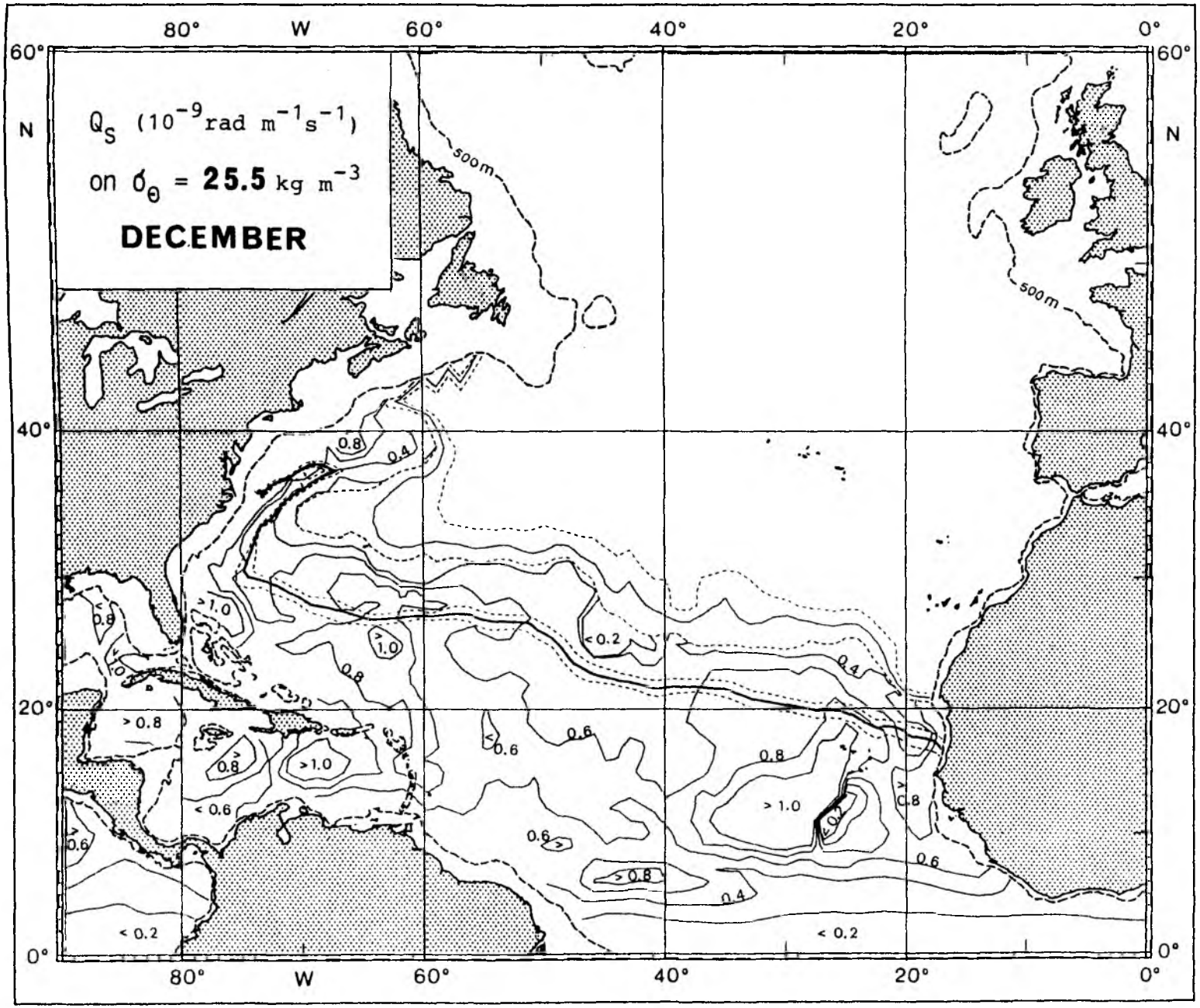
Q_S (10^{-9}rad $m^{-1}s^{-1}$)
on σ_θ = 25.5 kg m^{-3}
DECEMBER
80° W
60°
40°
20°
0°
60° N
40°
20°
0°
500m
500m
0.8
0.4
< 0.8
> 1.0
< 1.0
> 1.0
< 0.2
0.4
> 0.8
0.8
> 1.0
< 0.6
0.6
0.6
0.8
> 1.0
< 0.6
0.6
> 0.8
0.4
0.6
< 0.2
< 0.2

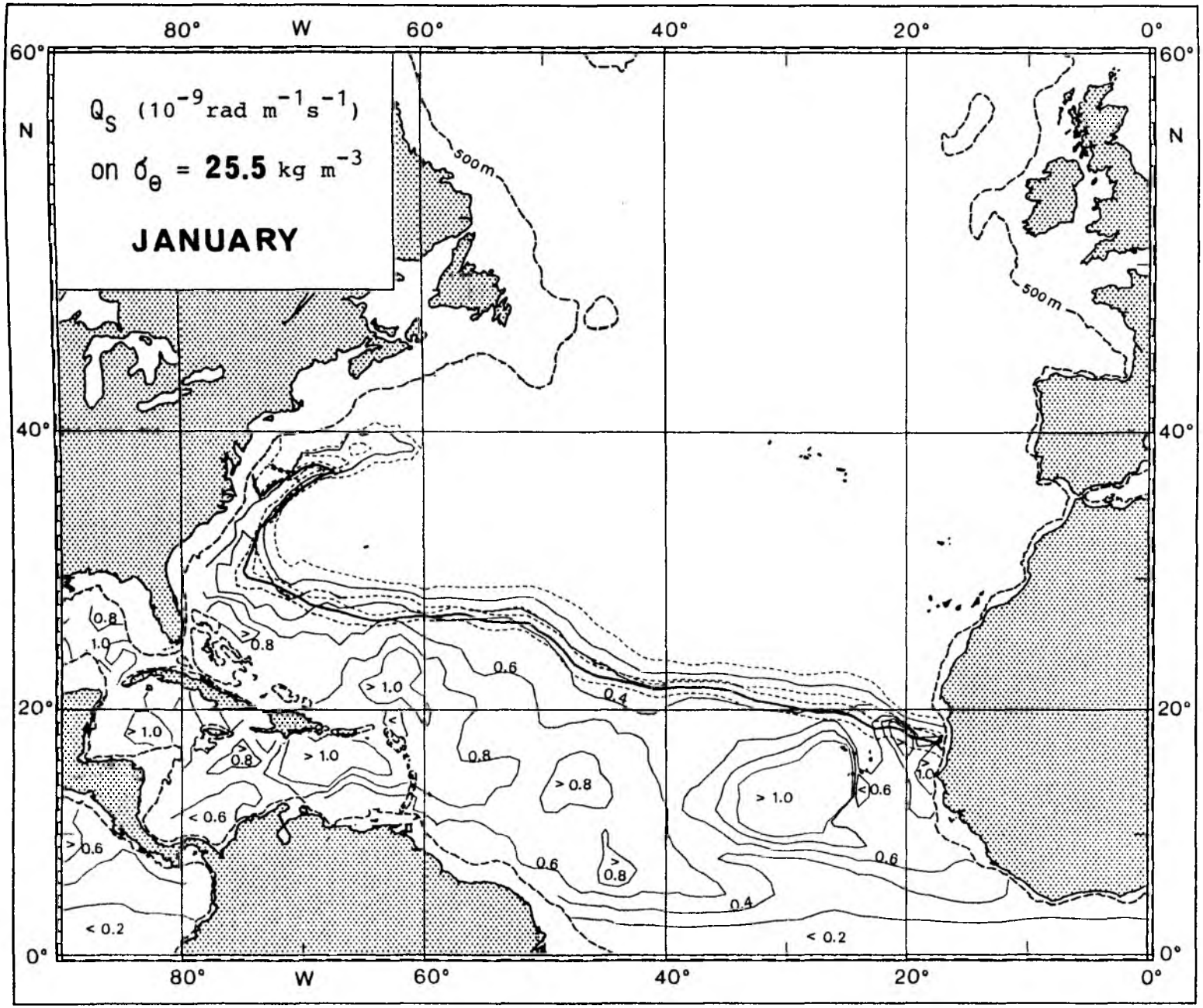
Q_S (10^{-9} rad $m^{-1}s^{-1}$)
on σ_θ = 25.5 kg m^{-3}
JANUARY
80° W
60°
40°
20°
0°
60° N
40°
20°
0°
500m
500m
0.8
1.0
0.8
0.6
0.4
> 1.0
> 1.0
0.8
0.8
> 0.8
> 1.0
< 0.6
> 1.0
< 0.6
1.0
< 0.6
> 0.6
0.6
0.6
0.8
0.4
< 0.2
< 0.2

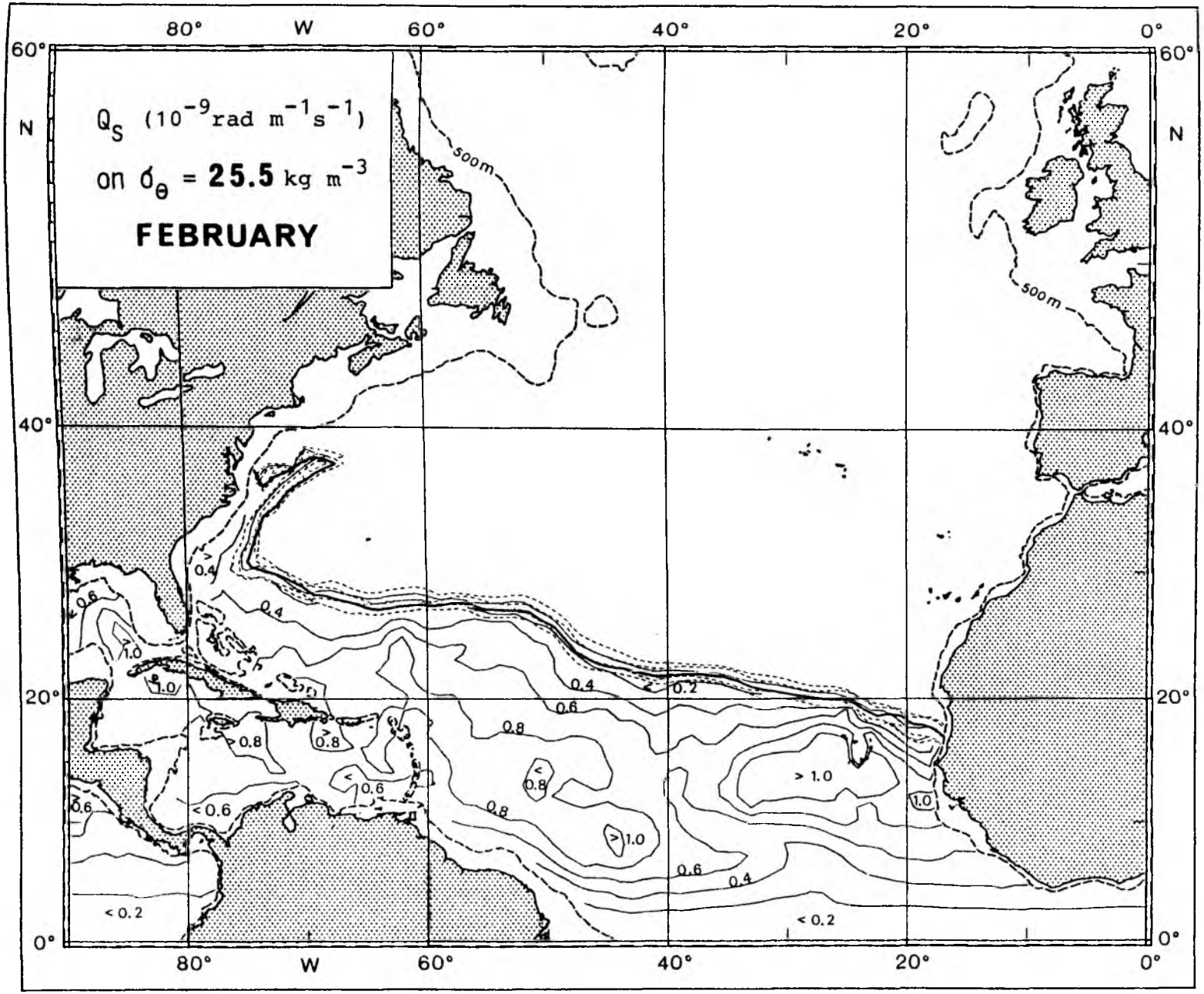
Q_S (10^{-9}rad $m^{-1}s^{-1}$)
on σ_θ = 25.5 kg m^{-3}
FEBRUARY
80° W
60°
40°
20°
0°
60° N
40°
20°
0°
500m
500m
0.4
0.6
1.0
0.8
0.2
> 1.0
< 0.6
< 0.2
< 0.2

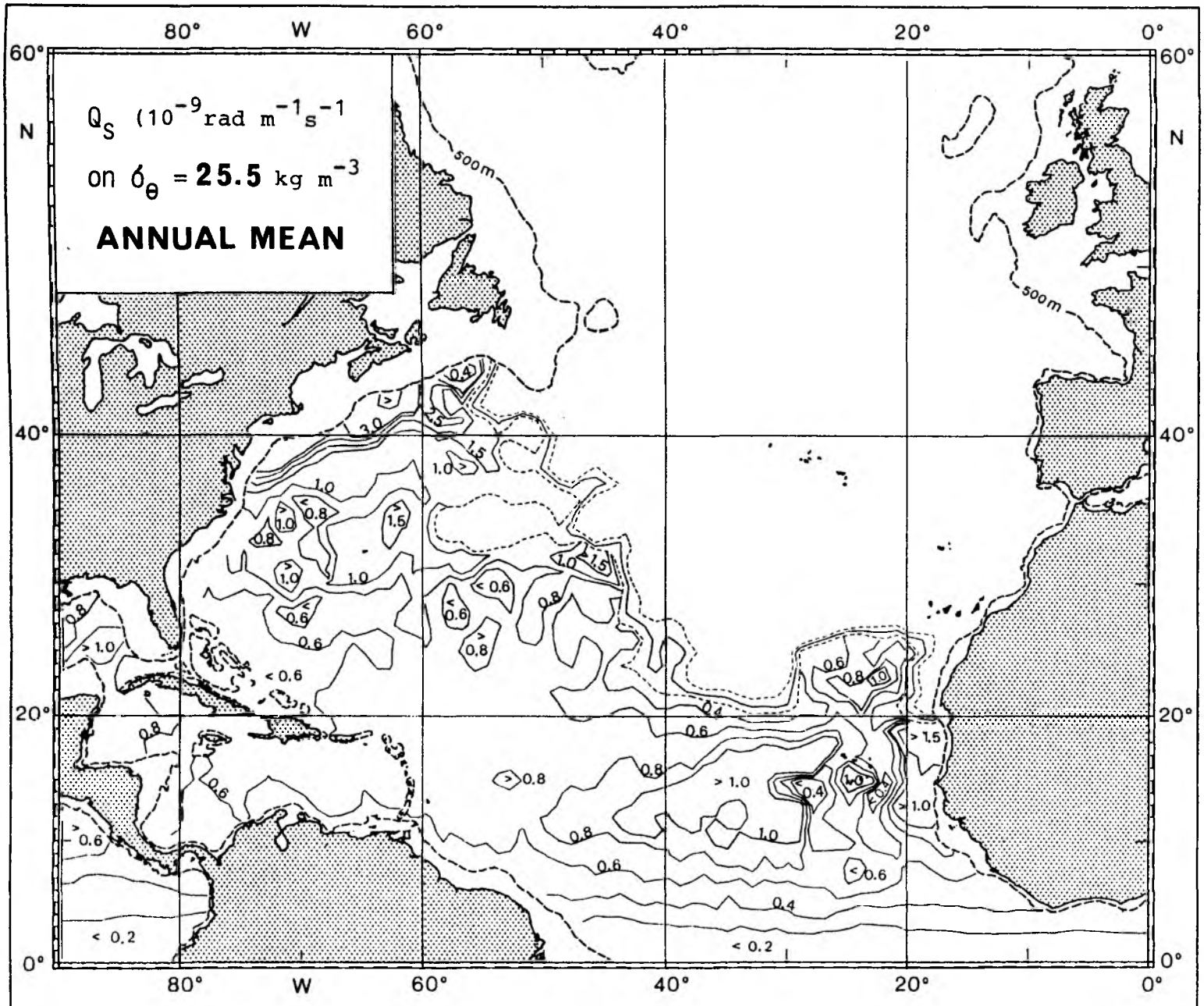
Q_S (10^{-9} rad $m^{-1}s^{-1}$
on σ_θ = 25.5 kg m^{-3}
ANNUAL MEAN
80° W 60° 40° 20° 0°
60° N
40°
20°
0°
500m
500m
< 0.2
< 0.2

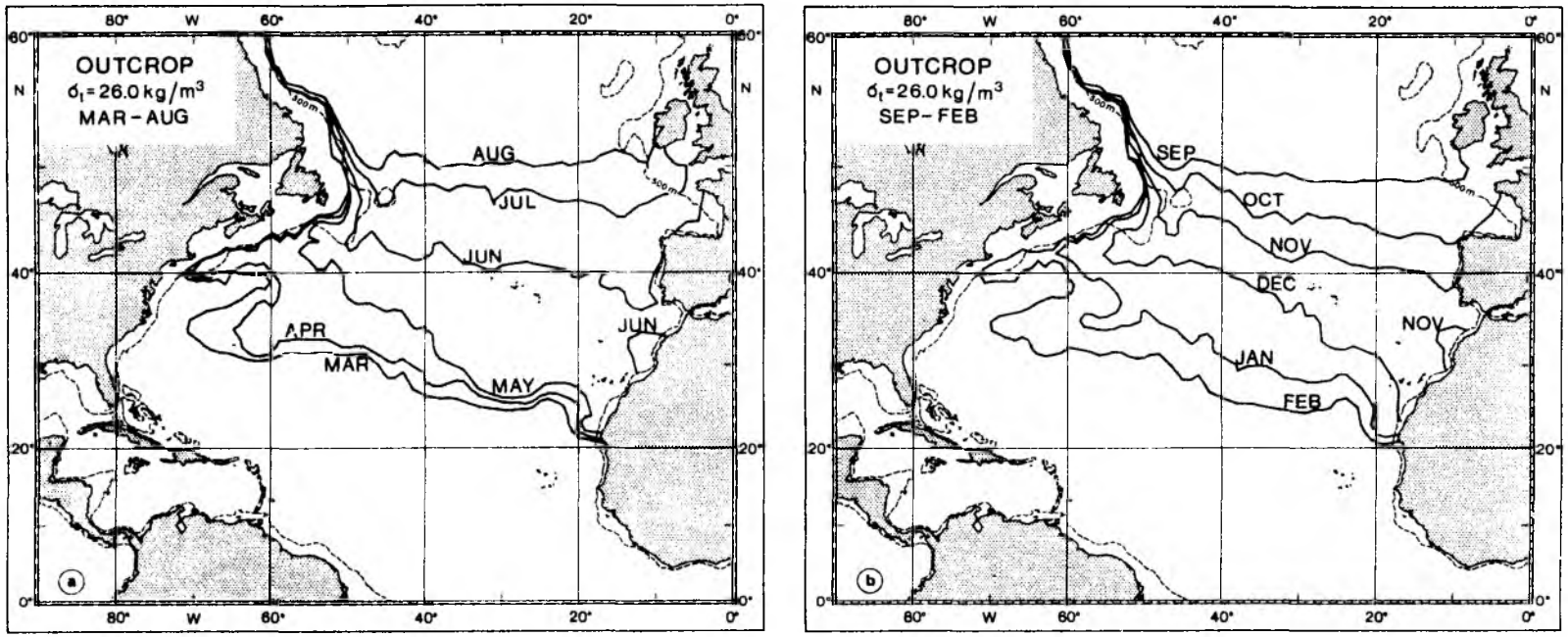

Seasonal migration of the outcrop of the isopycnal surface with σ_θ = 26.0 kg m^{-3};
(a) heating season, (b) cooling season.

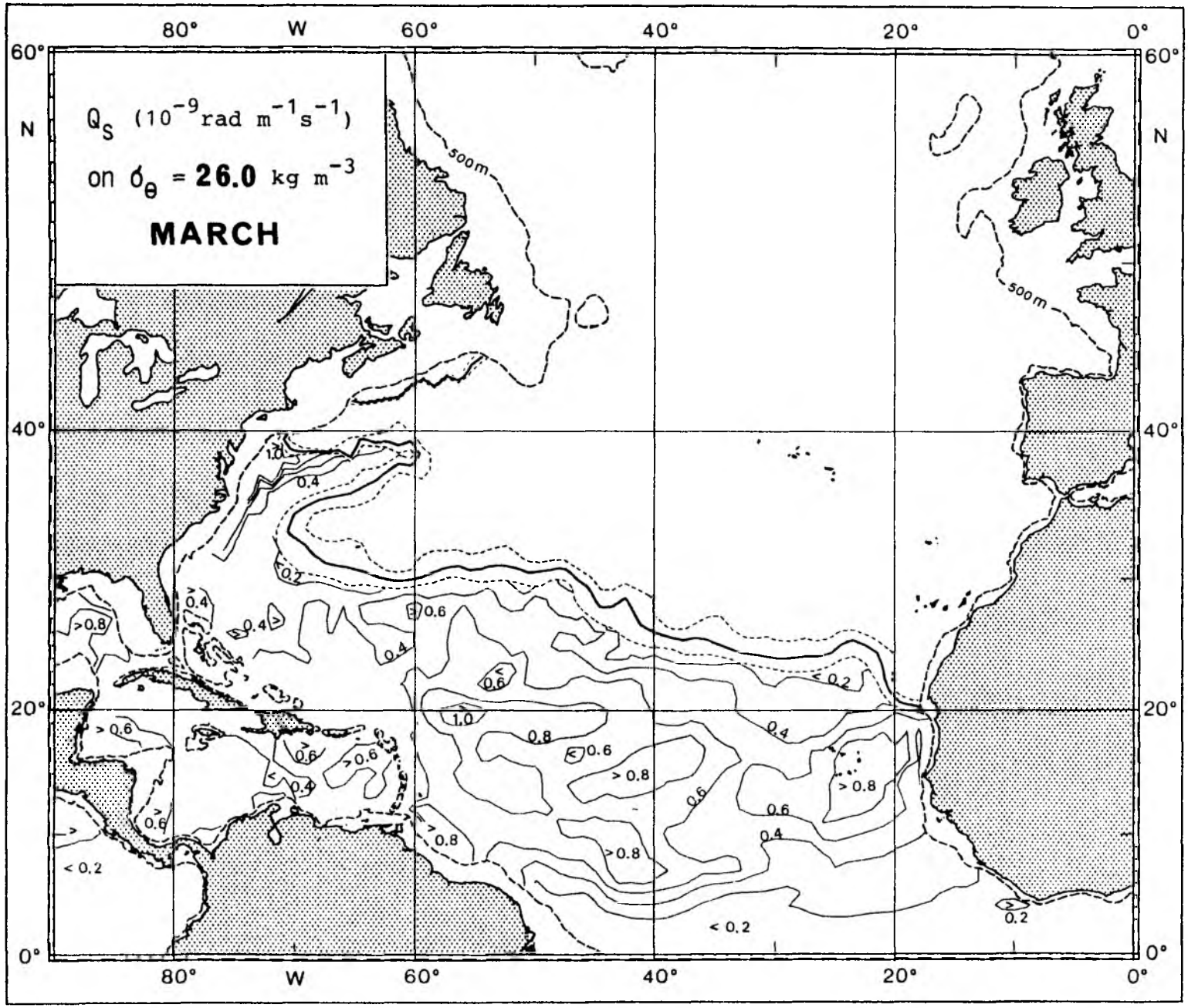
Q_S (10^{-9} rad $m^{-1}s^{-1}$)
on σ_θ = 26.0 kg m^{-3}
MARCH
80° W
60°
40°
20°
0°
60° N
40°
20°
0°
500m
500m
1.0
0.4
0.2
0.4
0.6
0.4
< 0.2
0.6
1.0
0.8
0.6
0.4
> 0.8
> 0.8
0.6
0.6
0.4
> 0.8
> 0.8
> 0.6
0.6
> 0.6
0.4
0.6
< 0.2
< 0.2
0.2

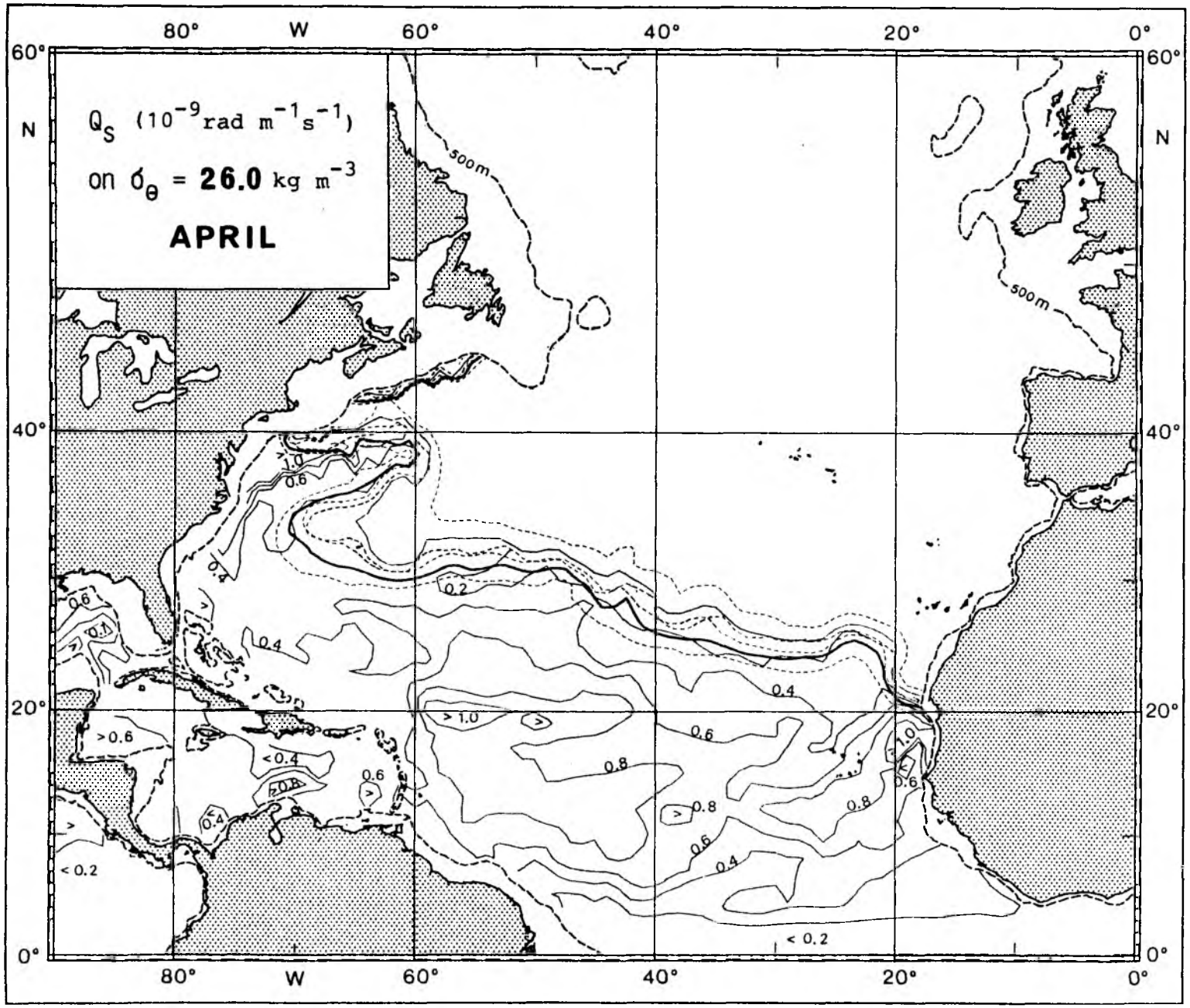
Q_S (10^{-9} rad $m^{-1}s^{-1}$)
on σ_θ = 26.0 kg m^{-3}
APRIL
80° W
60°
40°
20°
0°
60° N
40°
20°
0°
500m
500m
> 1.0
0.6
0.2
0.4
0.6
0.4
> 1.0
0.6
0.8
0.8
0.8
0.6
0.4
> 1.0
0.6
> 0.6
< 0.4
0.6
0.8
0.4
< 0.2
< 0.2

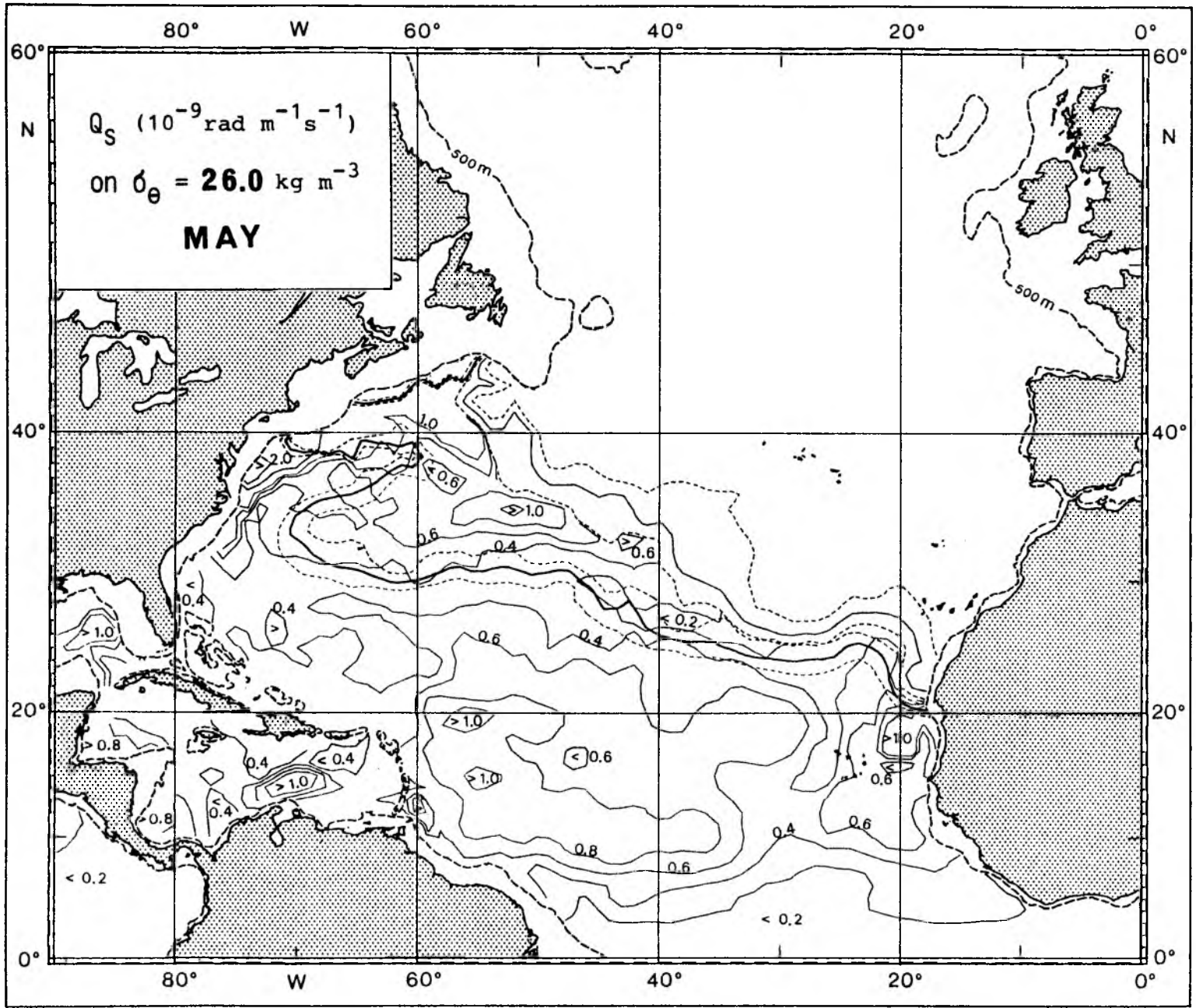
Q_S (10^{-9} rad $m^{-1}s^{-1}$)
on σ_θ = **26.0** kg m^{-3}
MAY
80° W
60°
40°
20°
0°
60° N
40°
20°
0°
500m
500m
1.0
2.0
< 0.6
> 1.0
> 0.6
0.6
0.4
< 0.4
> 0.4
> 1.0
< 0.2
0.6
0.4
> 1.0
> 0.8
0.4
< 0.4
> 1.0
< 0.6
> 1.0
> 1.0
0.6
< 0.8
0.4
0.8
0.4
0.6
0.6
< 0.2
< 0.2

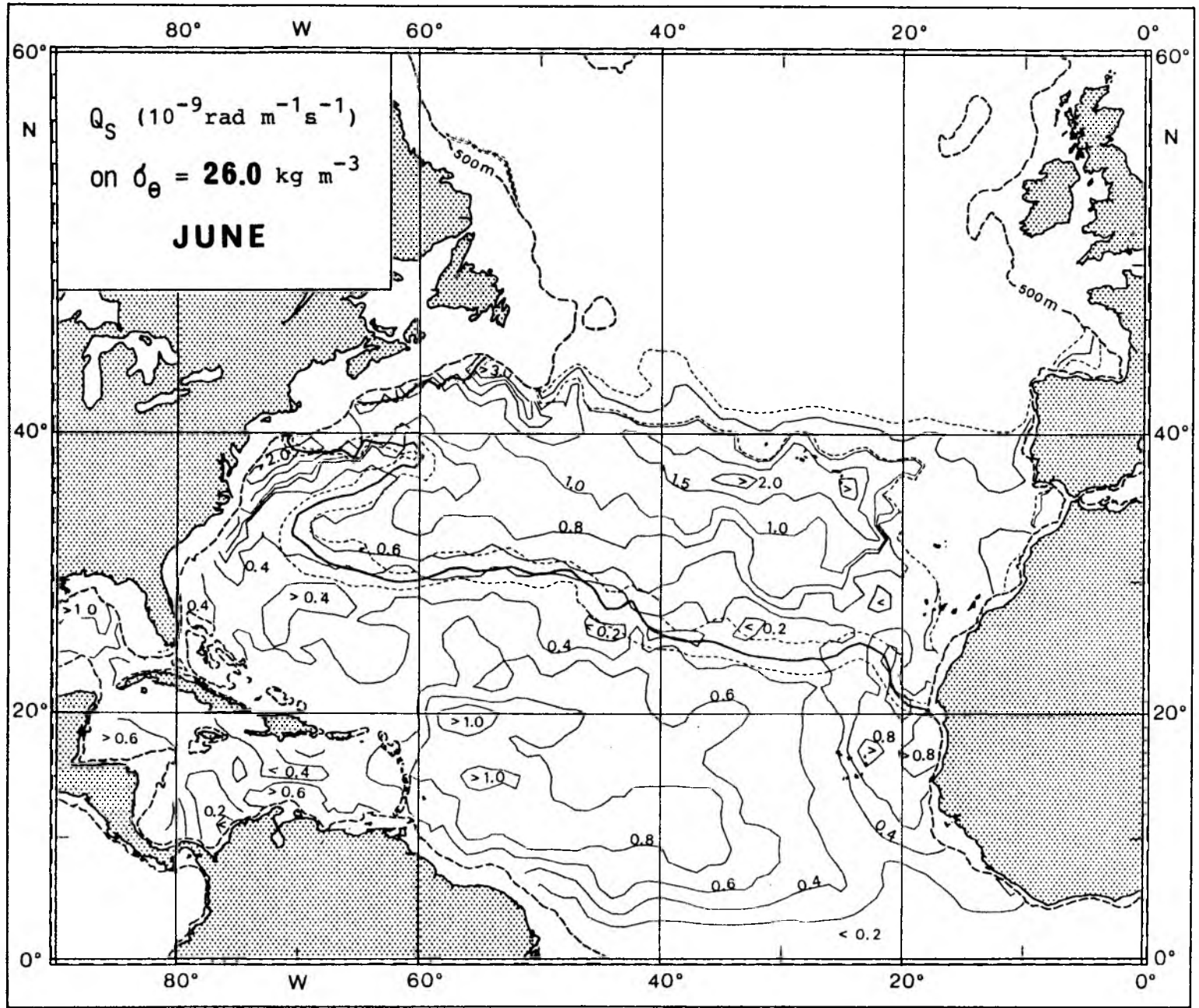
Q_S (10^{-9} rad $m^{-1}s^{-1}$)
on σ_θ = 26.0 kg m^{-3}
JUNE
80° W
60°
40°
20°
0°
60° N
40°
20°
0°
500m
500m
> 3.0
2.0
1.0
1.5
> 2.0
0.8
1.0
0.6
0.4
> 0.4
0.4
> 1.0
< 0.2
< 0.2
0.4
0.6
> 1.0
0.8
0.8
> 0.6
< 0.4
> 0.6
> 1.0
0.2
0.8
0.4
0.6
0.4
< 0.2

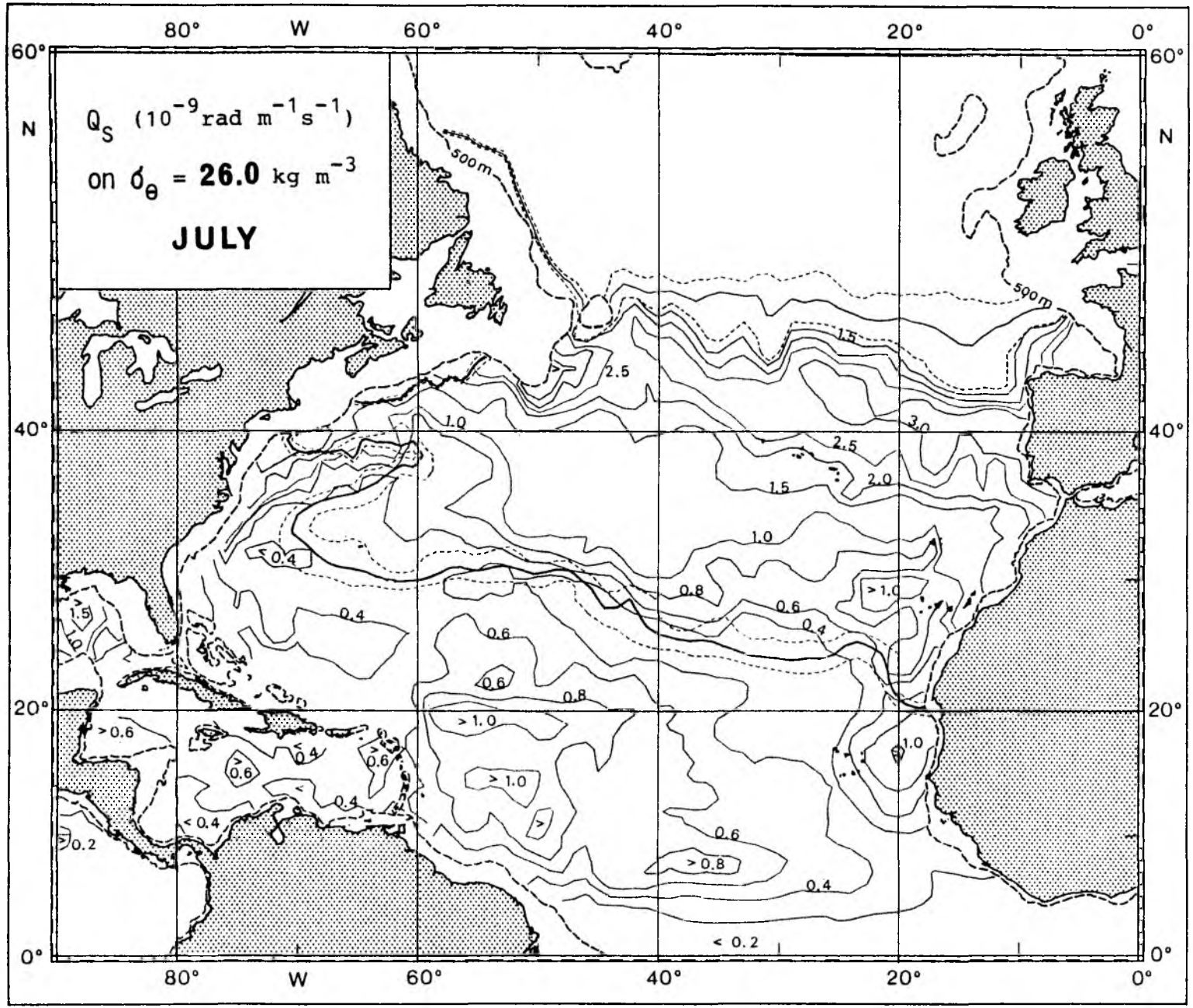
Q_S (10^{-9} rad m^{-1} s^{-1})
on σ_θ = 26.0 kg m^{-3}
JULY
80° W
60°
40°
20°
0°
60° N
40°
20°
0°
500m
500m
1.5
2.5
1.0
3.0
2.5
2.0
1.5
1.0
< 0.4
0.8
0.6
0.4
> 1.0
0.4
0.6
0.6
0.8
1.5
1.0
> 1.0
1.0
> 0.6
0.4
0.6
0.6
> 1.0
0.4
< 0.4
0.2
0.6
> 0.8
0.4
< 0.2

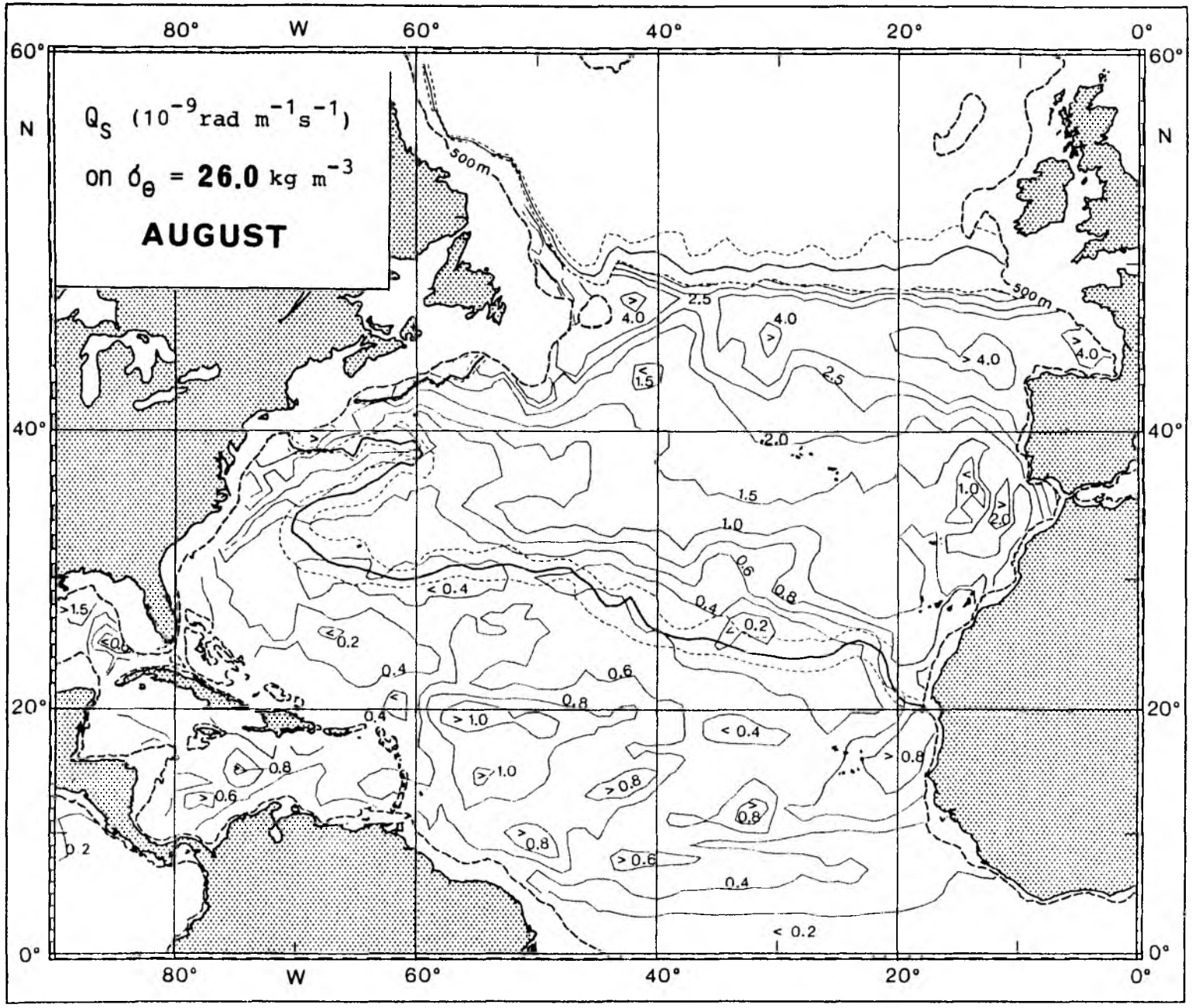
Q_S (10^{-9} rad $m^{-1}s^{-1}$)
on σ_θ = **26.0** kg m^{-3}
AUGUST
80° W
60°
40°
20°
0°
60° N
40°
20°
0°
500m
500m
4.0
2.5
1.5
2.0
1.0
0.6
0.8
0.4
0.2

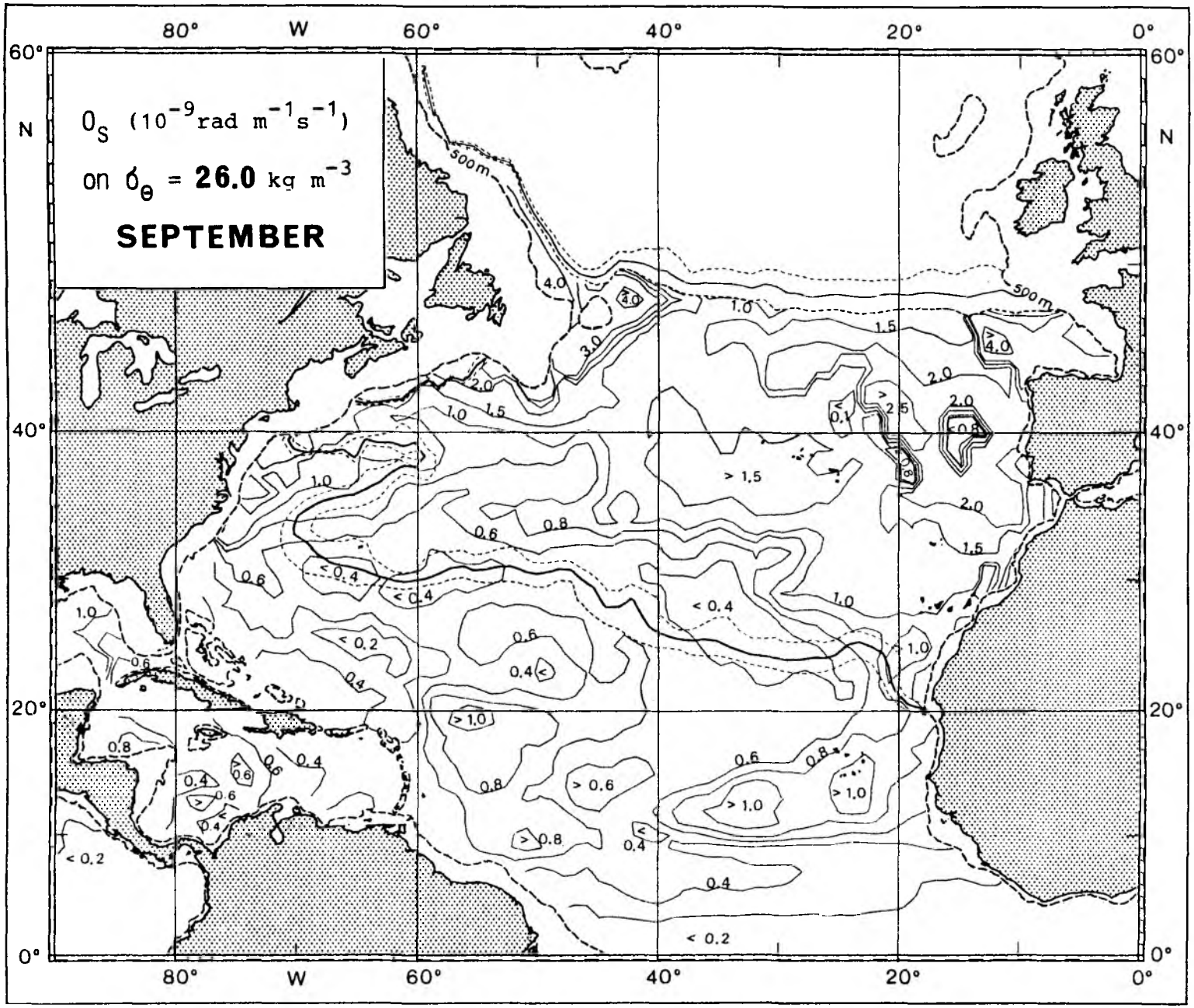
O_S (10^{-9} rad $m^{-1}s^{-1}$)
on σ_θ = 26.0 kg m^{-3}
SEPTEMBER
80° W
60°
40°
20°
0°
60° N
40°
20°
0°
500m
4.0
3.0
2.0
1.5
1.0
0.8
0.6
0.4
0.2
0.1
> 4.0
> 2.5
> 1.5
> 1.0
> 0.8
> 0.6
< 0.4
< 0.2

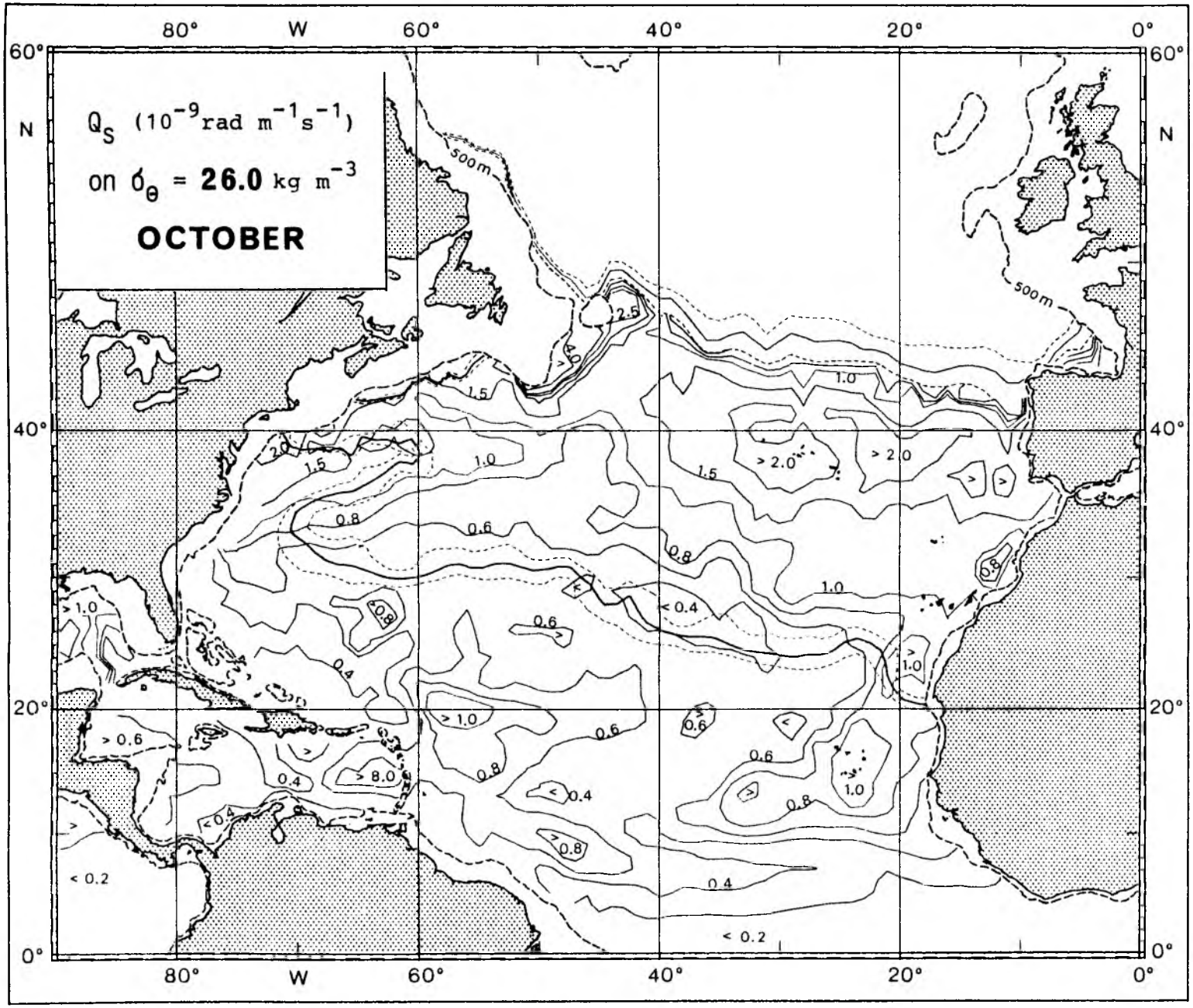
Q_S (10^{-9}rad $m^{-1}s^{-1}$)
on σ_θ = **26.0** kg m^{-3}
OCTOBER
80° W
60°
40°
20°
0°
60° N
40°
20°
0°
500m
2.5
2.0
1.5
1.0
0.8
0.6
0.4
< 0.2
> 1.0
> 0.6
> 8.0
< 0.4
> 2.0
> 0.8

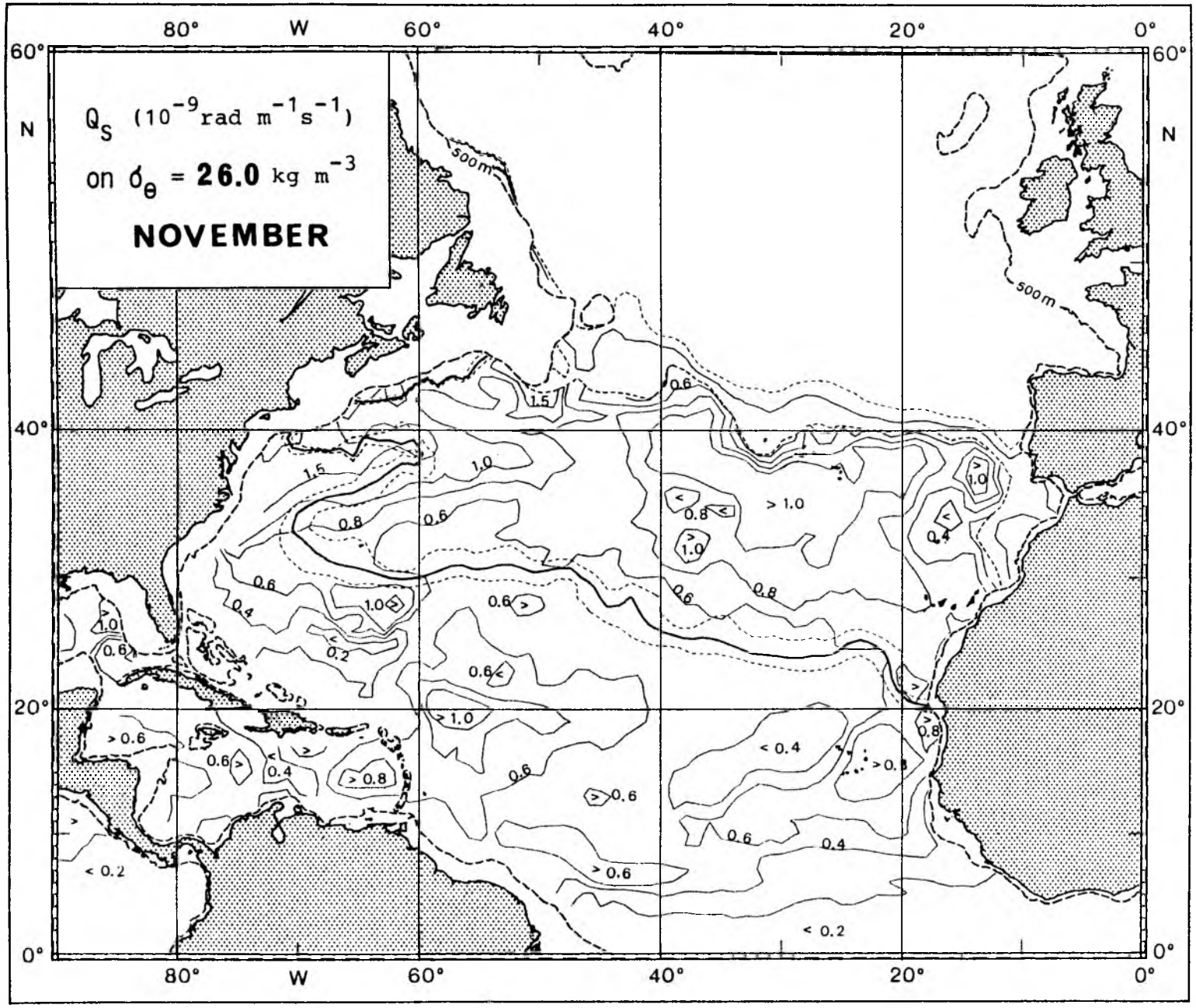
Q_S (10^{-9} rad $m^{-1}s^{-1}$)
on σ_θ = 26.0 kg m^{-3}
NOVEMBER
80° W
60°
40°
20°
0°
60° N
40°
20°
0°
500m
500m
1.5
1.0
0.8
0.6
0.4
0.2
> 1.0
> 0.6
> 0.8
< 0.4
< 0.2

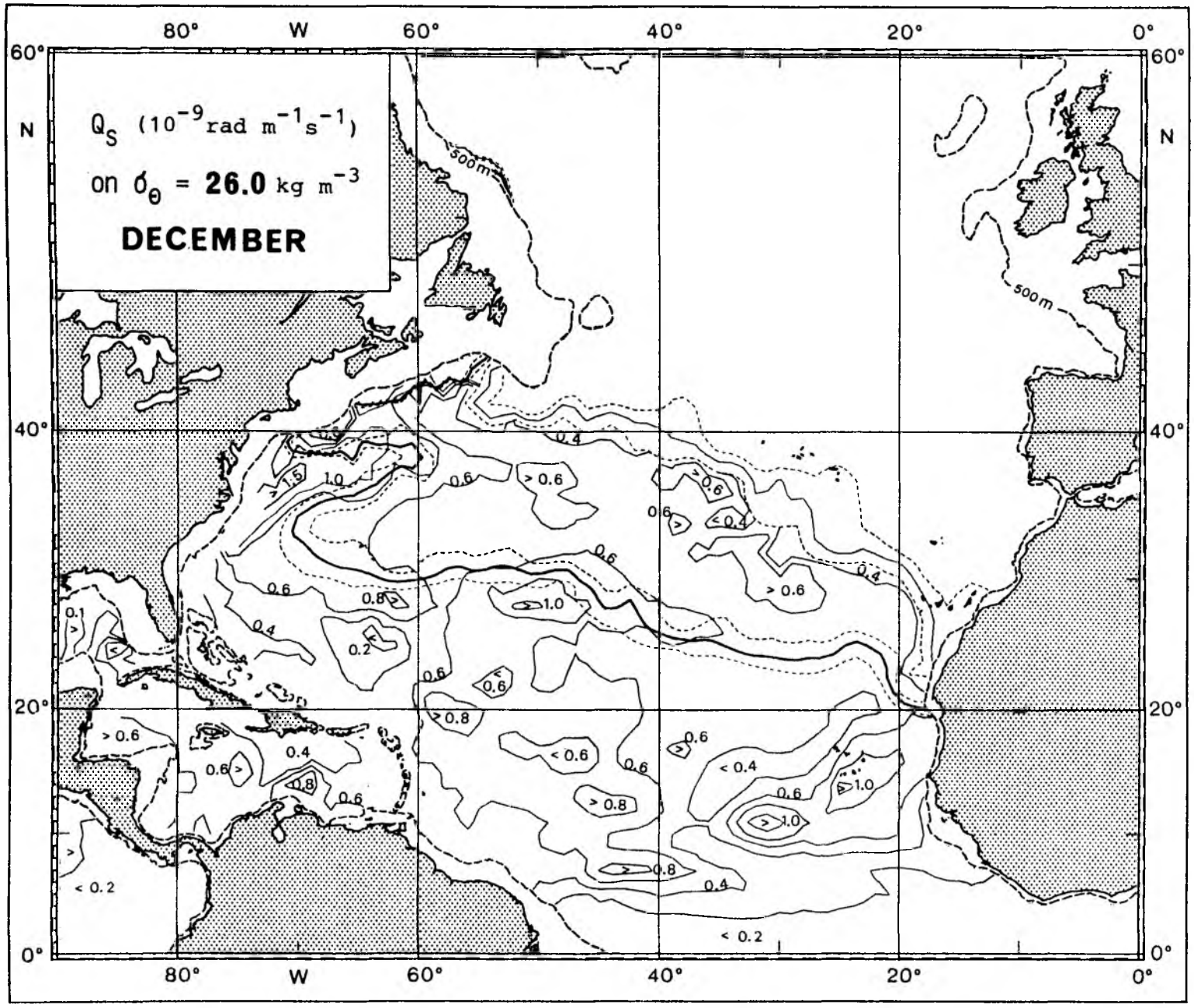
Q_S (10^{-9} rad $m^{-1}s^{-1}$)
on σ_θ = **26.0** kg m^{-3}
DECEMBER
80° W
60°
40°
20°
0°
60° N
40°
20°
0°
500m
500m
> 1.5
1.0
0.6
> 0.6
0.4
0.8
0.2
0.1
< 0.2
< 0.4
< 0.6
> 0.8
> 1.0

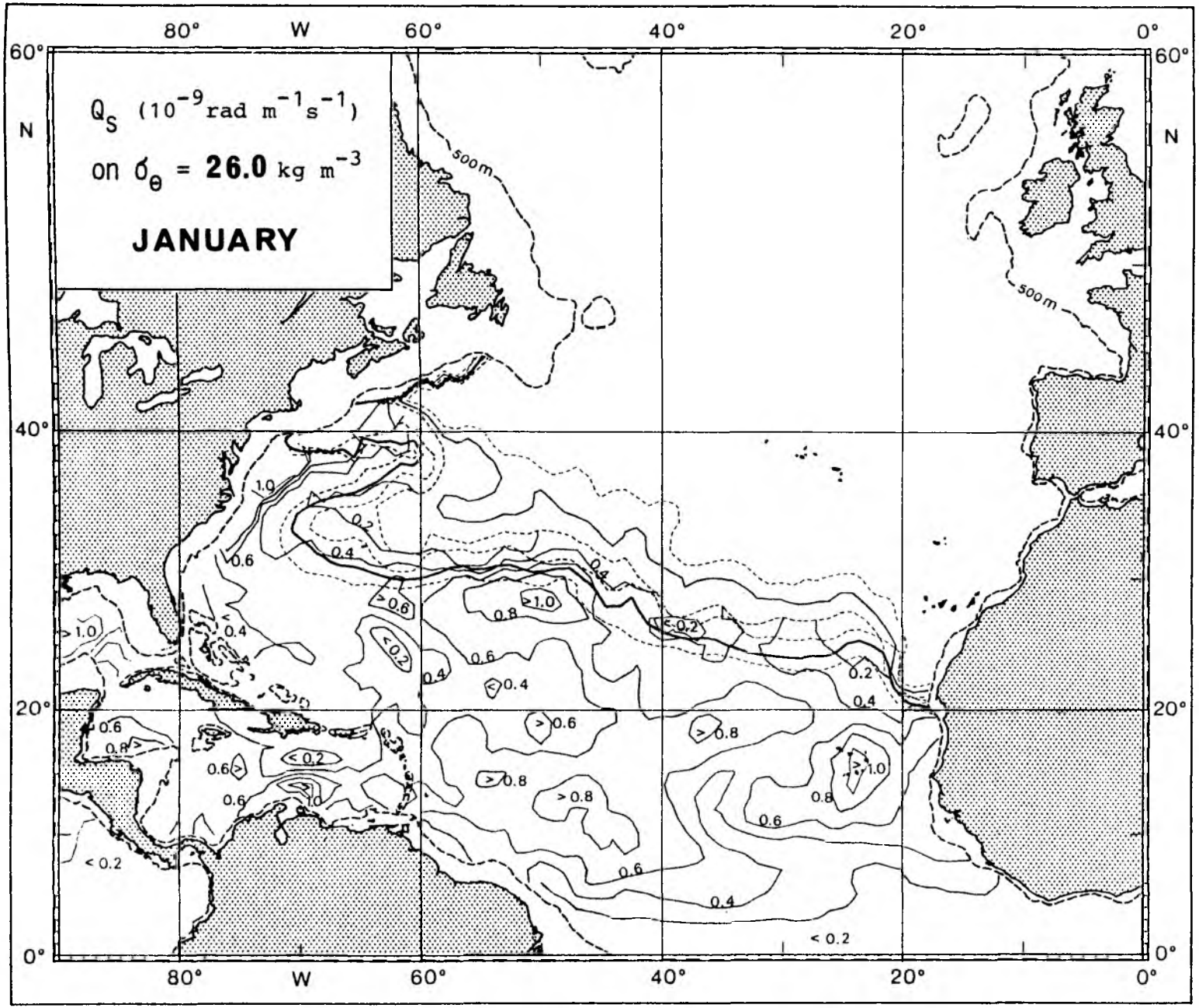
Q_S (10^{-9} rad $m^{-1}s^{-1}$)
on σ_θ = 26.0 kg m^{-3}
JANUARY
80° W 60° 40° 20° 0°
60° N
40°
20°
0°
500m
500m
1.0
0.6
0.4
0.2
> 0.6
< 0.2
0.8
> 1.0
> 0.8
> 0.4
< 0.4
> 0.2

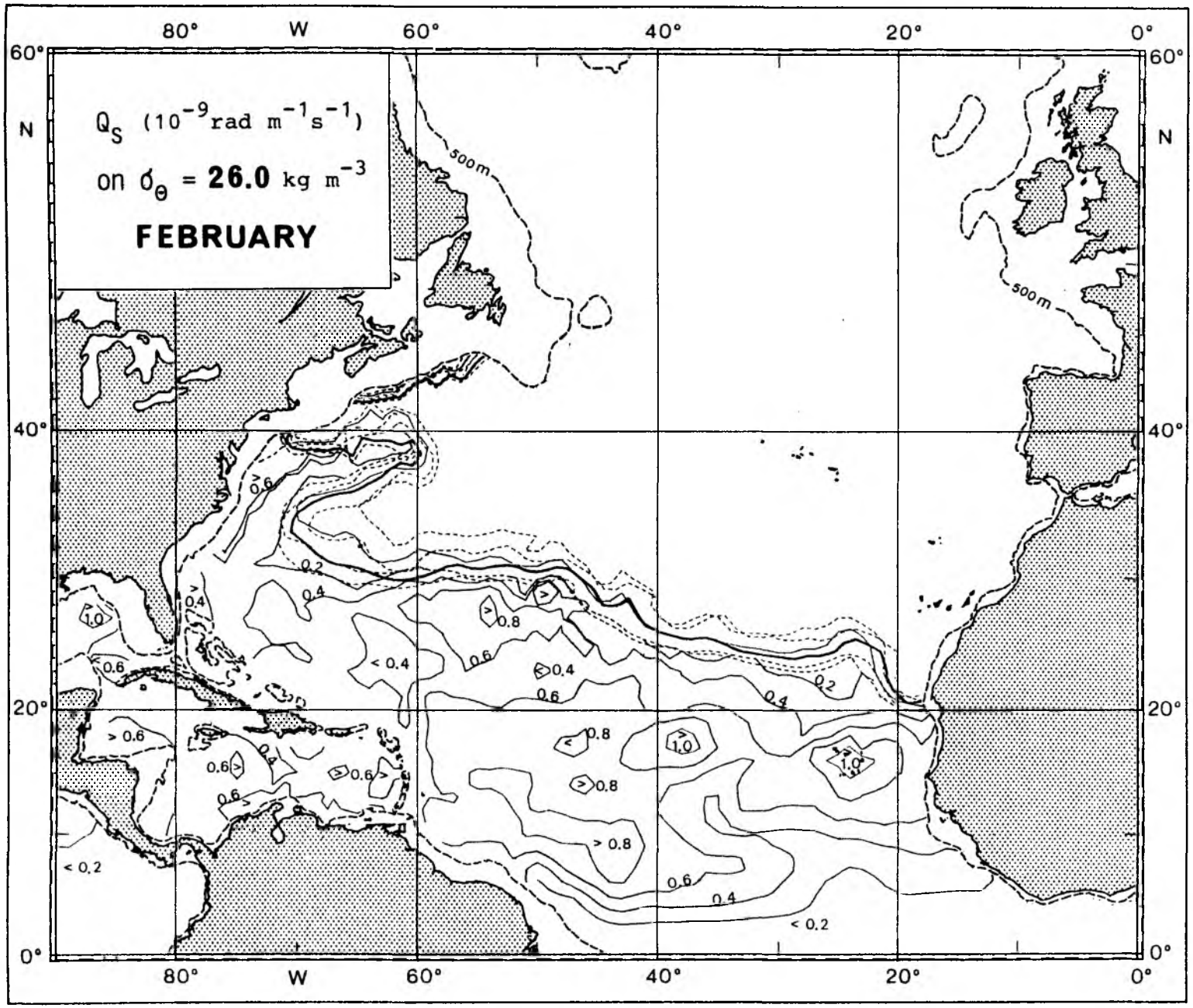
Q_S (10^{-9}rad $m^{-1}s^{-1}$)
on σ_θ = **26.0** kg m^{-3}
FEBRUARY
80° W
60°
40°
20°
0°
60° N
40°
20°
0°
500m
500m
1.0
0.6
0.4
0.2
< 0.4
0.8
> 0.6
< 0.2
> 0.8
< 0.8
1.0

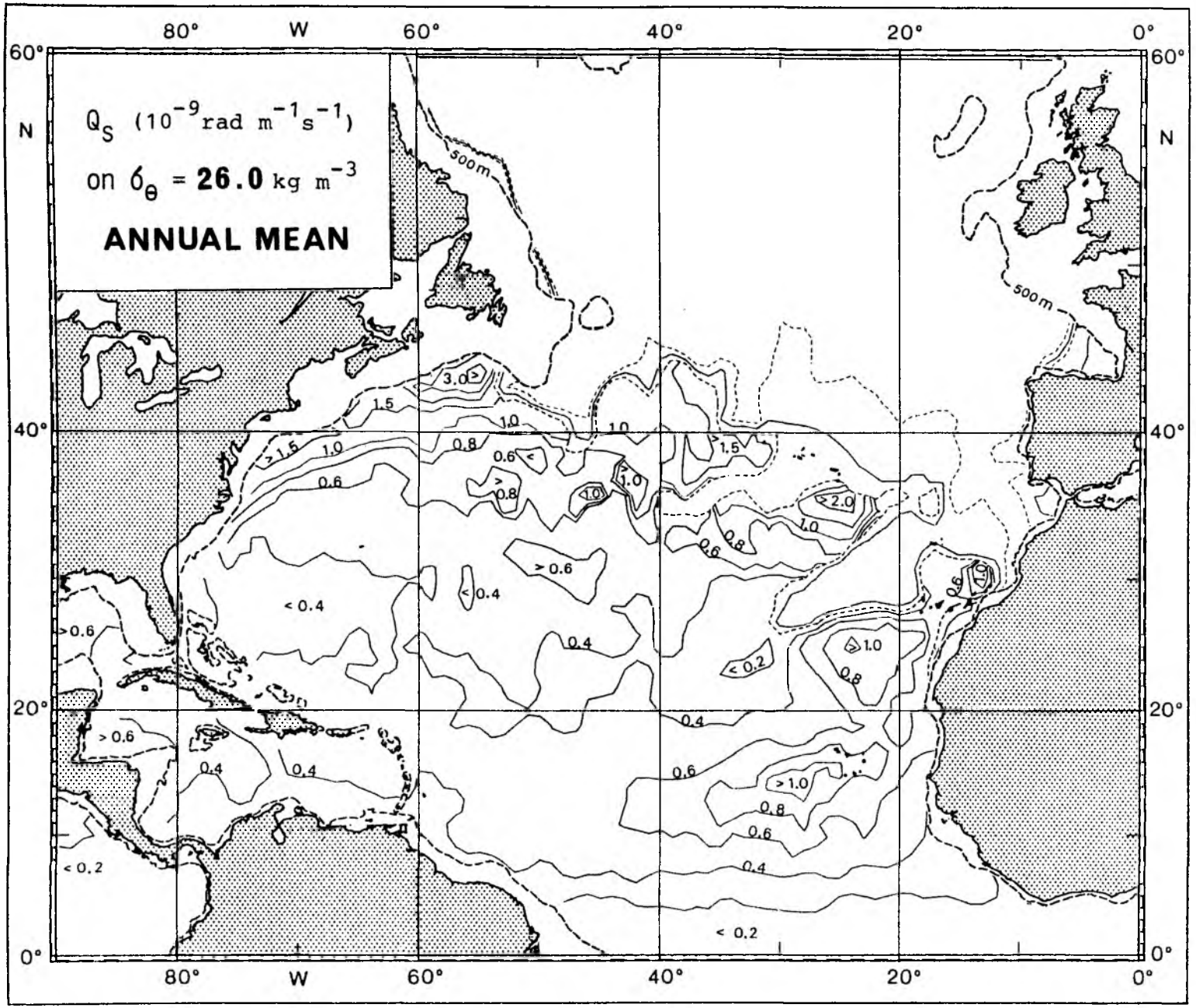
Q_S (10^{-9} rad $m^{-1}s^{-1}$)
on σ_θ = 26.0 kg m^{-3}
ANNUAL MEAN
80° W
60°
40°
20°
0°
60° N
40°
20°
0°
500m
500m
3.0
1.5
1.0
0.8
0.6
0.4
0.2

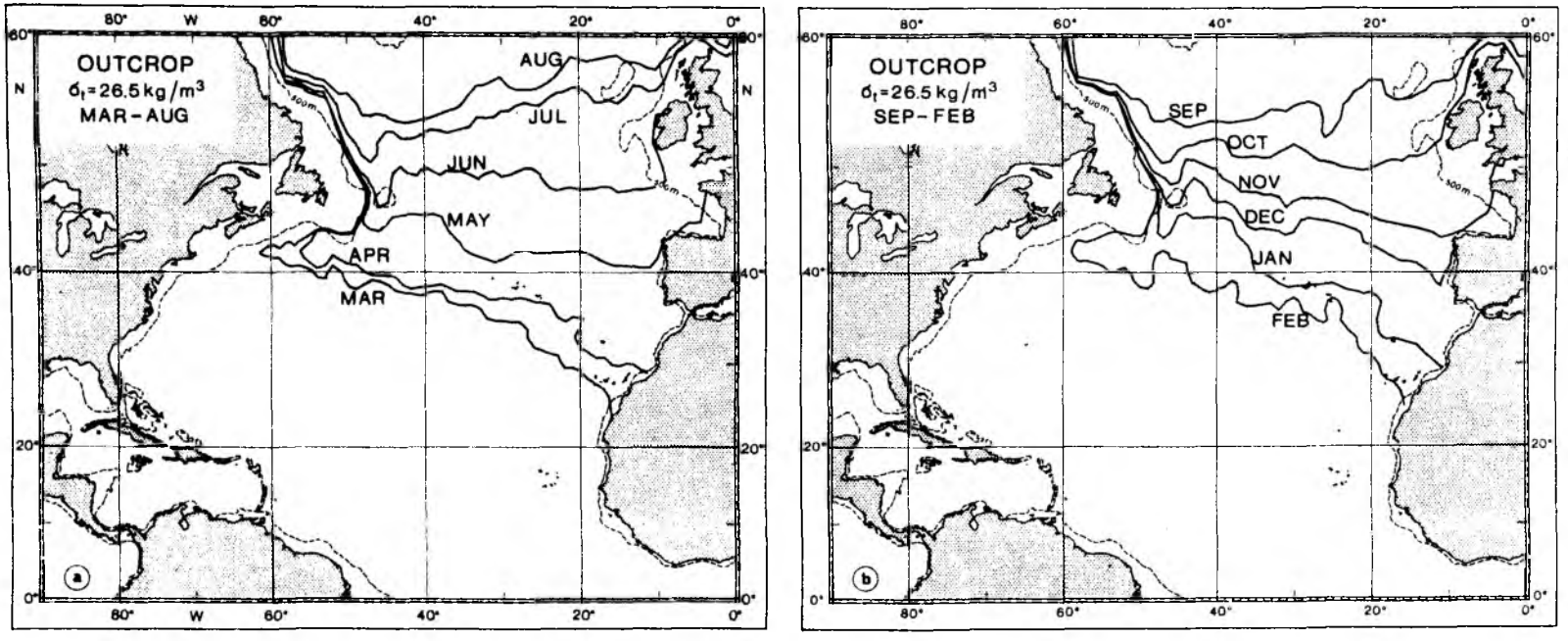

Seasonal migration of the outcrop of the isopycnal surface with σ_θ = 26.5 kg m^{-3};
(a) heating season, (b) cooling season.

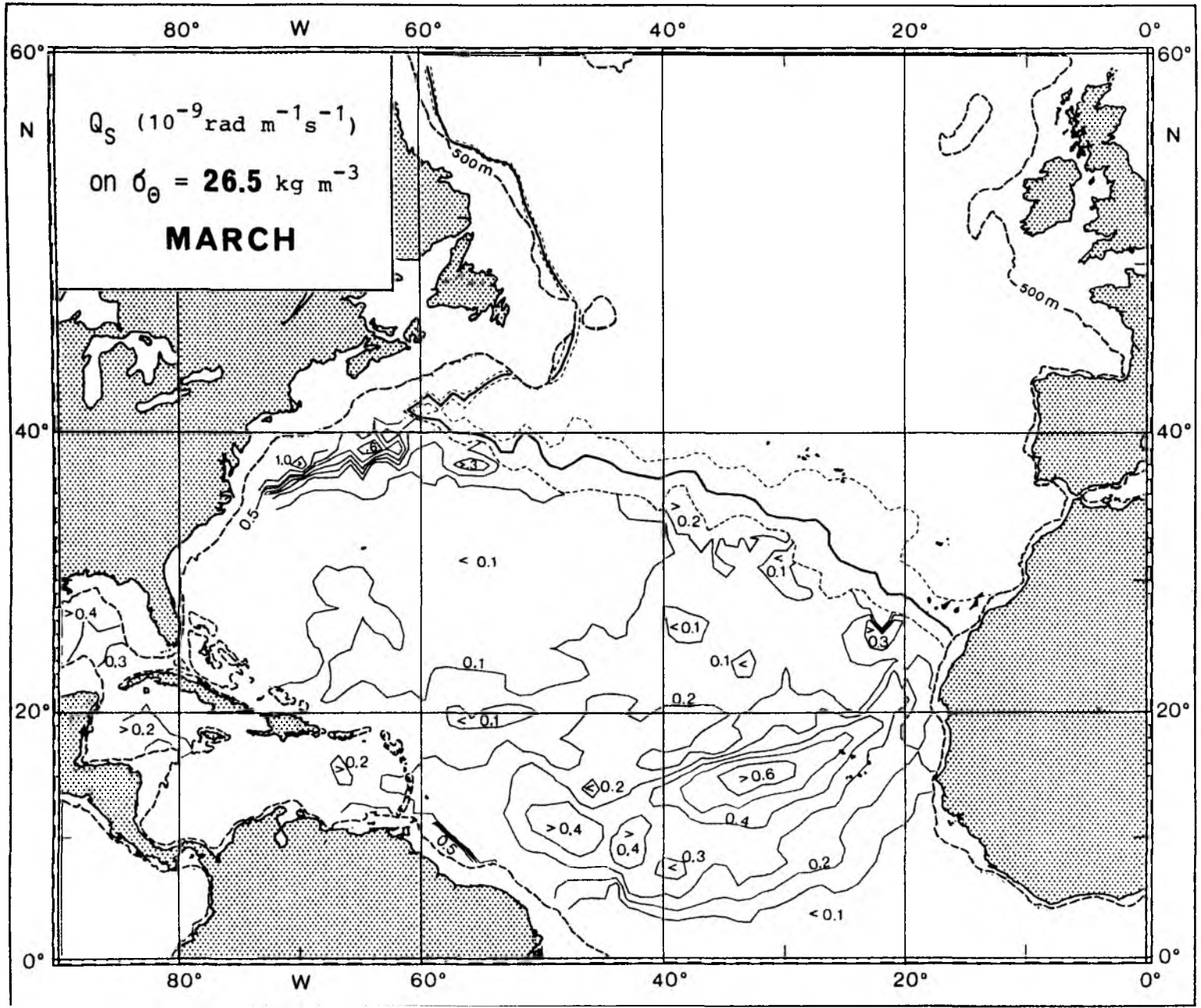
Q_S (10^{-9} rad $m^{-1}s^{-1}$)
on σ_θ = **26.5** kg m^{-3}
MARCH
80° W
60°
40°
20°
0°
60° N
40°
20°
0°
500 m
500 m
1.0
0.5
< 0.1
> 0.4
0.3
> 0.2
0.1
> 0.6
0.4
0.2

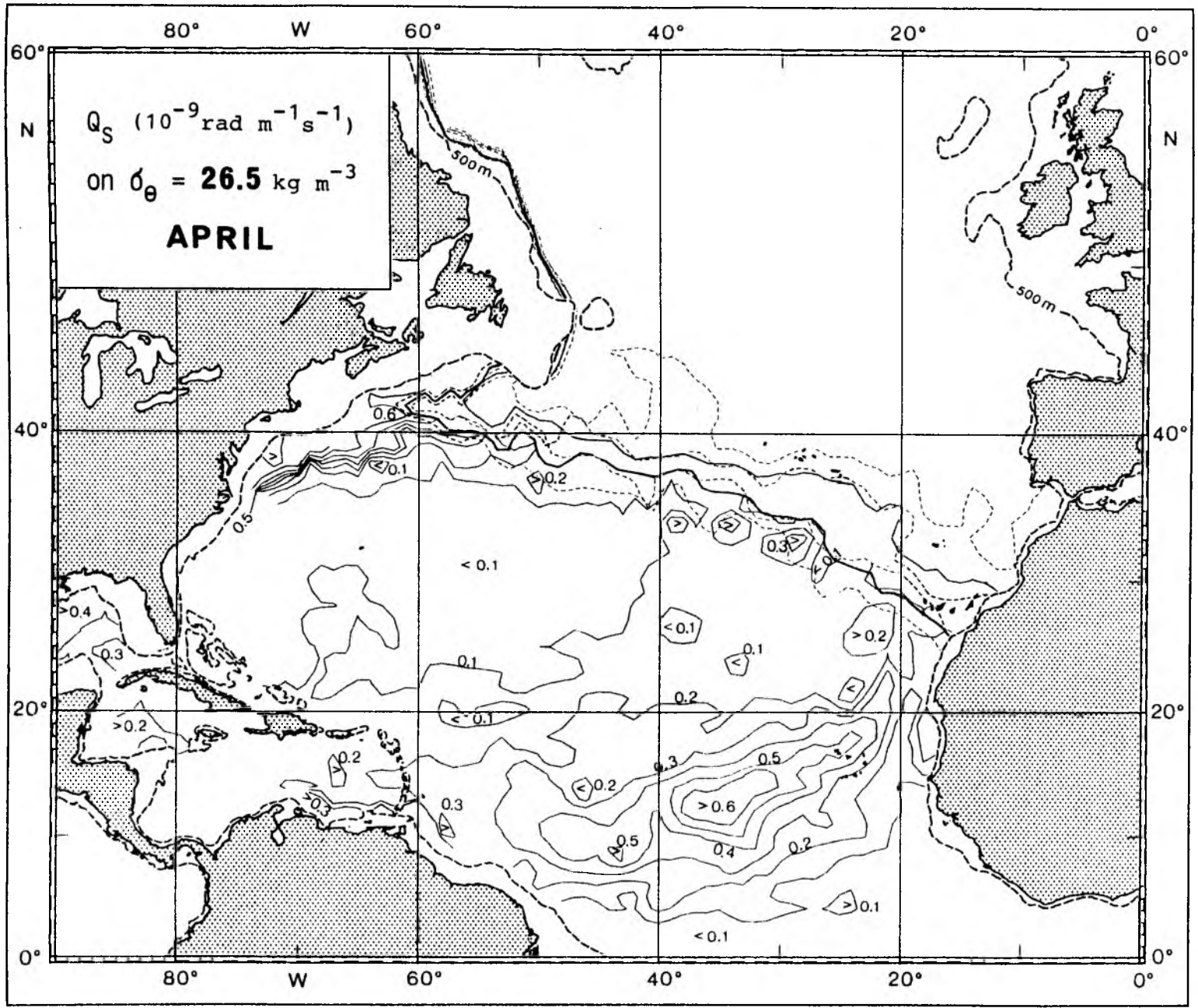
Q_S (10^{-9} rad $m^{-1}s^{-1}$)
on σ_θ = **26.5** kg m^{-3}
APRIL
80° W
60°
40°
20°
0°
60° N
40°
20°
0°
500 m
500 m
0.6
0.1
0.2
0.5
< 0.1
0.3
> 0.4
0.3
< 0.1
> 0.2
0.1
0.1
0.2
> 0.2
< 0.1
0.2
0.3
0.5
0.2
0.3
> 0.6
0.5
0.4
0.2
> 0.1
< 0.1

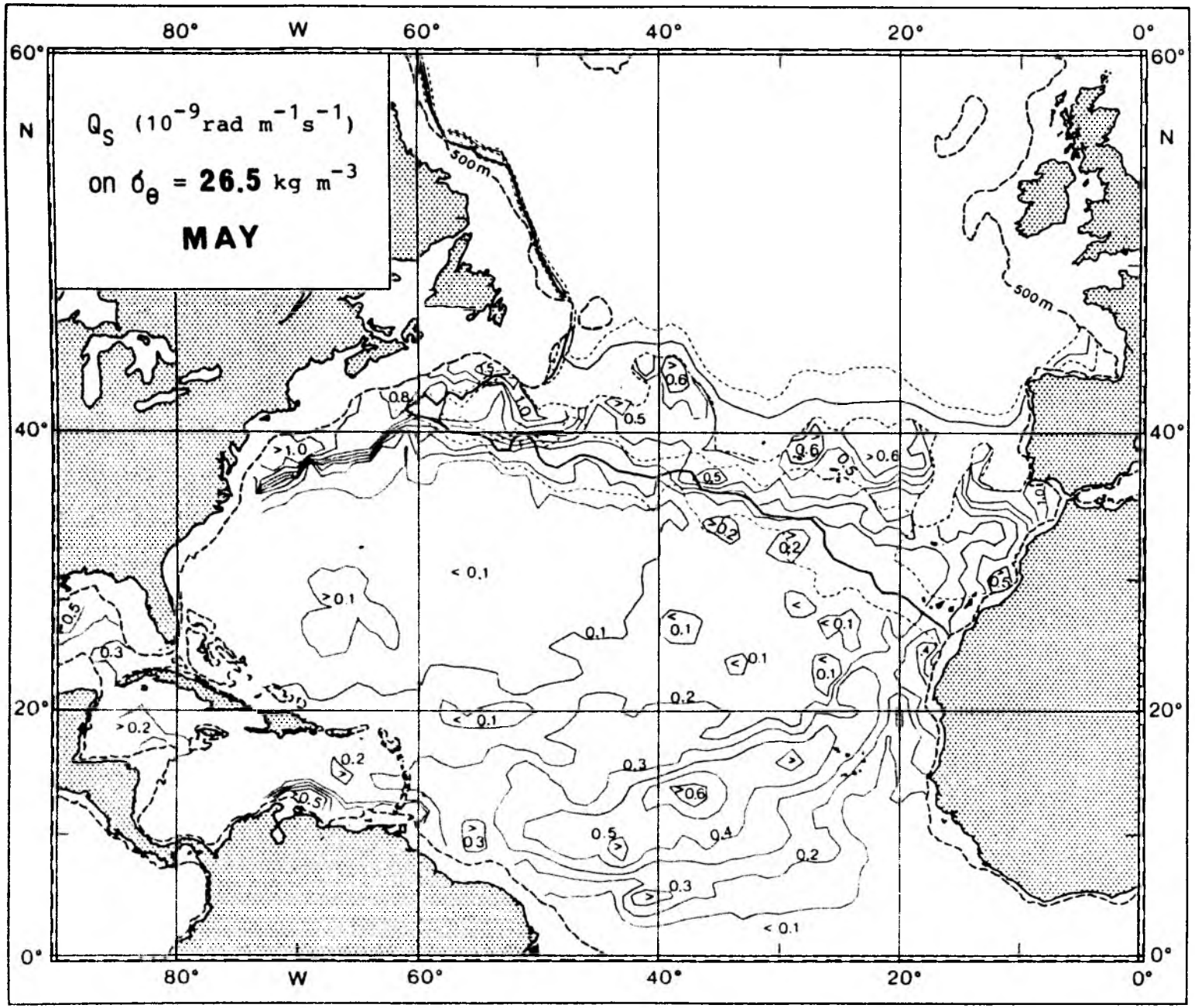
Q_S (10^{-9}rad $m^{-1}s^{-1}$)
on σ_θ = 26.5 kg m^{-3}
MAY
80° W 60° 40° 20° 0°
60° N
40°
20°
0°
500m
< 0.1
0.1
0.2
0.3
0.4
0.5
0.6
0.8
1.0
> 0.1
> 0.2
> 0.6
> 1.0

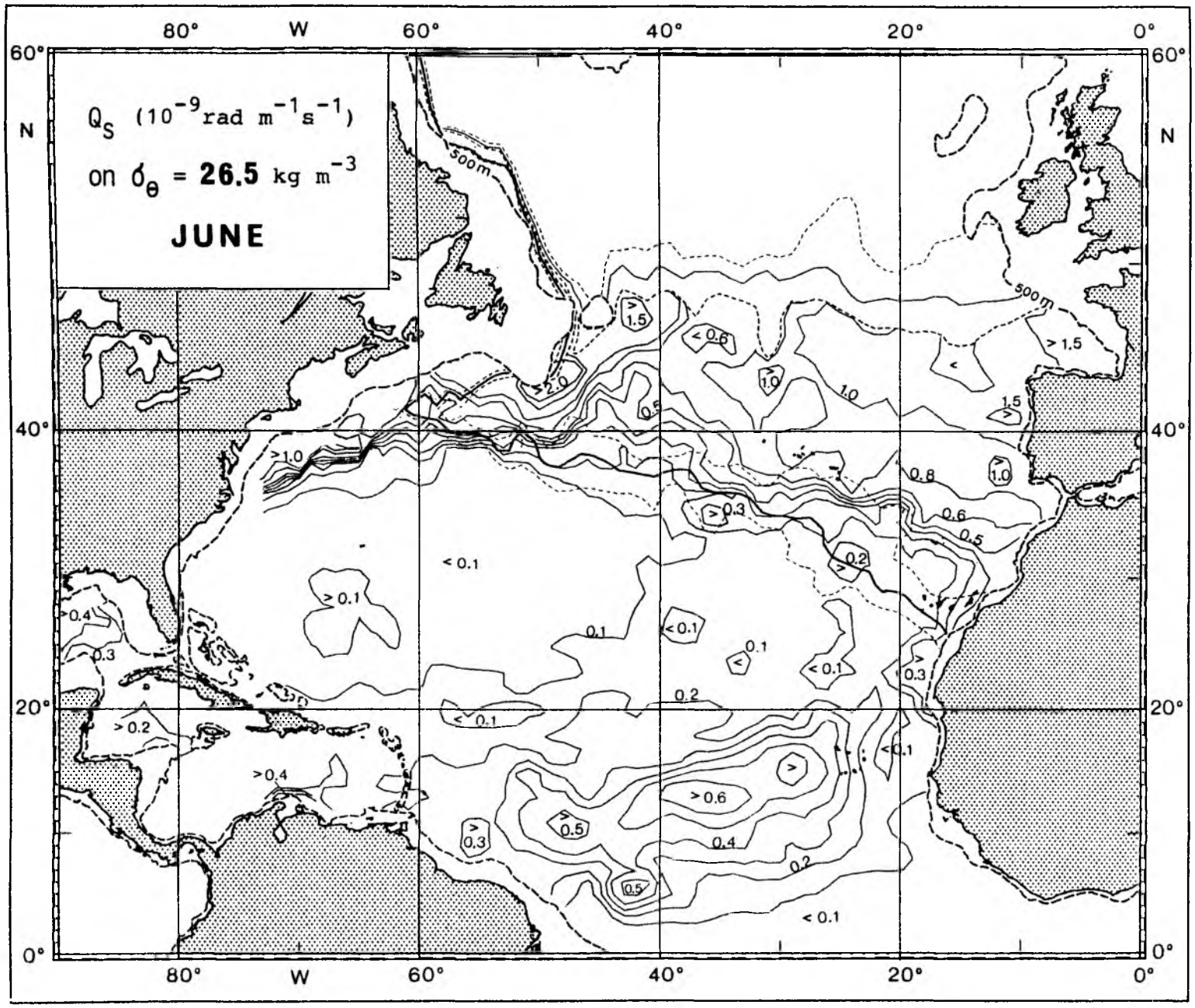
Q_S (10^{-9}rad $m^{-1}s^{-1}$)
on σ_θ = 26.5 kg m^{-3}
JUNE
80° W
60°
40°
20°
0°
60° N
40°
20°
0°
500m
500m
< 0.1
> 0.1
0.1
0.2
0.3
0.4
0.5
0.6
0.8
1.0
1.5
2.0
> 0.2
> 0.3
> 0.4
> 0.5
> 0.6
> 1.0
> 1.5

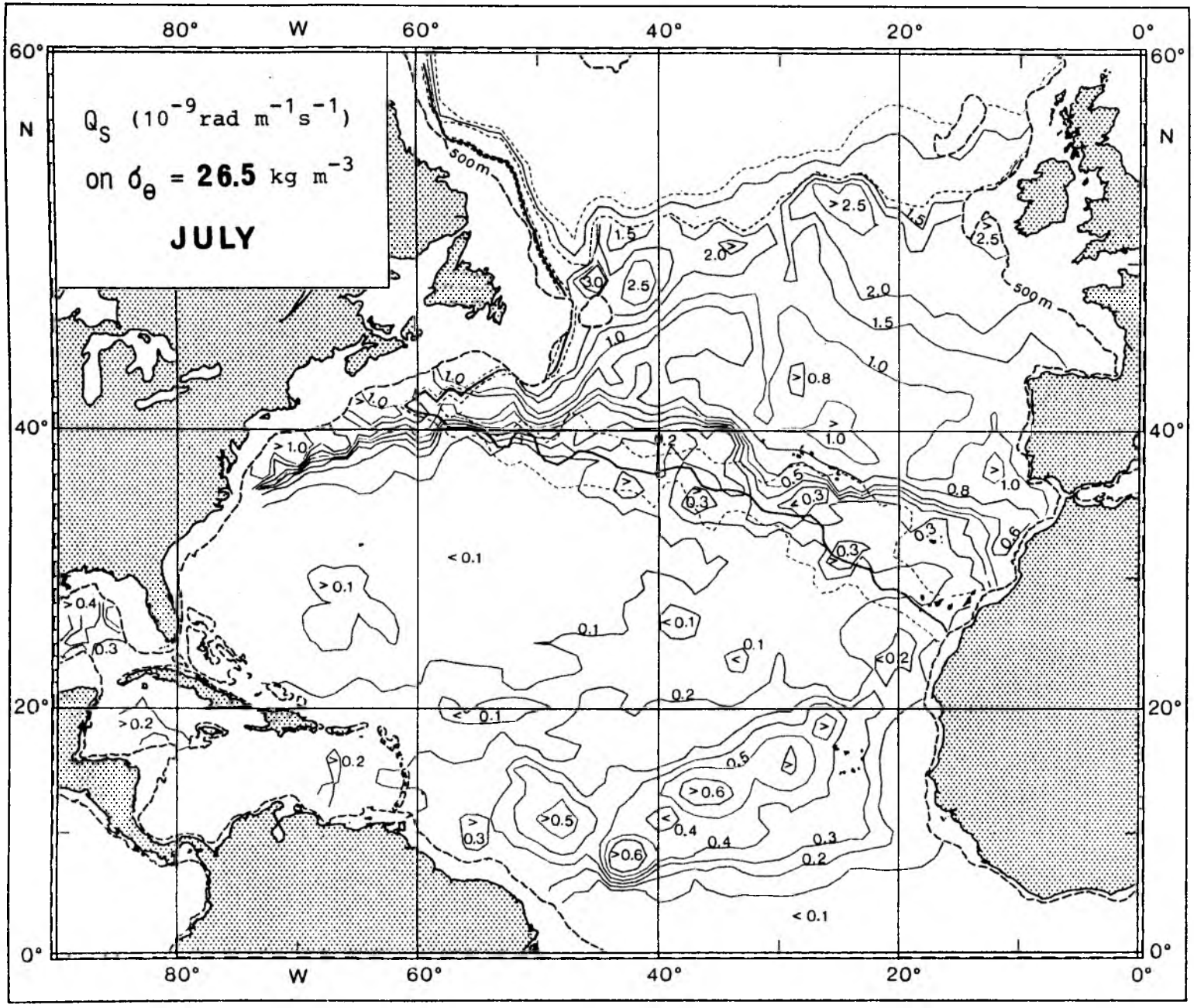
Q_S (10^{-9} rad $m^{-1}s^{-1}$)
on σ_θ = 26.5 kg m^{-3}
JULY
80° W 60° 40° 20° 0°
60° N
40°
20°
0°
500m
> 2.5
2.5
2.0
1.5
1.0
> 0.8
0.8
0.5
0.3
0.2
0.1
0.6
0.4
> 1.0
> 0.1
> 0.4
> 0.2
< 0.1
< 0.2
> 0.6
> 0.5
> 0.3

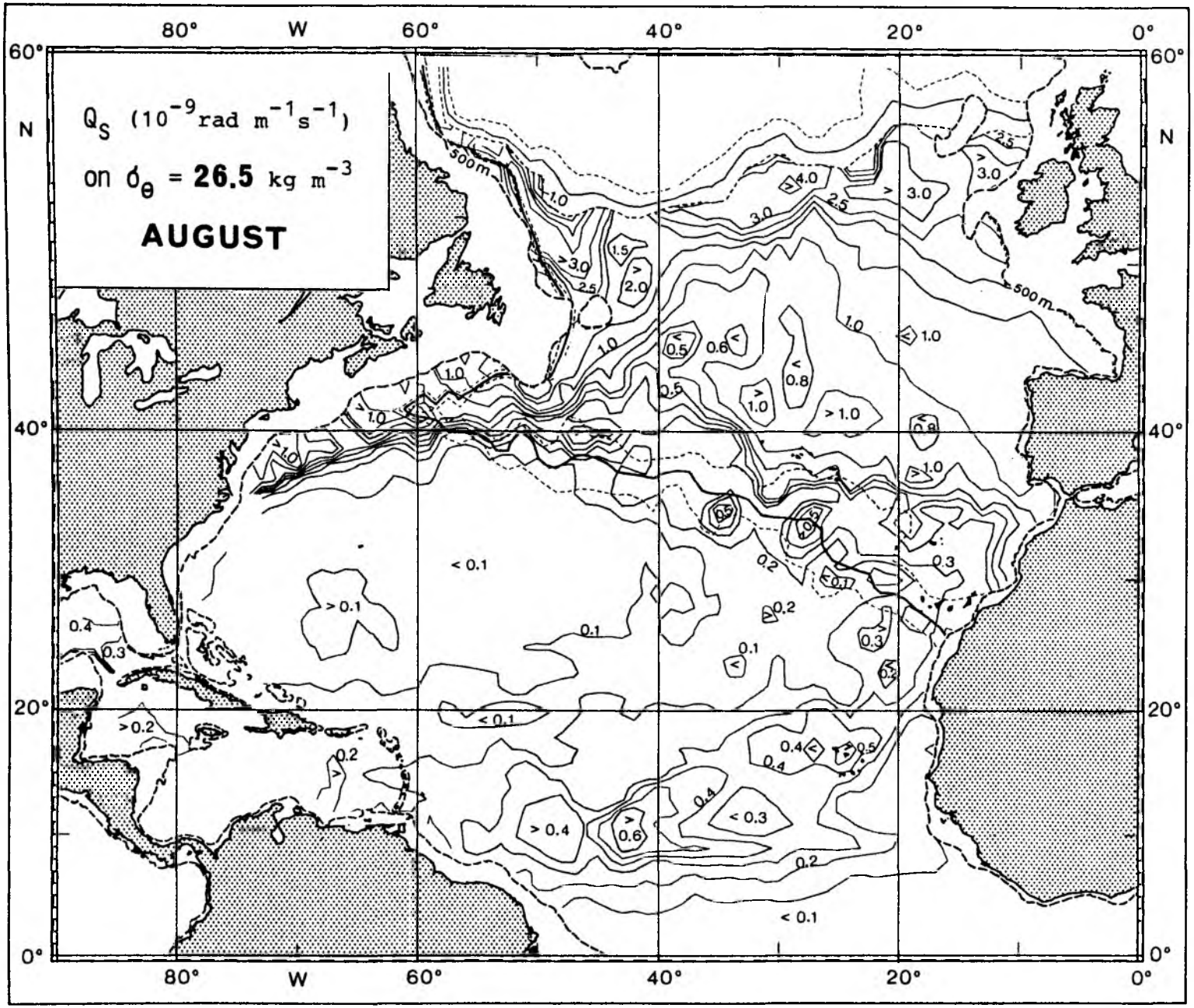
Q_S (10^{-9} rad $m^{-1}s^{-1}$)
on σ_θ = 26.5 kg m^{-3}
AUGUST
80° W
60°
40°
20°
0°
60° N
40°
20°
0°
500 m
< 0.1
> 0.1
> 0.2
> 0.4
< 0.3
1.0
2.0
3.0
4.0

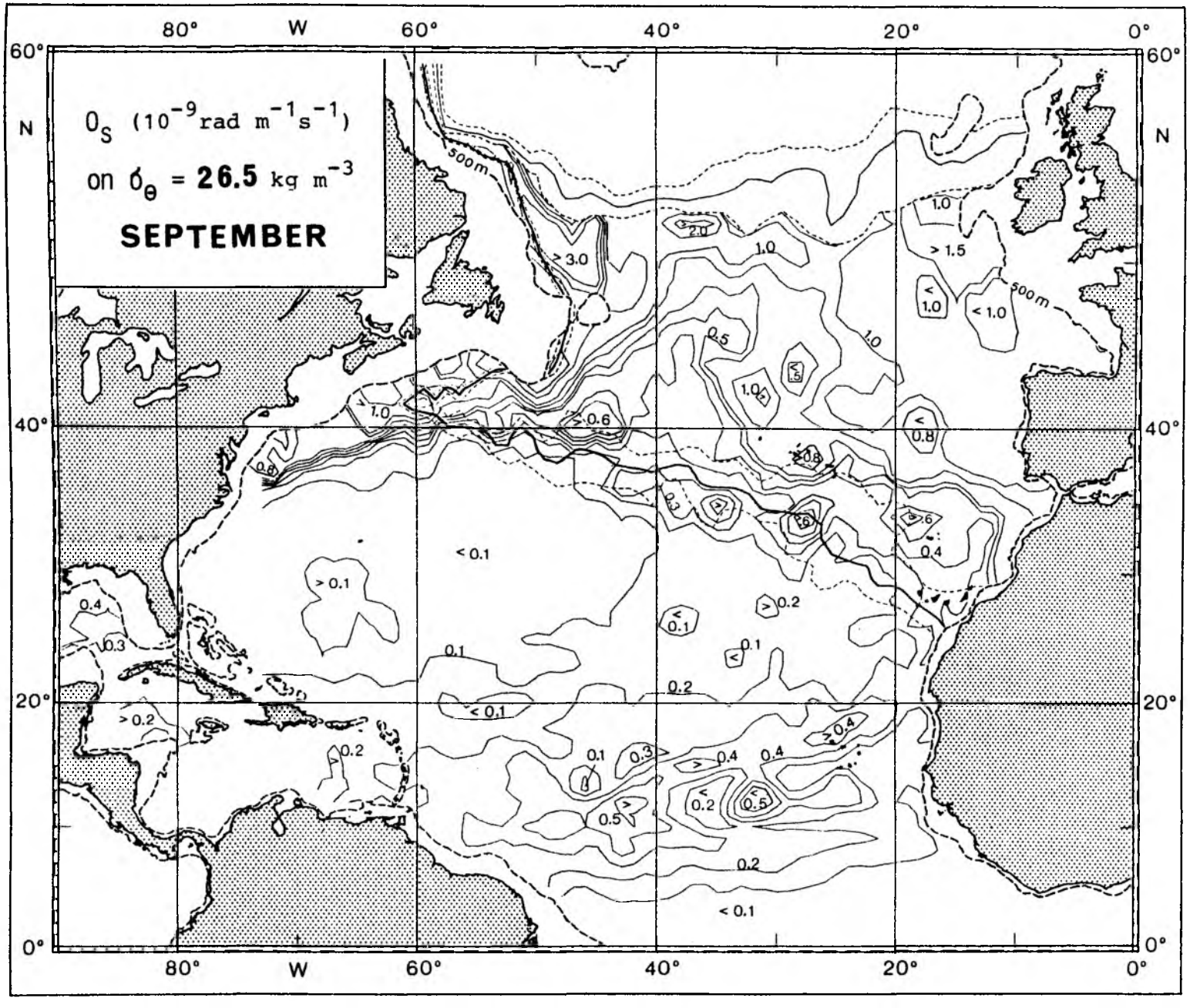
O_S (10^{-9} rad $m^{-1}s^{-1}$)
on σ_θ = 26.5 kg m^{-3}
SEPTEMBER
80° W
60°
40°
20°
0°
60° N
40°
20°
0°
500 m
> 3.0
2.0
1.0
> 1.5
< 1.0
0.5
> 0.6
0.8
0.6
0.3
0.4
< 0.1
> 0.1
0.1
> 0.2
0.2
0.4
0.3
0.5

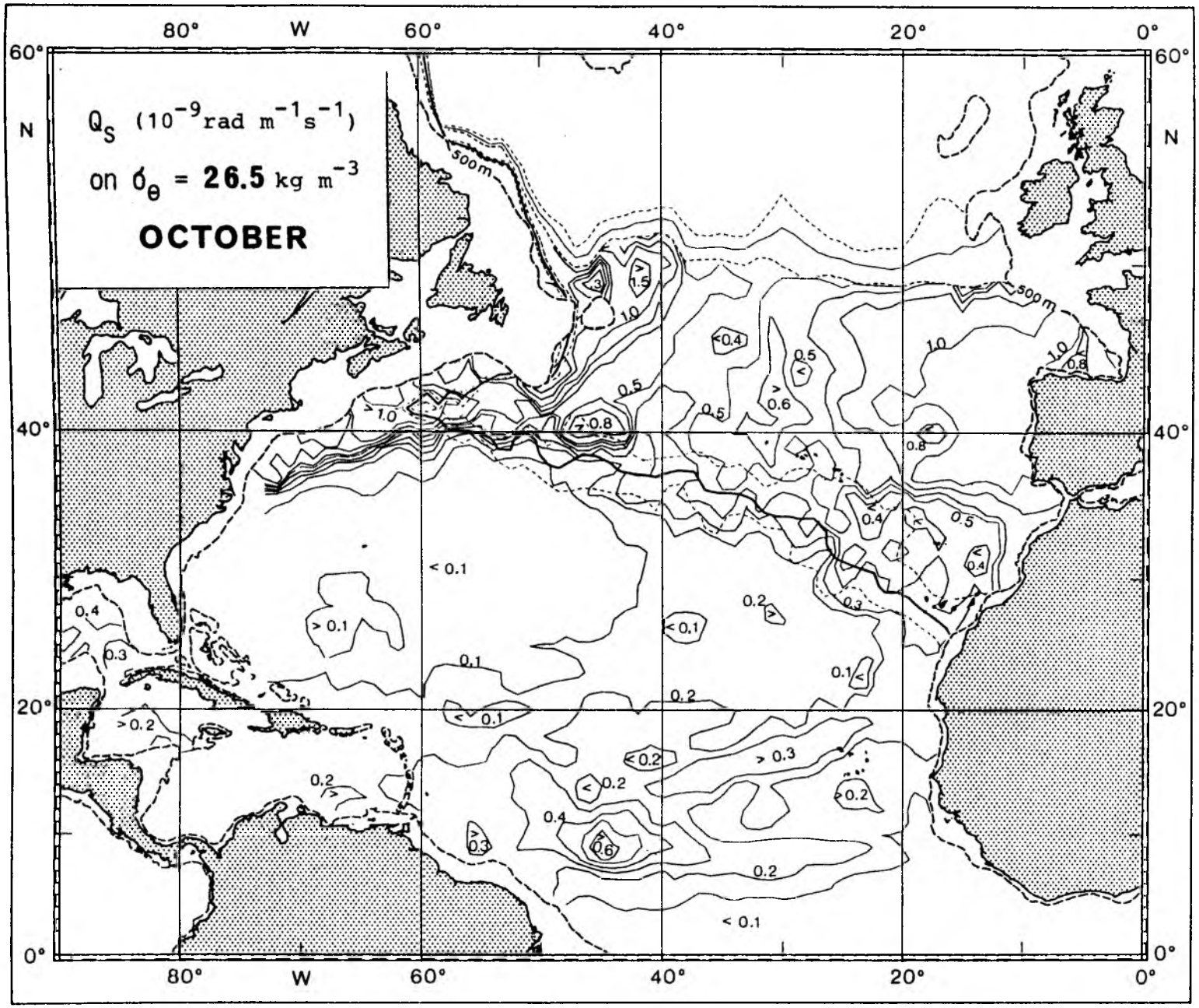
Q_S (10^{-9}rad $m^{-1}s^{-1}$)
on σ_θ = 26.5 kg m^{-3}
OCTOBER
80° W
60°
40°
20°
0°
60° N
40°
20°
0°
500m
< 0.1
> 0.1
0.1
0.2
0.3
0.4
0.5
0.6
0.8
1.0
1.5

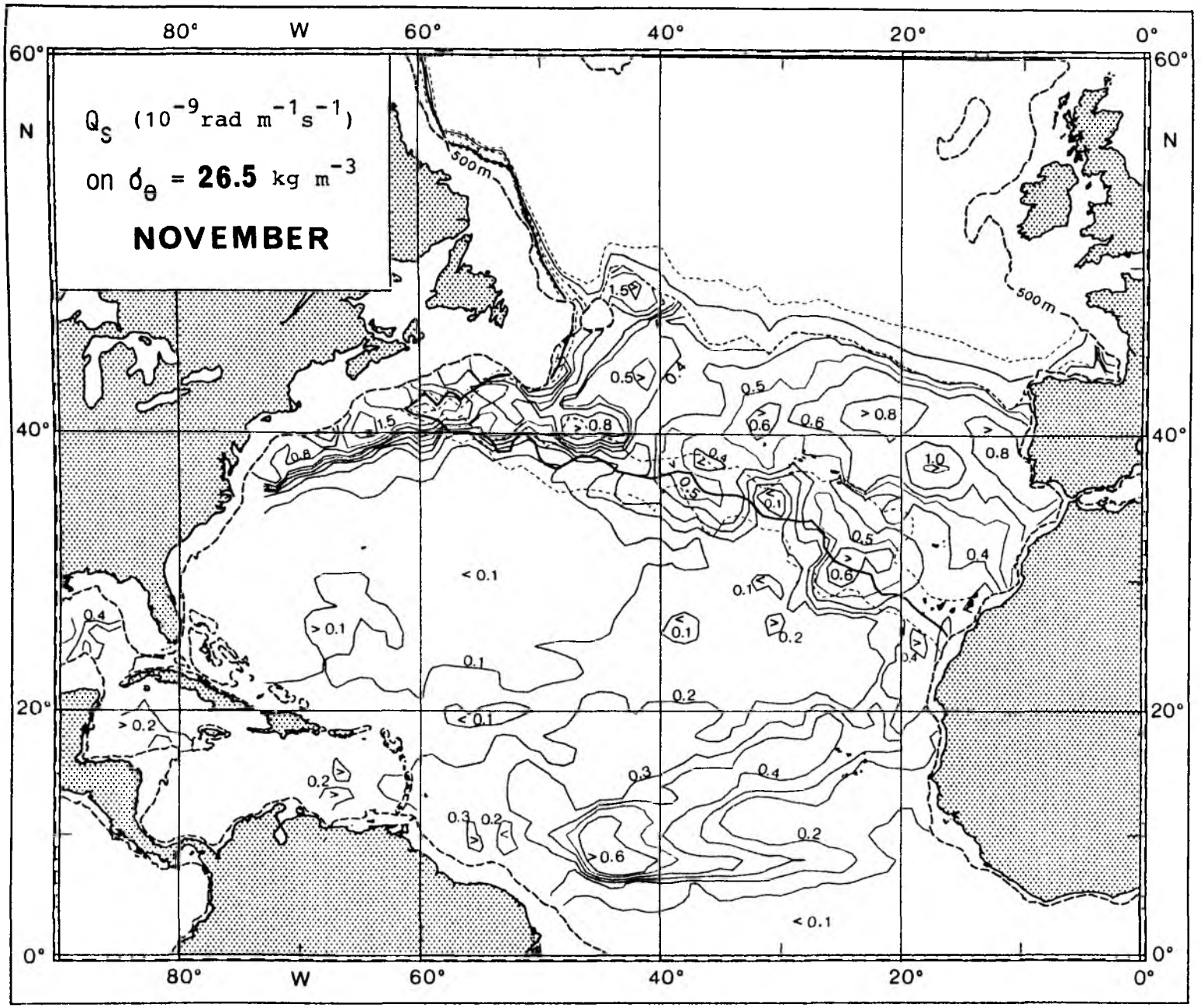
Q_S (10^{-9}rad $m^{-1}s^{-1}$)
on σ_θ = **26.5** kg m^{-3}
NOVEMBER
80° W
60°
40°
20°
0°
60° N
40°
20°
0°
500m
1.5
0.5
0.6
> 0.8
0.8
1.0
0.4
0.1
< 0.1
> 0.1
0.2
0.3
> 0.2
> 0.6

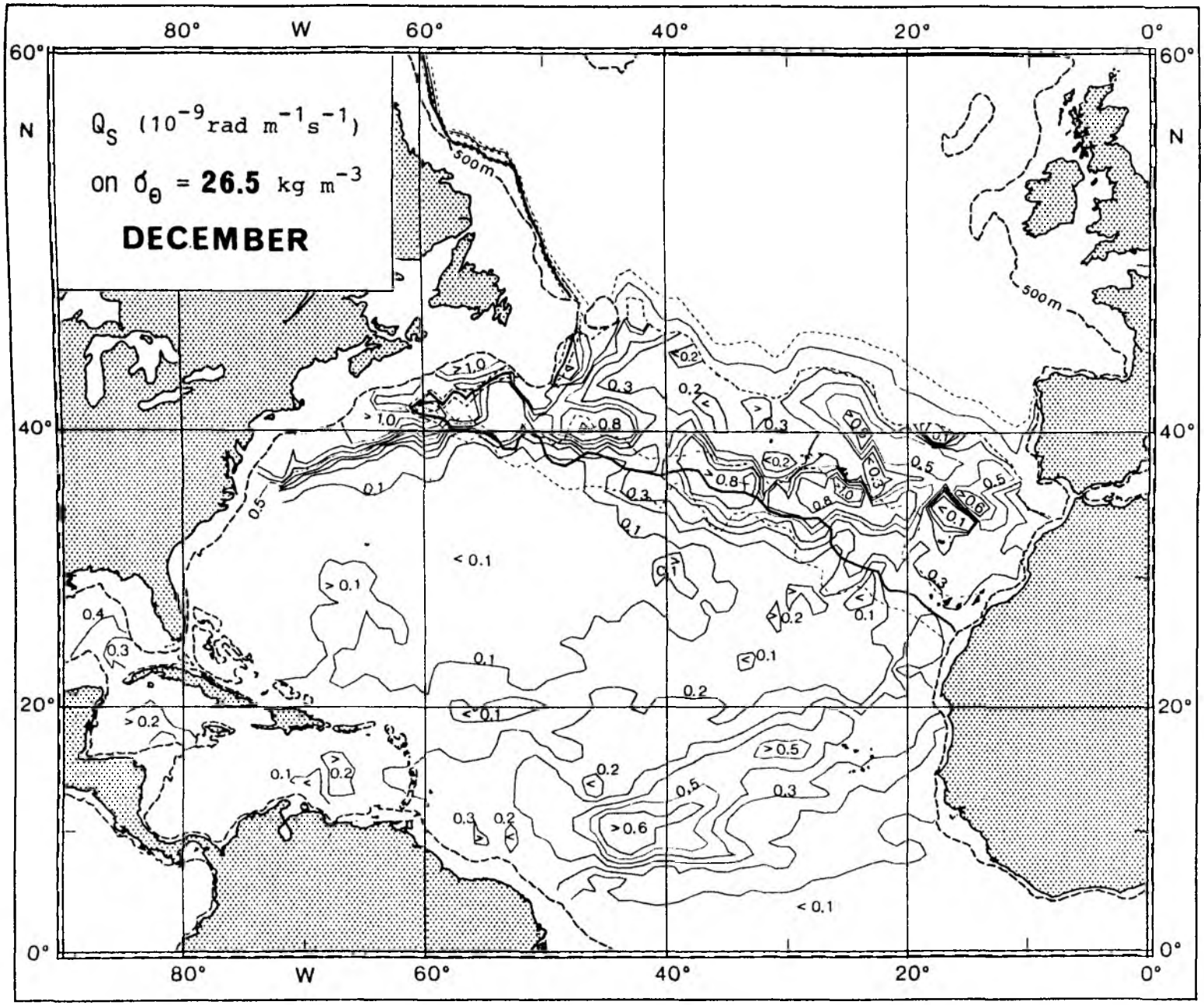
Q_S (10^{-9}rad $m^{-1}s^{-1}$)
on σ_θ = **26.5** kg m^{-3}
DECEMBER
80° W
60°
40°
20°
0°
60° N
40°
20°
0°
500m
500m
< 0.1
> 0.1
> 0.2
> 0.5
> 0.6
> 0.8
> 1.0

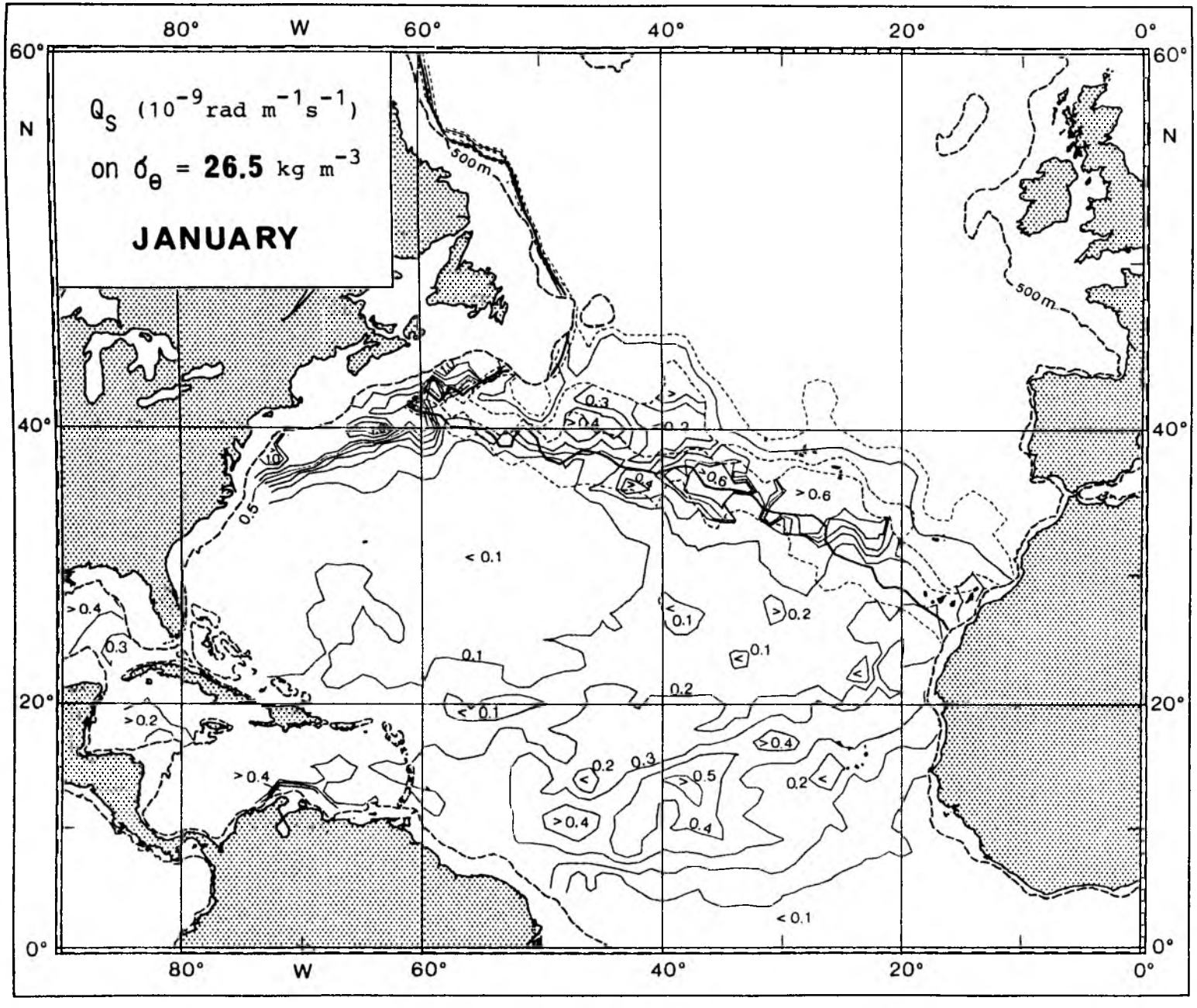
Q_S (10^{-9} rad $m^{-1}s^{-1}$)
on σ_θ = 26.5 kg m^{-3}
JANUARY
80° W
60°
40°
20°
0°
60° N
40°
20°
0°
500 m
500 m
< 0.1
> 0.4
0.3
> 0.2
0.1
0.2
> 0.4
0.3
> 0.5
0.2
> 0.4
0.4
< 0.1
0.5
1.0
> 0.6
> 0.6
> 0.2
0.3
> 0.4

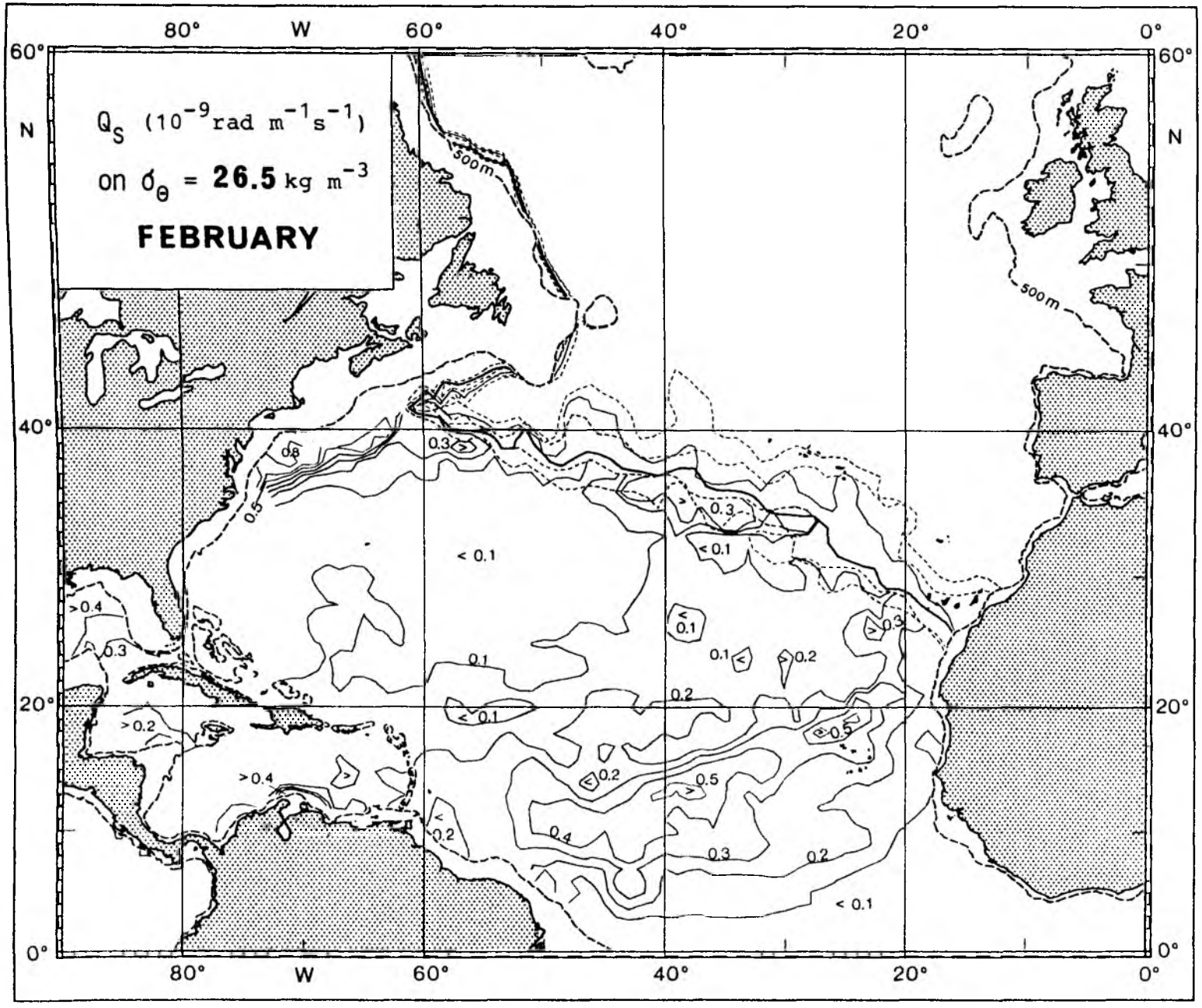
Q_S (10^{-9} rad $m^{-1}s^{-1}$)
on σ_θ = **26.5** kg m^{-3}
FEBRUARY
80° W
60°
40°
20°
0°
60° N
40°
20°
0°
500 m
500 m
0.8
0.5
0.3
< 0.1
> 0.4
0.3
0.1
> 0.2
< 0.1
> 0.4
< 0.2
0.4
0.3
0.2
< 0.1
0.3
< 0.1
< 0.1
0.1
0.1
> 0.2
0.2
0.5
0.2
0.5

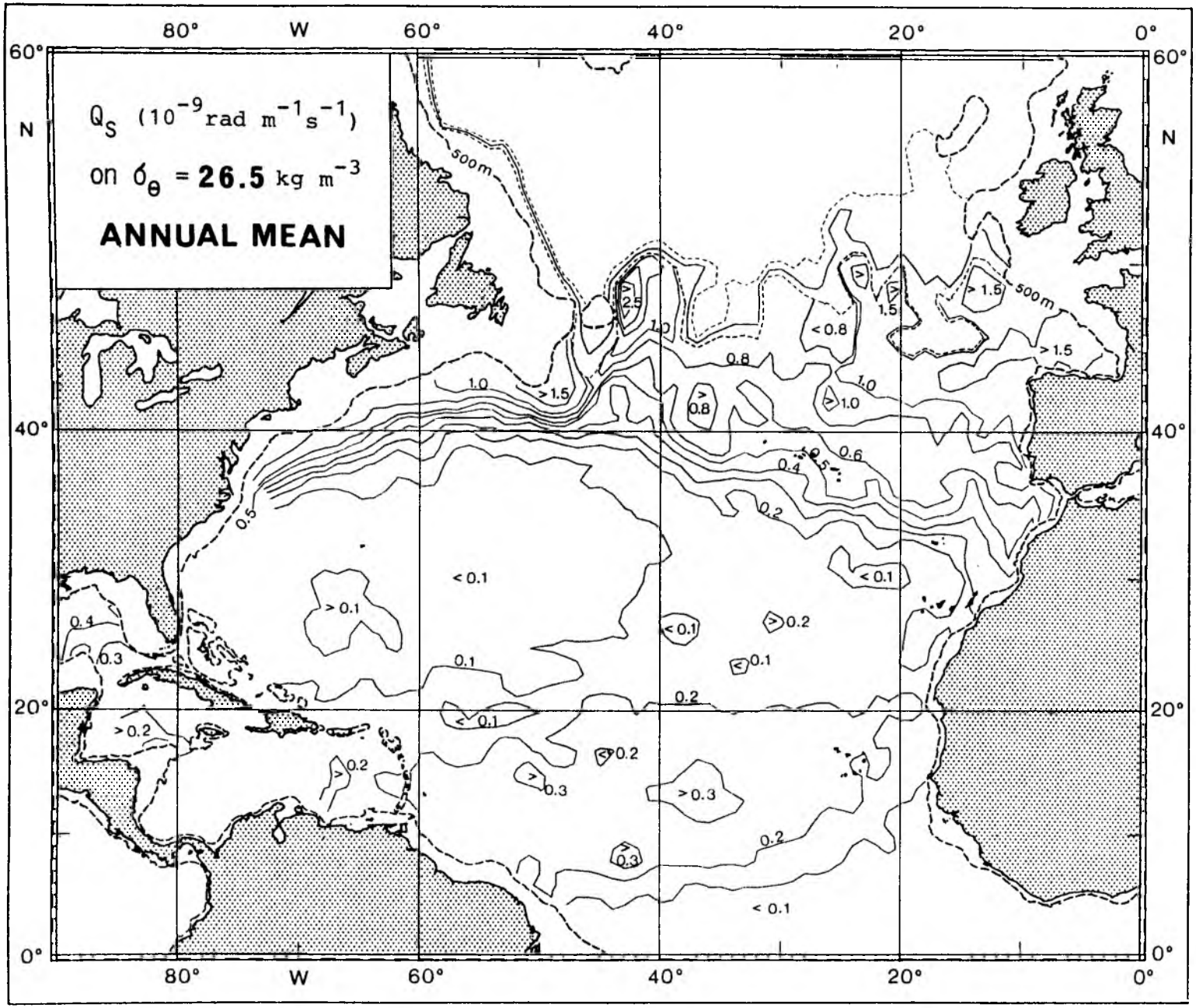
Q_S (10^{-9} rad $m^{-1}s^{-1}$)
on σ_θ = 26.5 kg m^{-3}
ANNUAL MEAN
80° W
60°
40°
20°
0°
60° N
40°
20°
0°
500m
< 0.8
0.8
1.0
1.5
> 1.5
2.5
0.5
0.6
0.4
0.2
< 0.1
> 0.1
0.1
0.3
> 0.2
> 0.3

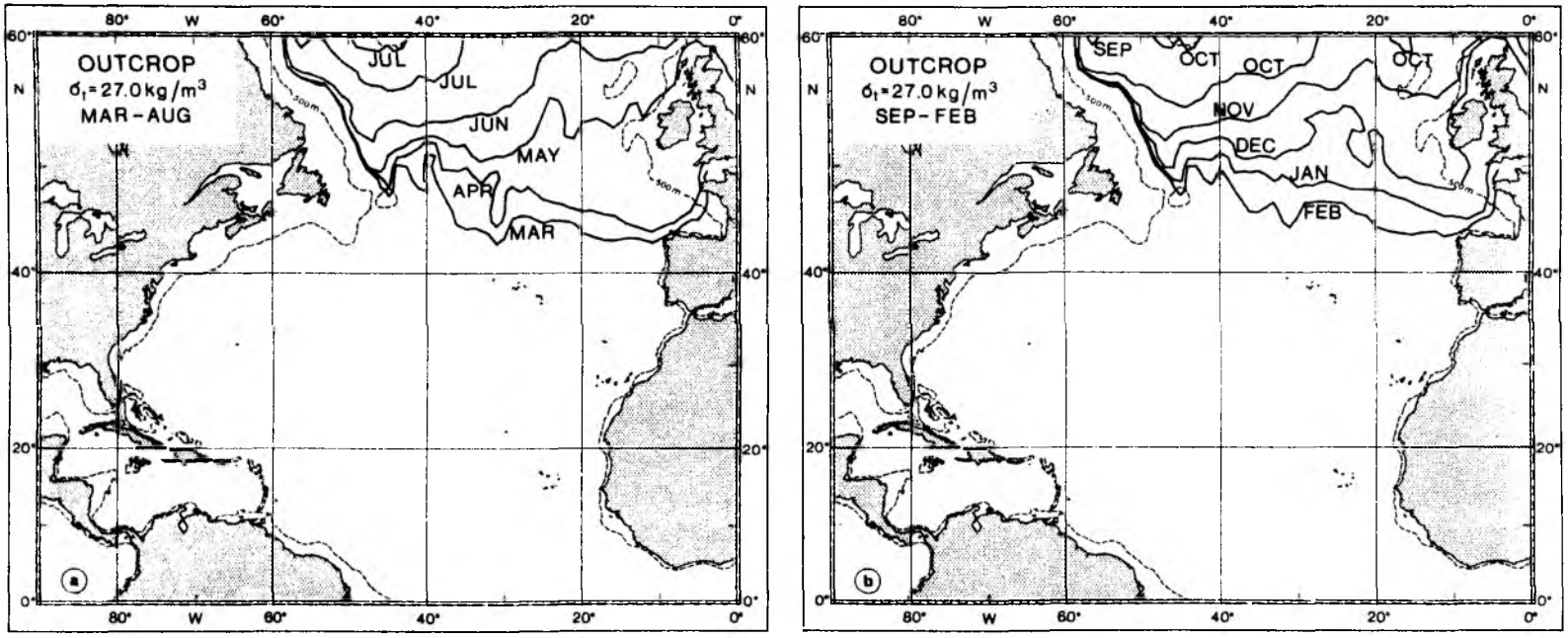

Seasonal migration of the outcrop of the isopycnal surface with σ_θ = 27.0 kg m^{-3};
(a) heating season, (b) cooling season.

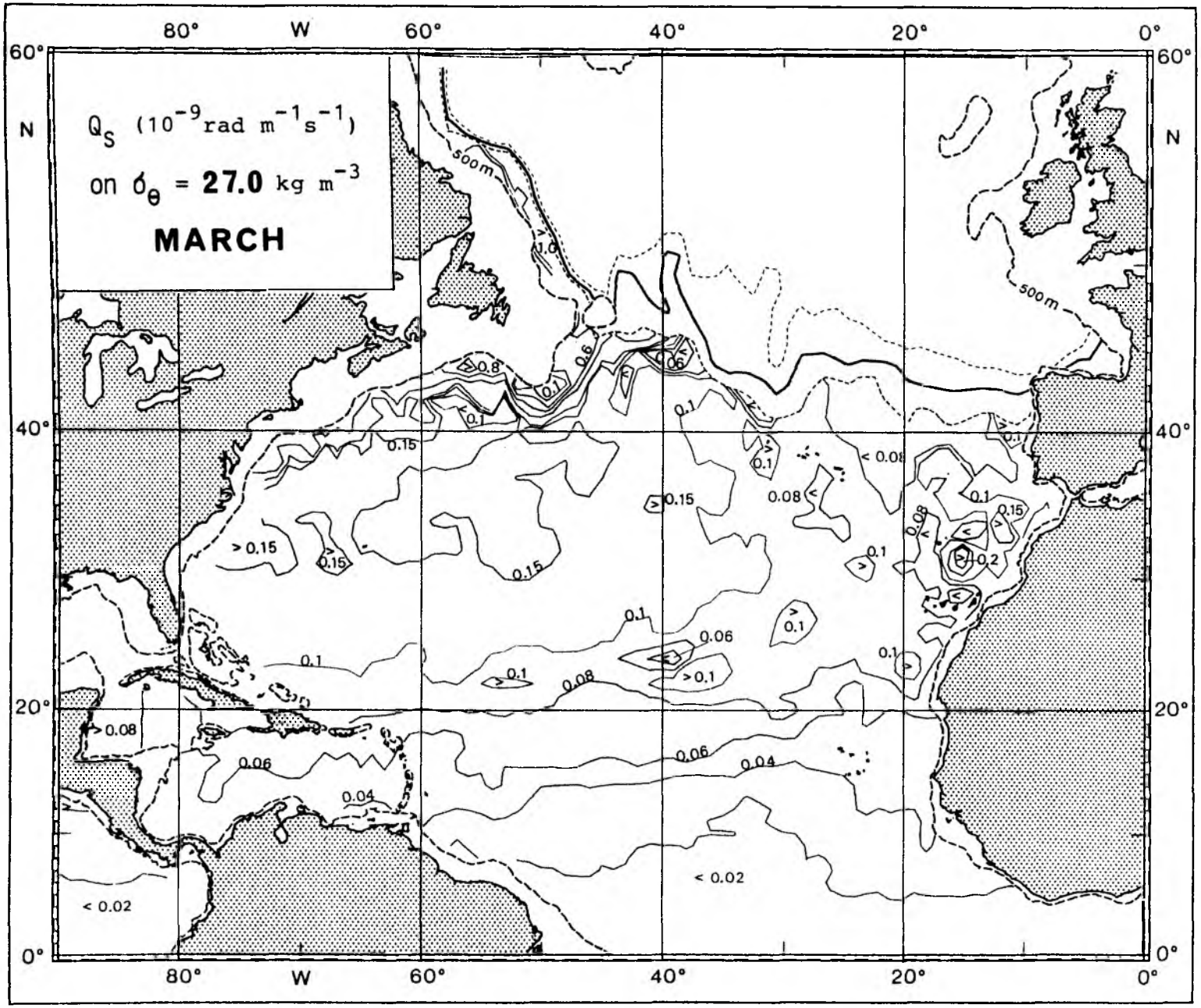
Q_S (10^{-9}rad $m^{-1}s^{-1}$)
on σ_θ = **27.0** kg m^{-3}
MARCH
80° W
60°
40°
20°
0°
60° N
40°
20°
0°
500m
1.0
0.8
0.6
0.1
0.15
0.08
0.2
0.06
0.04
0.02
< 0.02
< 0.08
> 0.15
> 0.1
> 0.08

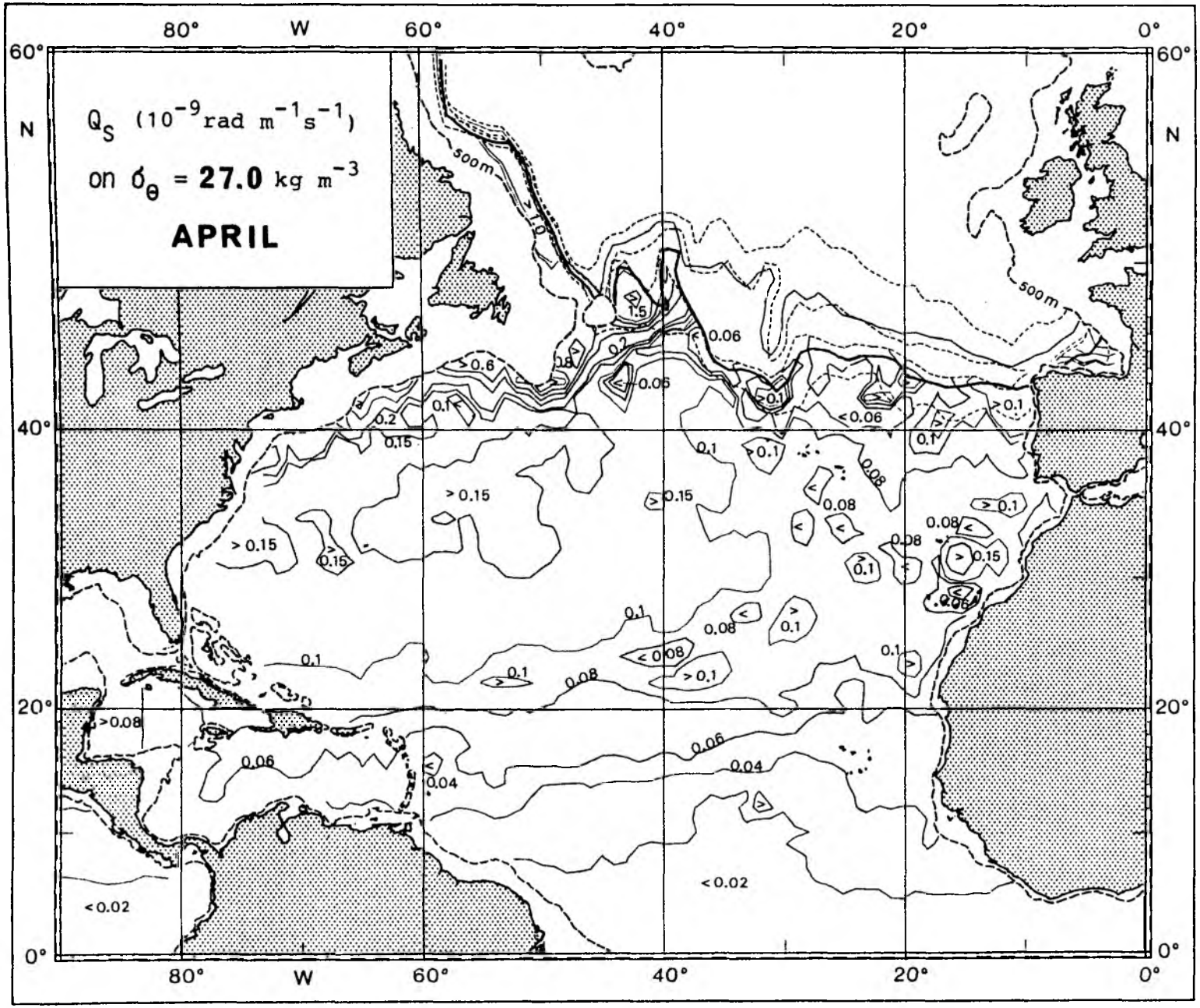
Q_S (10^{-9} rad $m^{-1}s^{-1}$)
on σ_θ = 27.0 kg m^{-3}
APRIL
80° W
60°
40°
20°
0°
60° N
40°
20°
0°
500 m
1.5
1.0
0.6
0.2
0.15
0.1
0.08
0.06
0.04
0.02
< 0.02

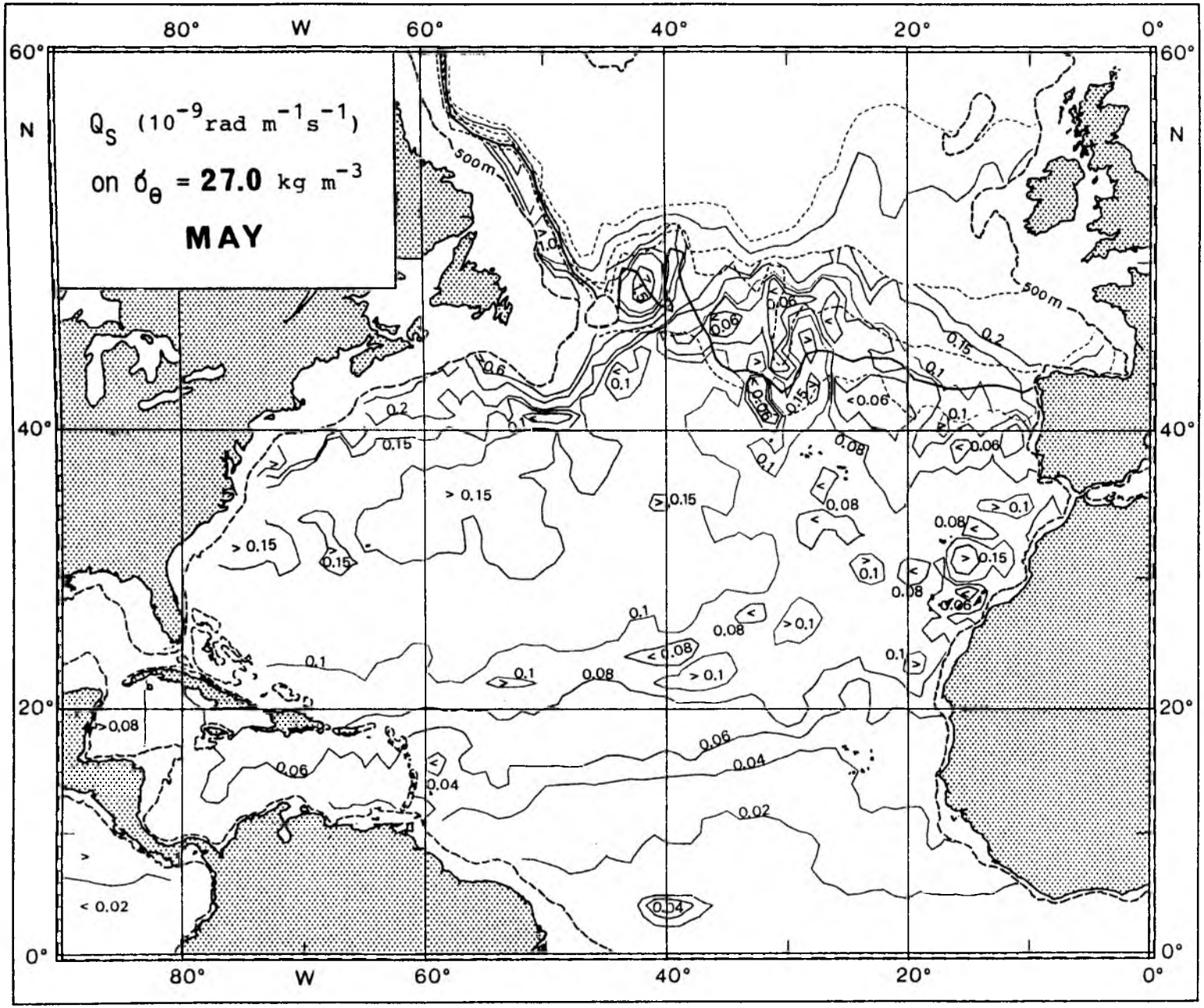
Q_S (10^{-9} rad $m^{-1}s^{-1}$)
on σ_θ = 27.0 kg m^{-3}
MAY
80° W
60°
40°
20°
0°
60° N
40°
20°
0°
500m
0.2
0.15
0.1
0.08
0.06
0.04
0.02
> 0.15
< 0.02

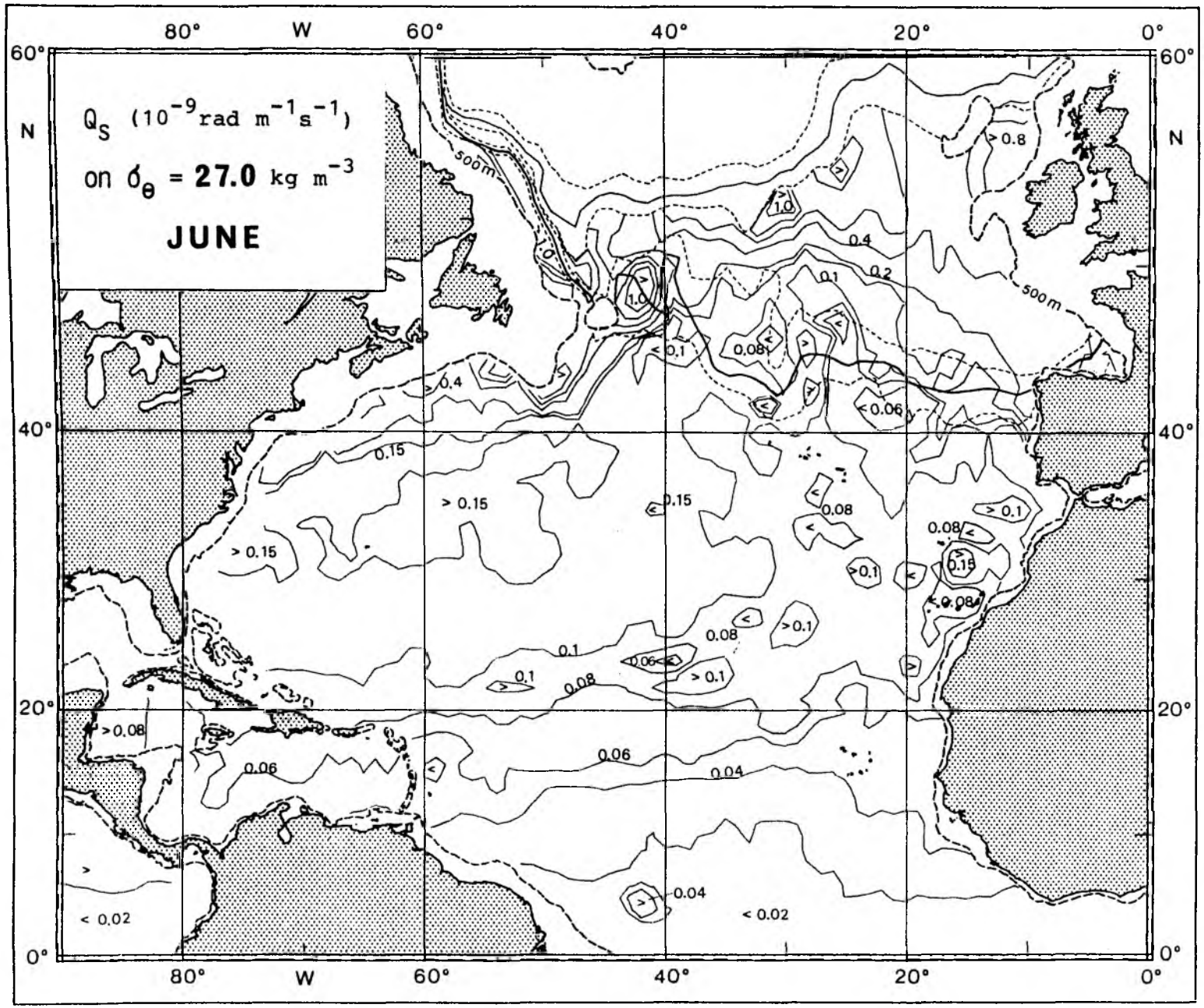
Q_S (10^{-9} rad $m^{-1}s^{-1}$)
on σ_θ = 27.0 kg m^{-3}
JUNE
80° W
60°
40°
20°
0°
60° N
40°
20°
0°
500m
> 0.8
1.0
0.4
0.2
0.1
< 0.1
0.08
< 0.06
> 0.4
0.15
> 0.15
< 0.02
> 0.1
0.06
0.04

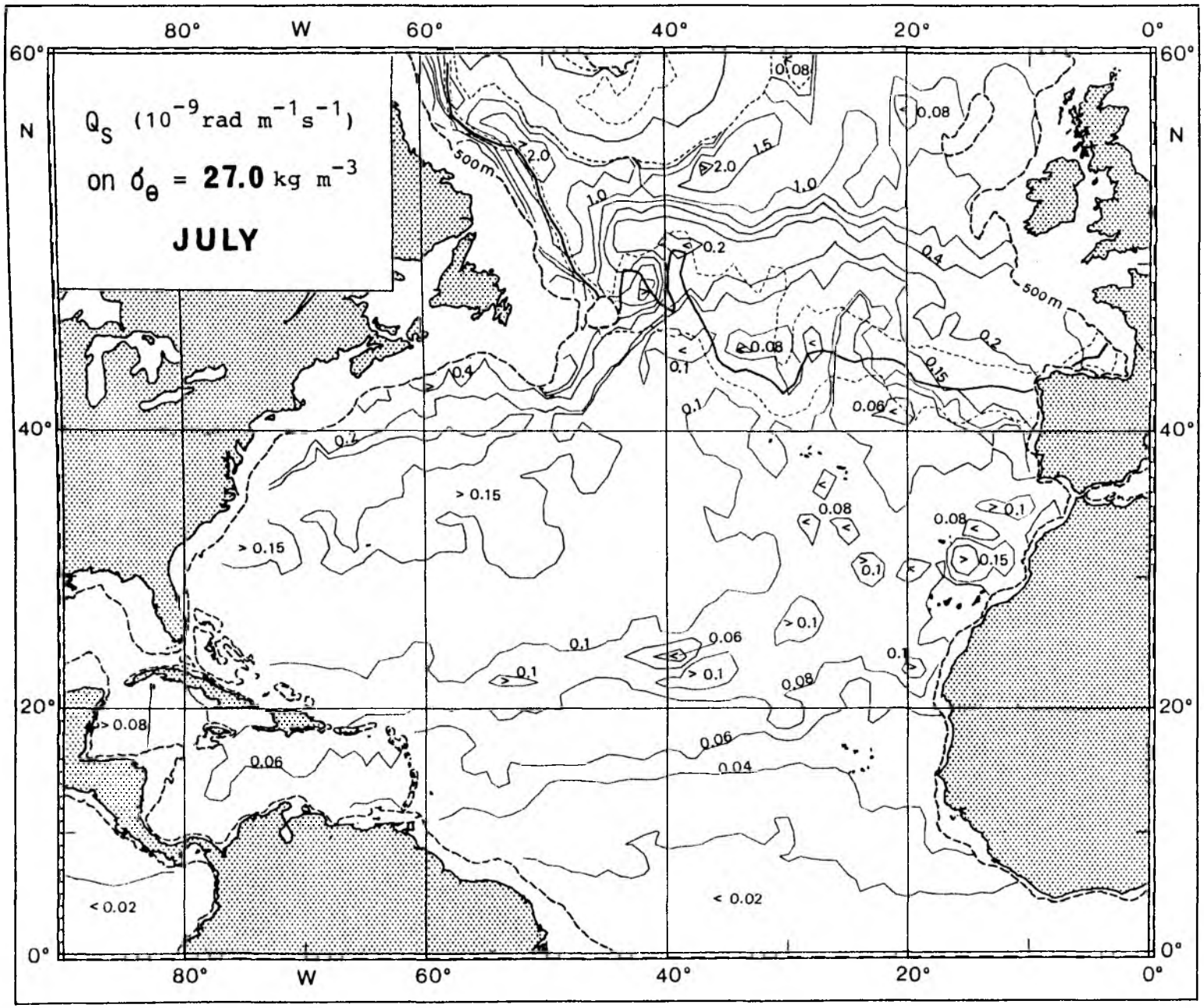
Q_S (10^{-9}rad $m^{-1}s^{-1}$)
on σ_θ = 27.0 kg m^{-3}
JULY
80° W
60°
40°
20°
0°
60° N
40°
20°
0°
500m
> 0.15
< 0.02
> 0.08
0.06
0.04
> 0.1
0.1
0.08
0.2
0.4
1.0
1.5
2.0
0.15
0.06

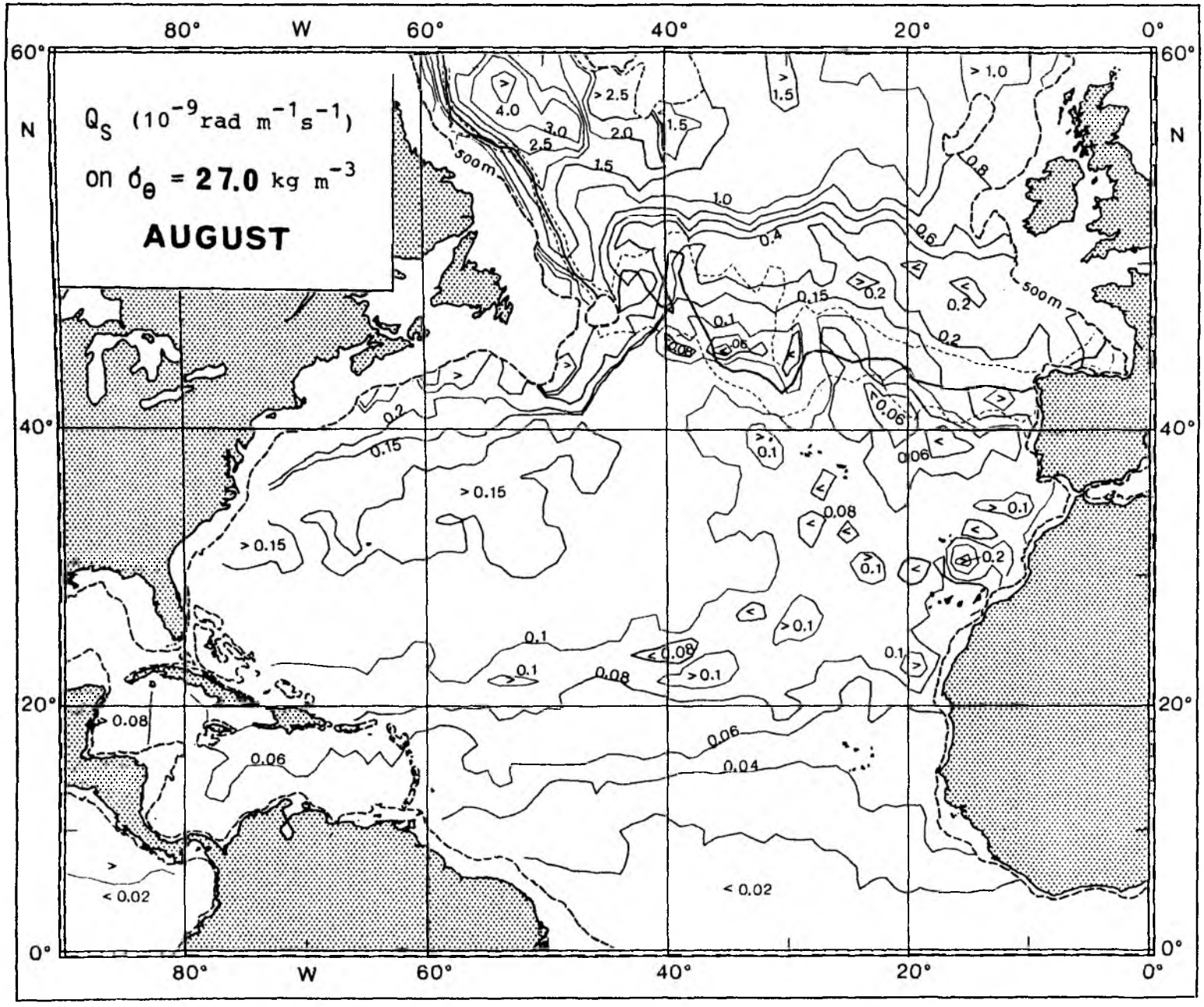
Q_S (10^{-9} rad $m^{-1}s^{-1}$)
on σ_θ = 27.0 kg m^{-3}
AUGUST
80° W
60°
40°
20°
0°
60° N
40°
20°
0°
500m
> 4.0
> 2.5
3.0
2.5
2.0
1.5
> 1.5
> 1.0
1.0
0.8
0.6
0.4
0.2
0.15
0.1
0.08
0.06
> 0.15
> 0.1
< 0.08
< 0.06
< 0.02
0.04

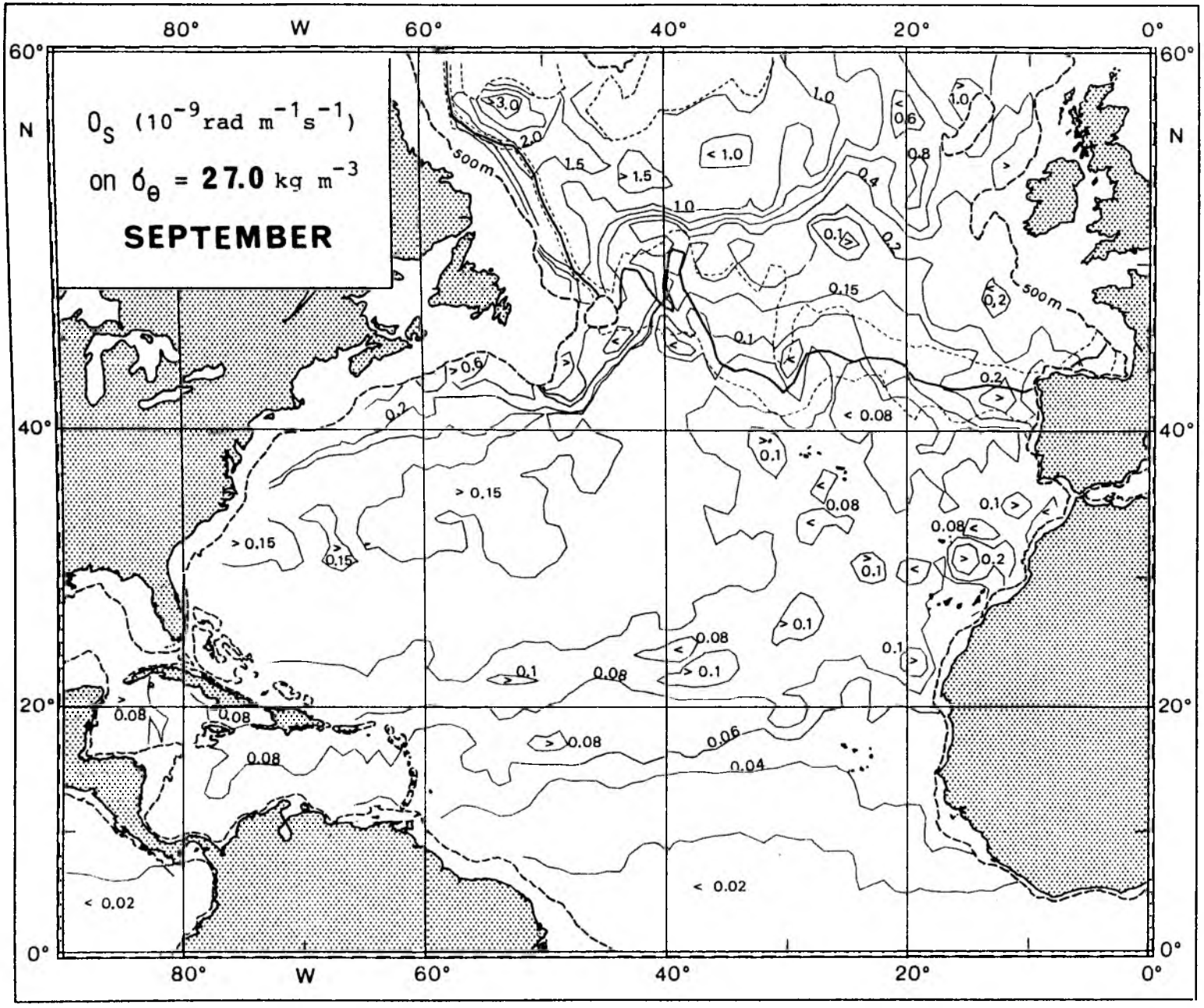
O_S (10^{-9} rad $m^{-1}s^{-1}$)
on σ_θ = 27.0 kg m^{-3}
SEPTEMBER
80° W
60°
40°
20°
0°
60° N
40°
20°
0°
500m
3.0
2.0
1.5
1.0
< 1.0
> 1.5
0.6
0.8
0.4
0.2
0.15
0.1
< 0.08
0.08
0.06
0.04
< 0.02

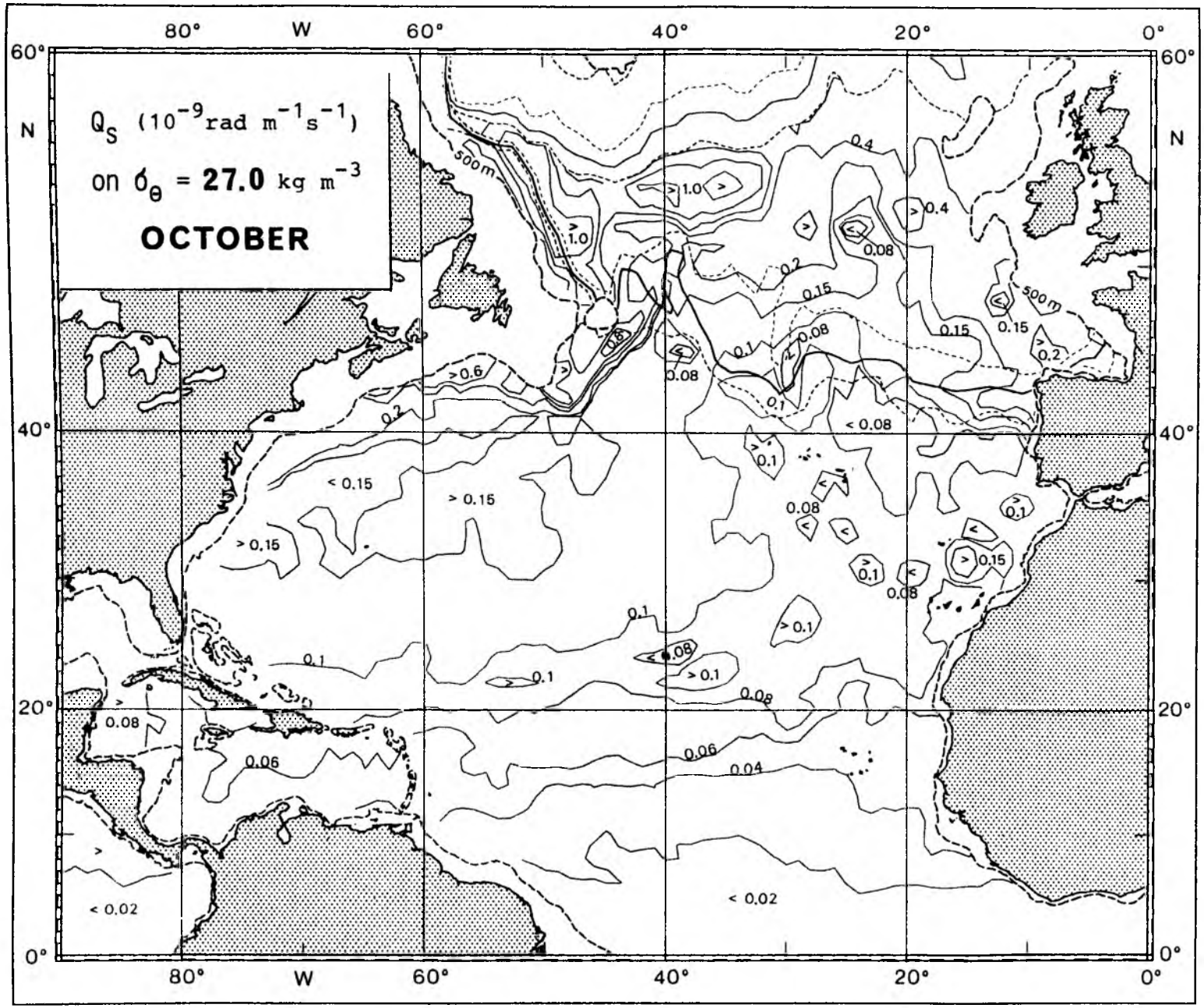
Q_S (10^{-9}rad $m^{-1}s^{-1}$)
on σ_θ = 27.0 kg m^{-3}
OCTOBER
80° W
60°
40°
20°
0°
60° N
40°
20°
0°
500m
1.0
0.4
0.2
0.15
0.1
0.08
0.06
0.04
0.02
> 0.6
< 0.15
> 0.15
> 0.1
< 0.08
< 0.02

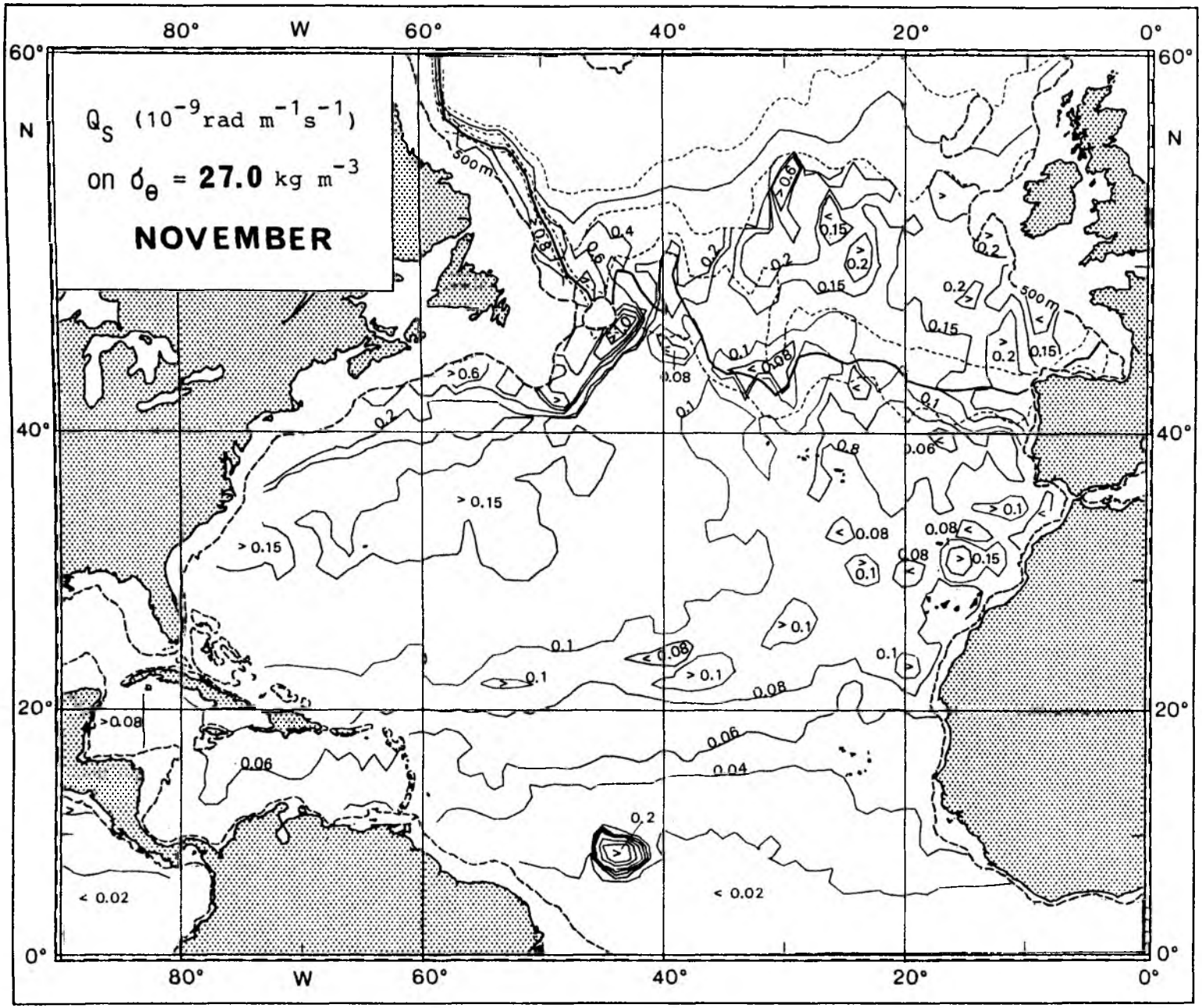
Q_S (10^{-9} rad $m^{-1}s^{-1}$)
on σ_θ = **27.0** kg m^{-3}
NOVEMBER
80° W
60°
40°
20°
0°
60° N
40°
20°
0°
500m
> 0.6
0.4
0.2
0.15
0.1
0.08
0.06
0.04
> 0.15
> 0.1
> 0.08
< 0.02

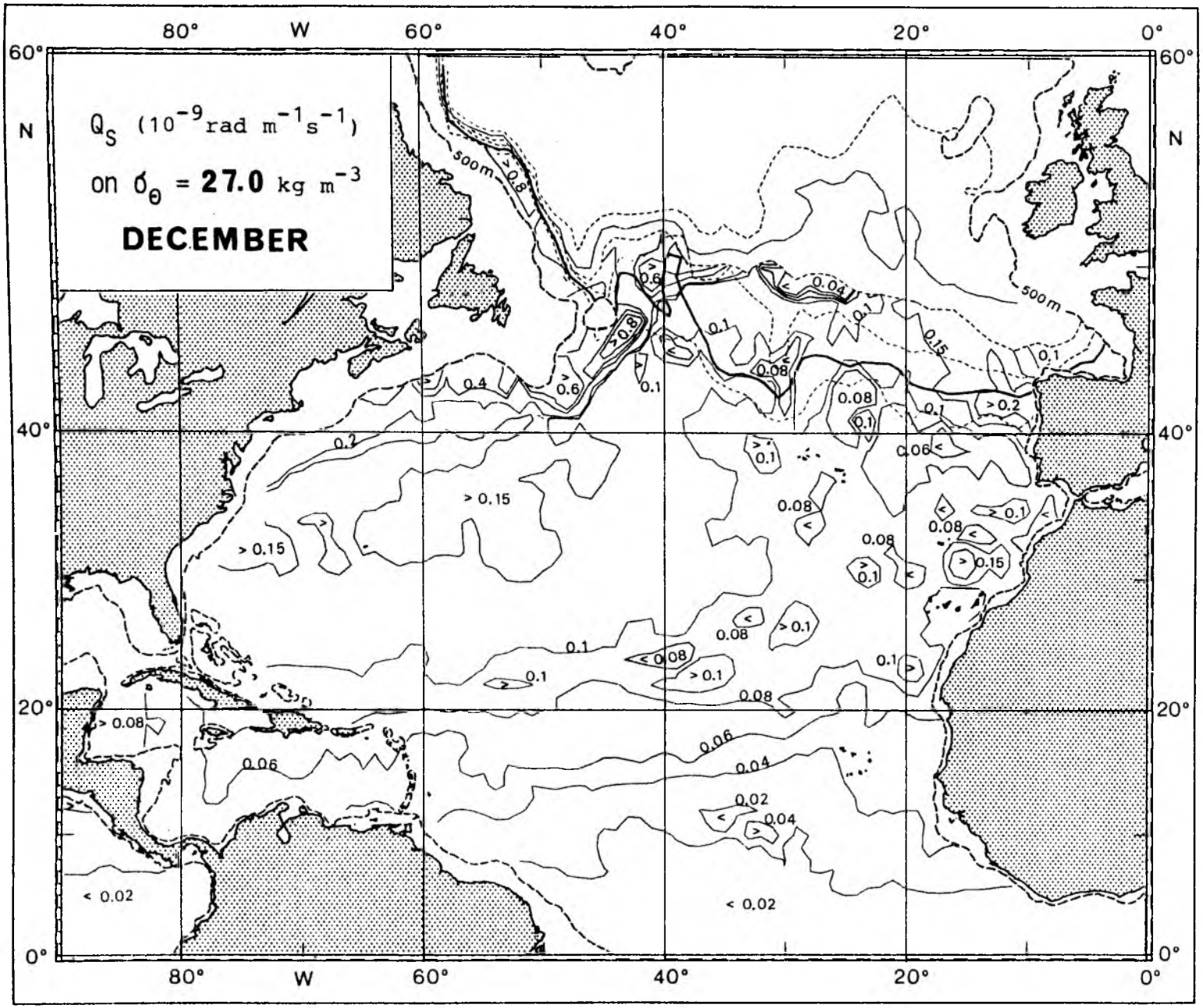
Q_S (10^{-9} rad $m^{-1}s^{-1}$)
on σ_θ = 27.0 kg m^{-3}
DECEMBER
80° W
60°
40°
20°
0°
60° N
40°
20°
0°
500m
> 0.8
> 0.6
0.4
0.2
> 0.15
0.1
0.08
0.06
0.04
0.02
> 0.2
< 0.02

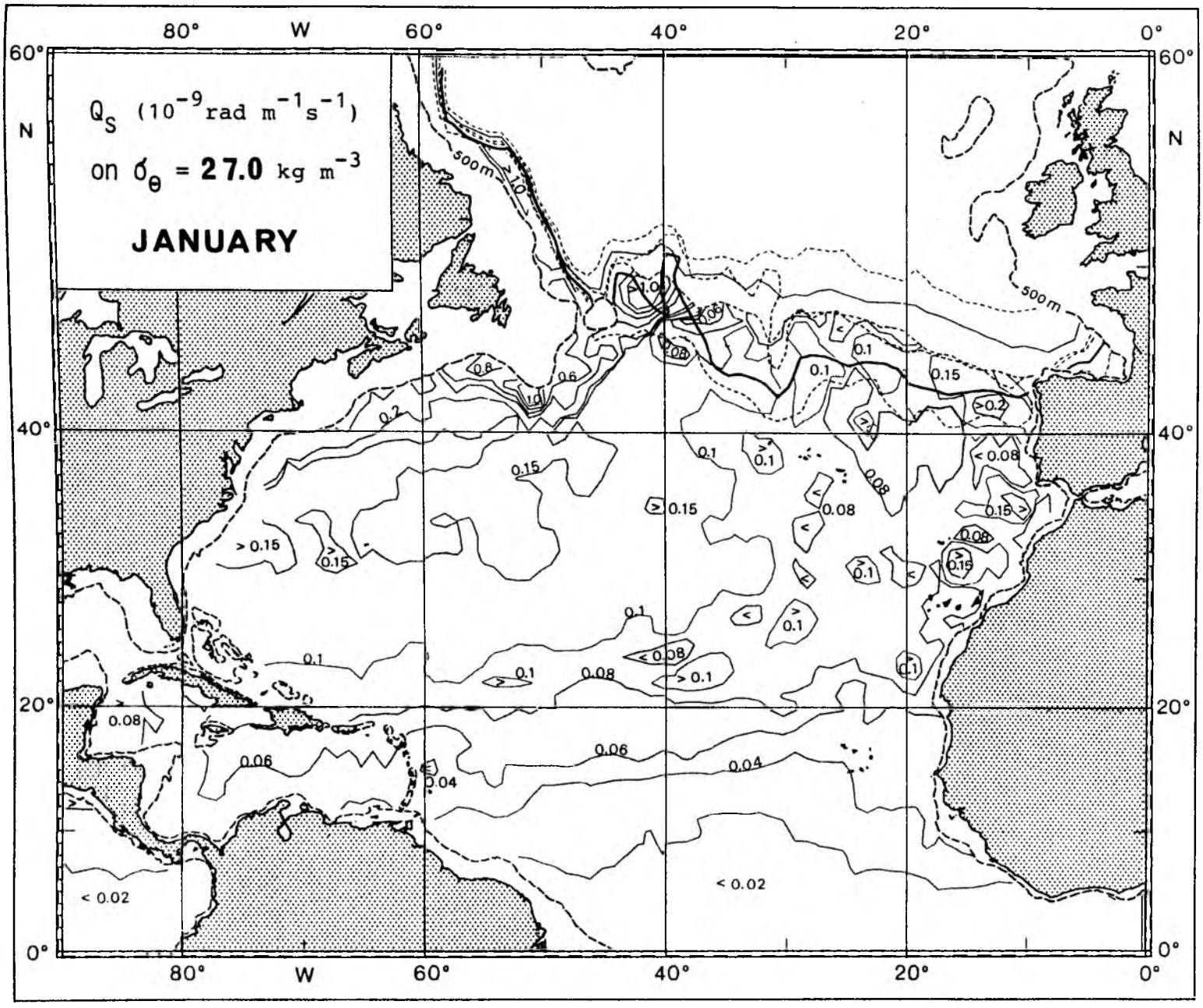
Q_S (10^{-9} rad $m^{-1}s^{-1}$)
on σ_θ = 27.0 kg m^{-3}
JANUARY
80° W
60°
40°
20°
0°
60° N
40°
20°
0°
500 m
< 0.02
0.04
0.06
0.08
0.1
0.15
0.2
0.6
0.8
1.0

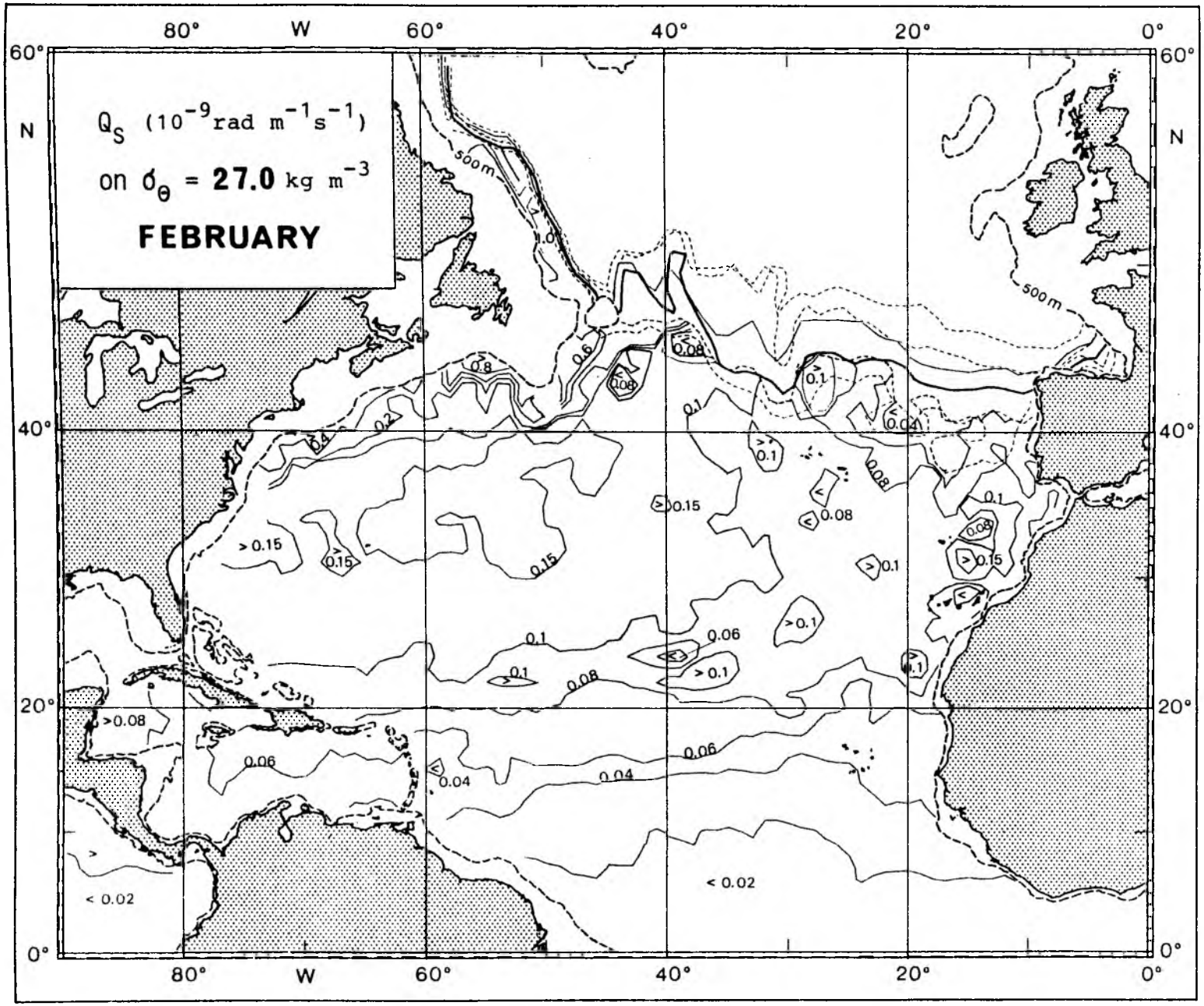
Q_S (10^{-9} rad $m^{-1}s^{-1}$)
on σ_θ = 27.0 kg m^{-3}
FEBRUARY
80° W
60°
40°
20°
0°
60° N
40°
20°
0°
500 m
0.8
0.6
0.4
0.2
0.08
0.1
0.04
0.15
0.06
0.02

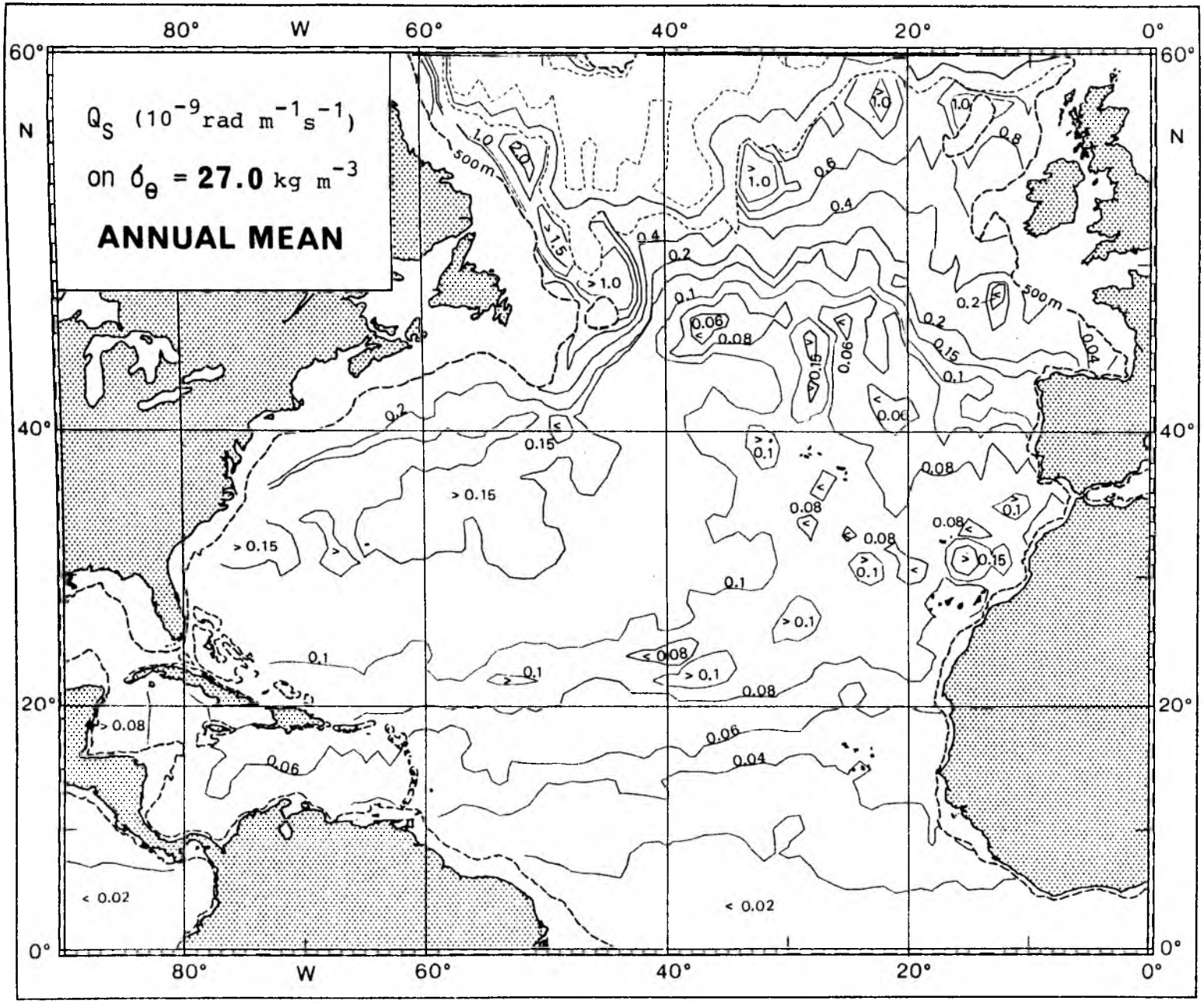
Q_S (10^{-9}rad $m^{-1}s^{-1}$)
on σ_θ = 27.0 kg m^{-3}
ANNUAL MEAN
80° W 60° 40° 20° 0°
60° N
40°
20°
0°
500m
1.0
2.0
0.8
0.6
0.4
0.2
0.1
0.08
0.06
0.04
0.15
> 1.0
> 0.15
> 0.1
< 0.08
< 0.02

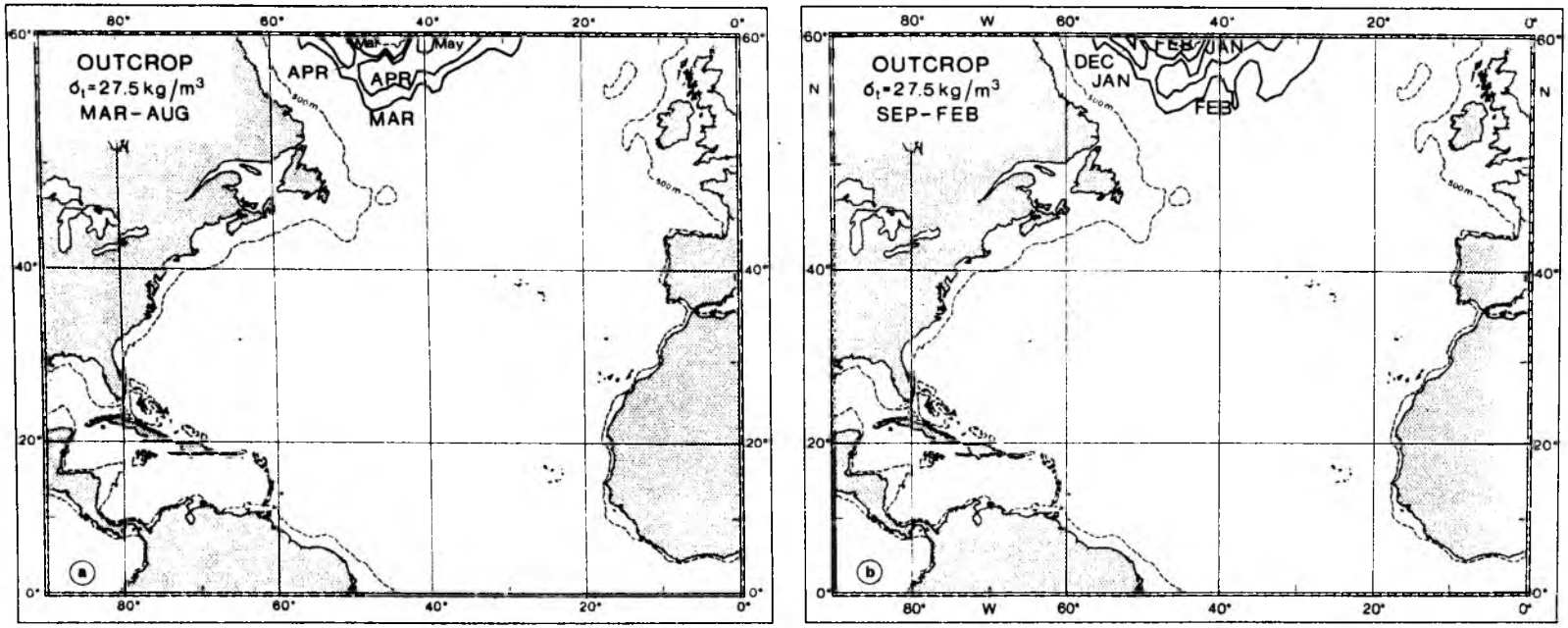

Seasonal migration of the outcrop of the isopycnal surface with σ_θ = 27.5 kg m^{-3};
(a) heating season, (b) cooling season.

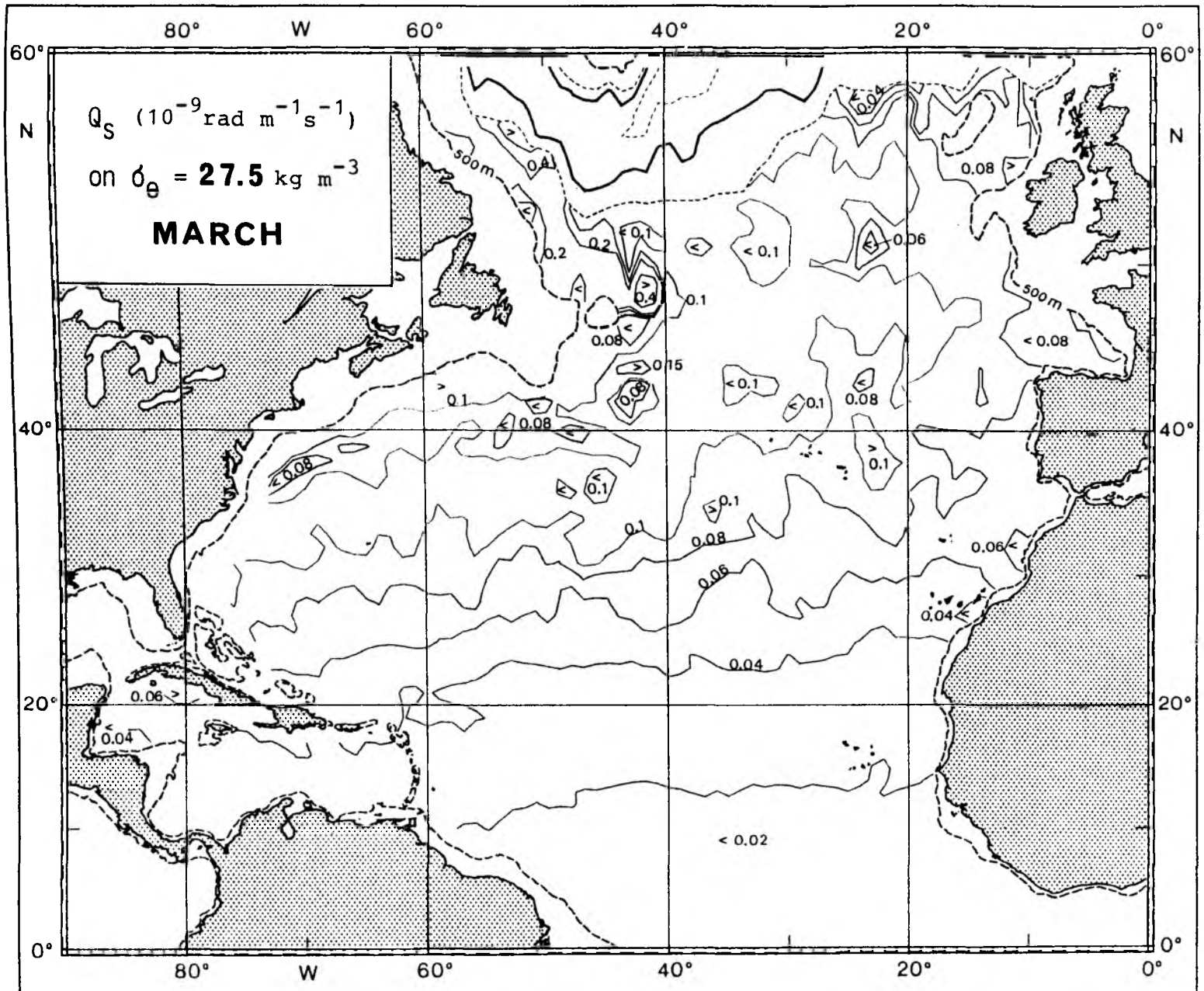
Q_S (10^{-9} rad $m^{-1}s^{-1}$)
on σ_θ = 27.5 kg m^{-3}
MARCH
80° W
60°
40°
20°
0°
60° N
40°
20°
0°
500m
< 0.1
0.1
0.2
0.08
0.15
0.06
0.04
0.02

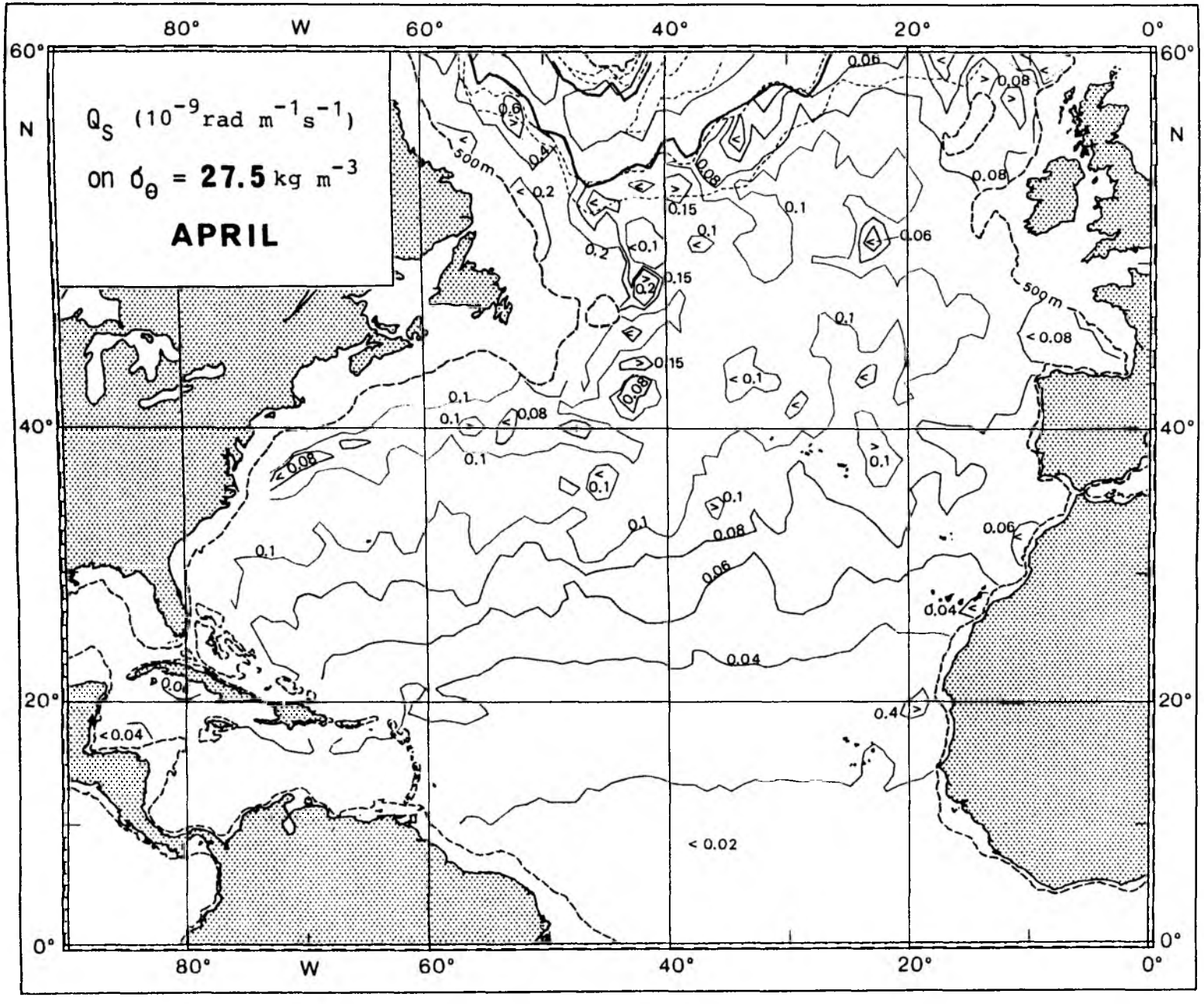
Q_S (10^{-9} rad $m^{-1}s^{-1}$)
on σ_θ = 27.5 kg m^{-3}
APRIL
80° W
60°
40°
20°
0°
60° N
40°
20°
0°
500m
< 0.02

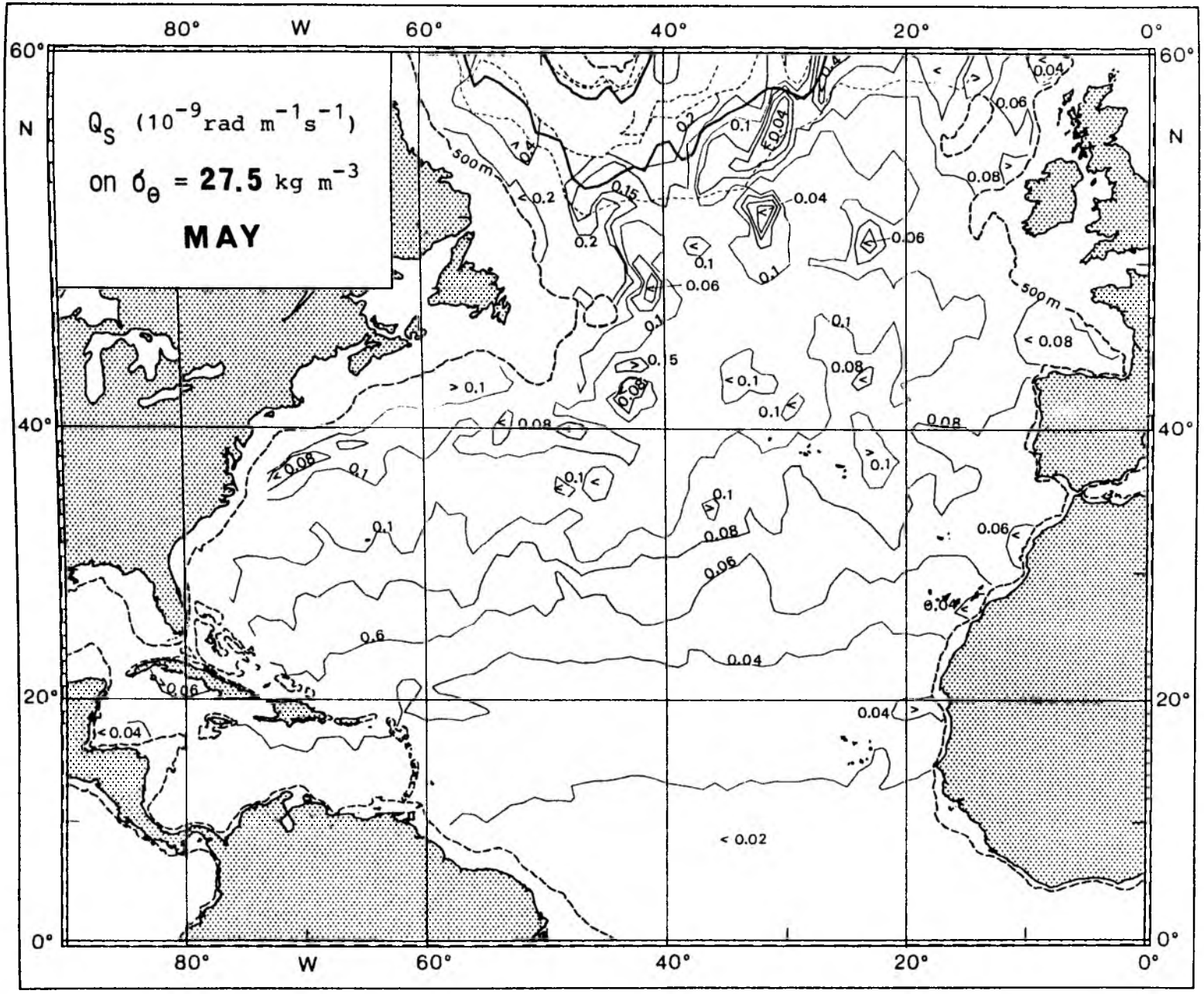
Q_S (10^{-9}rad $m^{-1}s^{-1}$)
on σ_θ = 27.5 kg m^{-3}
MAY
80° W
60°
40°
20°
0°
60° N
40°
20°
0°
500m
< 0.02
< 0.04
0.04
0.06
0.08
0.1
0.2
0.5
0.6

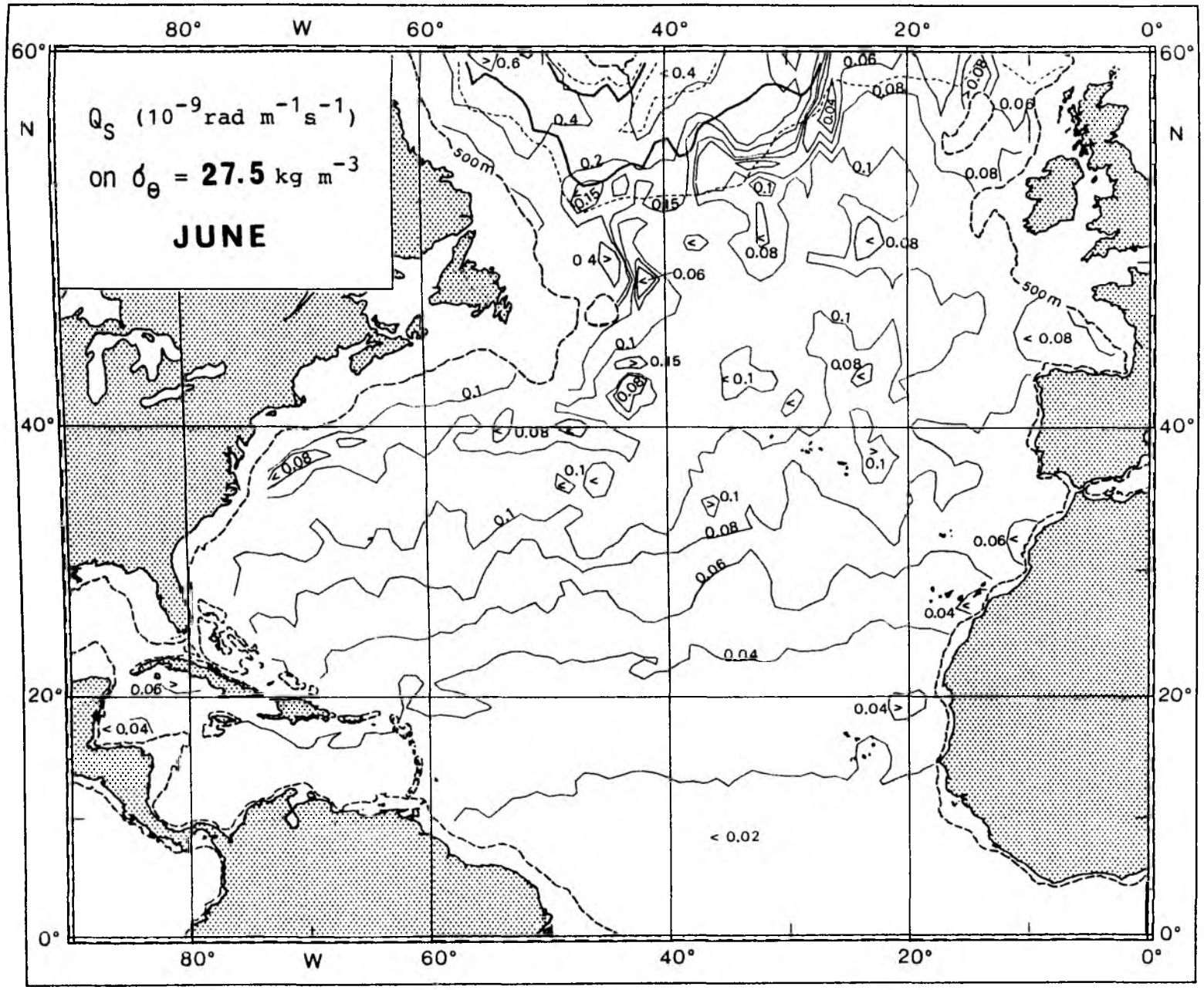
Q_S (10^{-9} rad m^{-1} s^{-1})
on σ_θ = 27.5 kg m^{-3}
JUNE
80° W
60°
40°
20°
0°
60° N
40°
20°
0°
500m
> 0.6
0.4
0.2
0.15
0.1
0.08
0.06
0.04
< 0.02

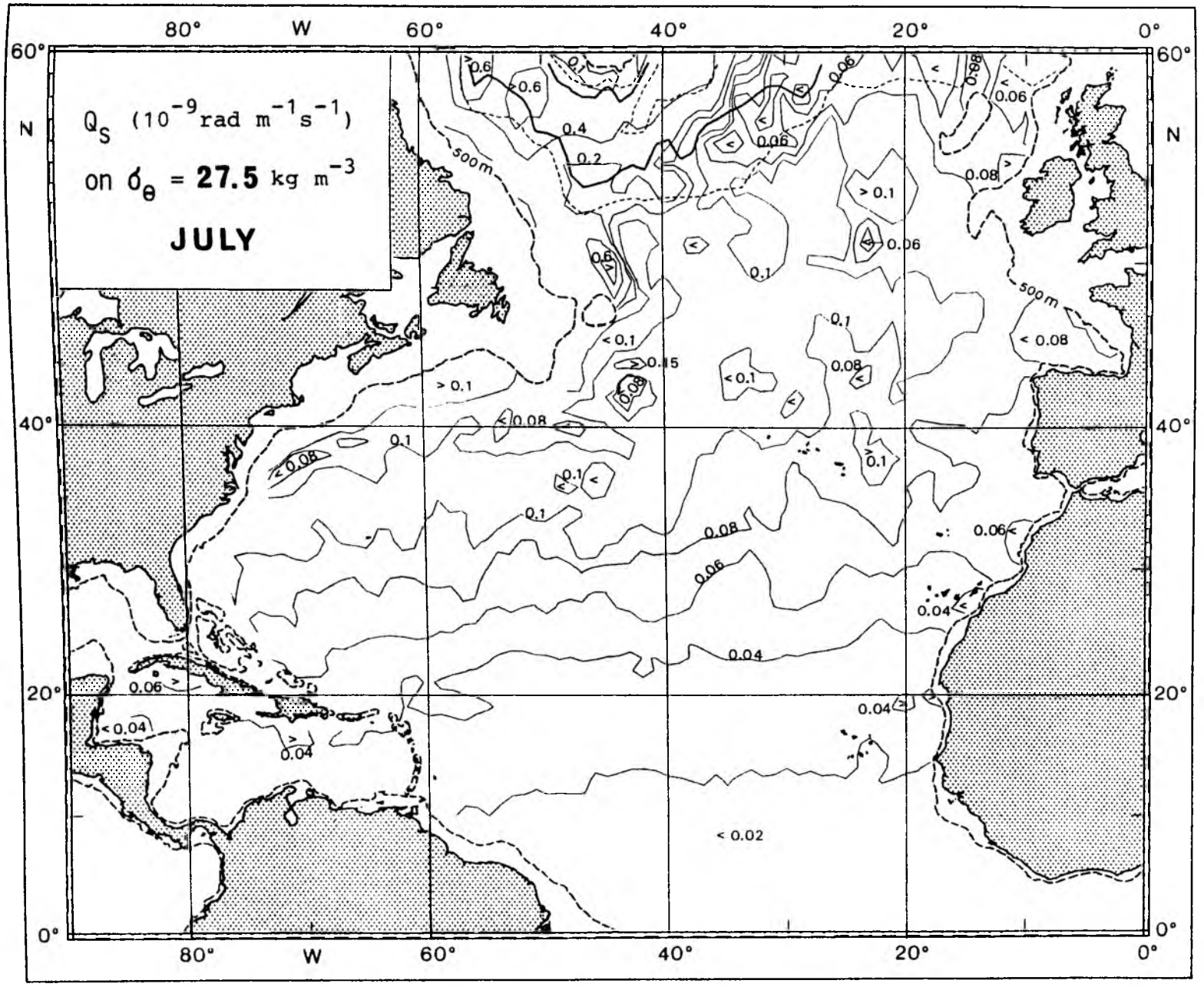
Q_S (10^{-9} rad $m^{-1}s^{-1}$)
on σ_θ = 27.5 kg m^{-3}
JULY
80° W
60°
40°
20°
0°
60° N
40°
20°
0°
500m
> 0.6
0.4
0.2
0.1
< 0.1
> 0.1
0.15
0.08
< 0.08
0.06
< 0.06
0.04
< 0.04
< 0.02

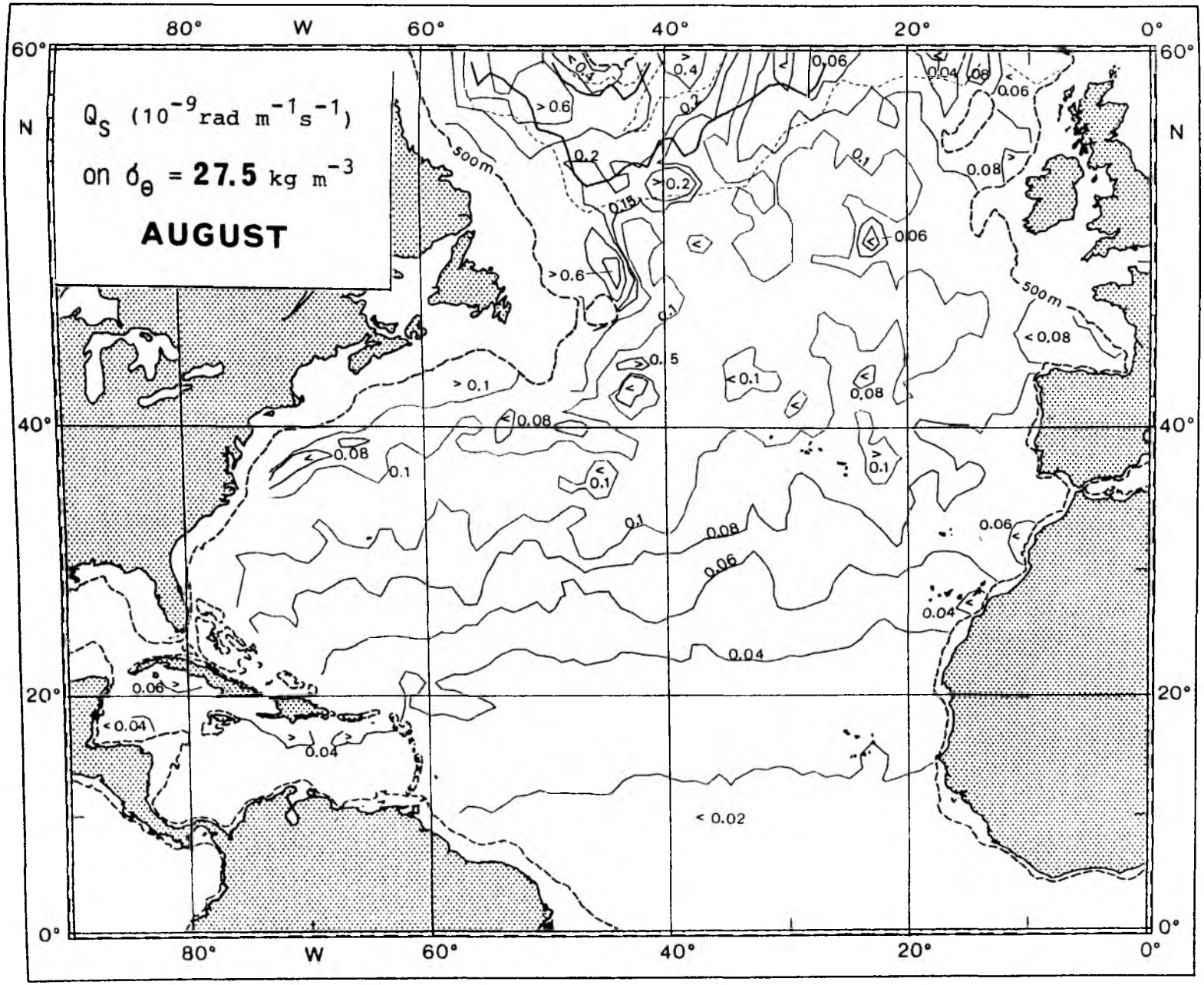
Q_S (10^{-9} rad $m^{-1}s^{-1}$)
on σ_θ = 27.5 kg m^{-3}
AUGUST
80° W
60°
40°
20°
0°
60° N
40°
20°
0°
500m
< 0.04
> 0.4
0.2
> 0.6
0.15
> 0.2
0.1
< 0.06
0.08
< 0.08
> 0.1
0.5
< 0.1
0.06
0.04
< 0.02

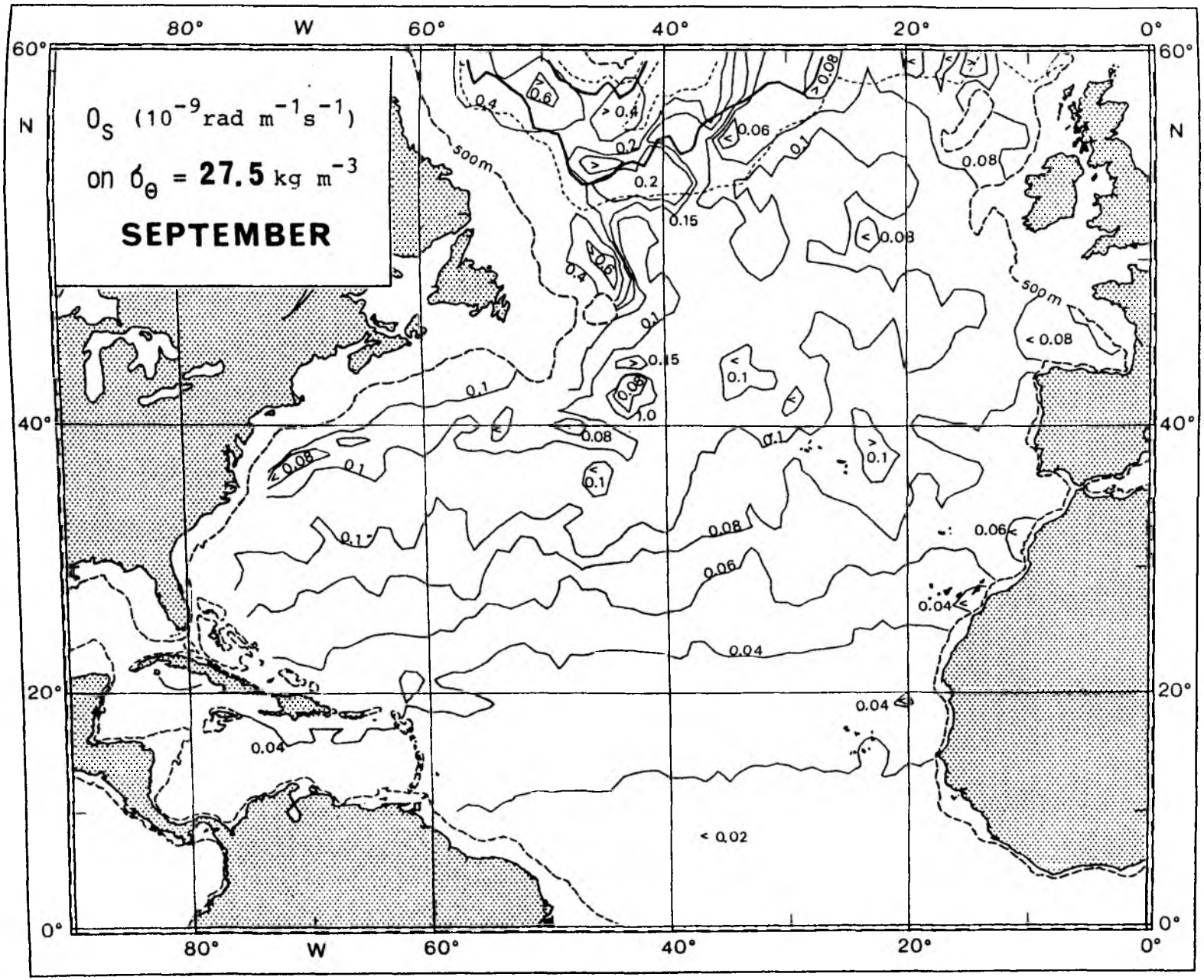
O_S (10^{-9} rad $m^{-1}s^{-1}$)
on σ_θ = 27.5 kg m^{-3}
SEPTEMBER
80° W
60°
40°
20°
0°
60° N
40°
20°
0°
500m
0.4
0.6
0.2
0.15
0.1
0.08
0.06
0.04
1.0
< 0.02

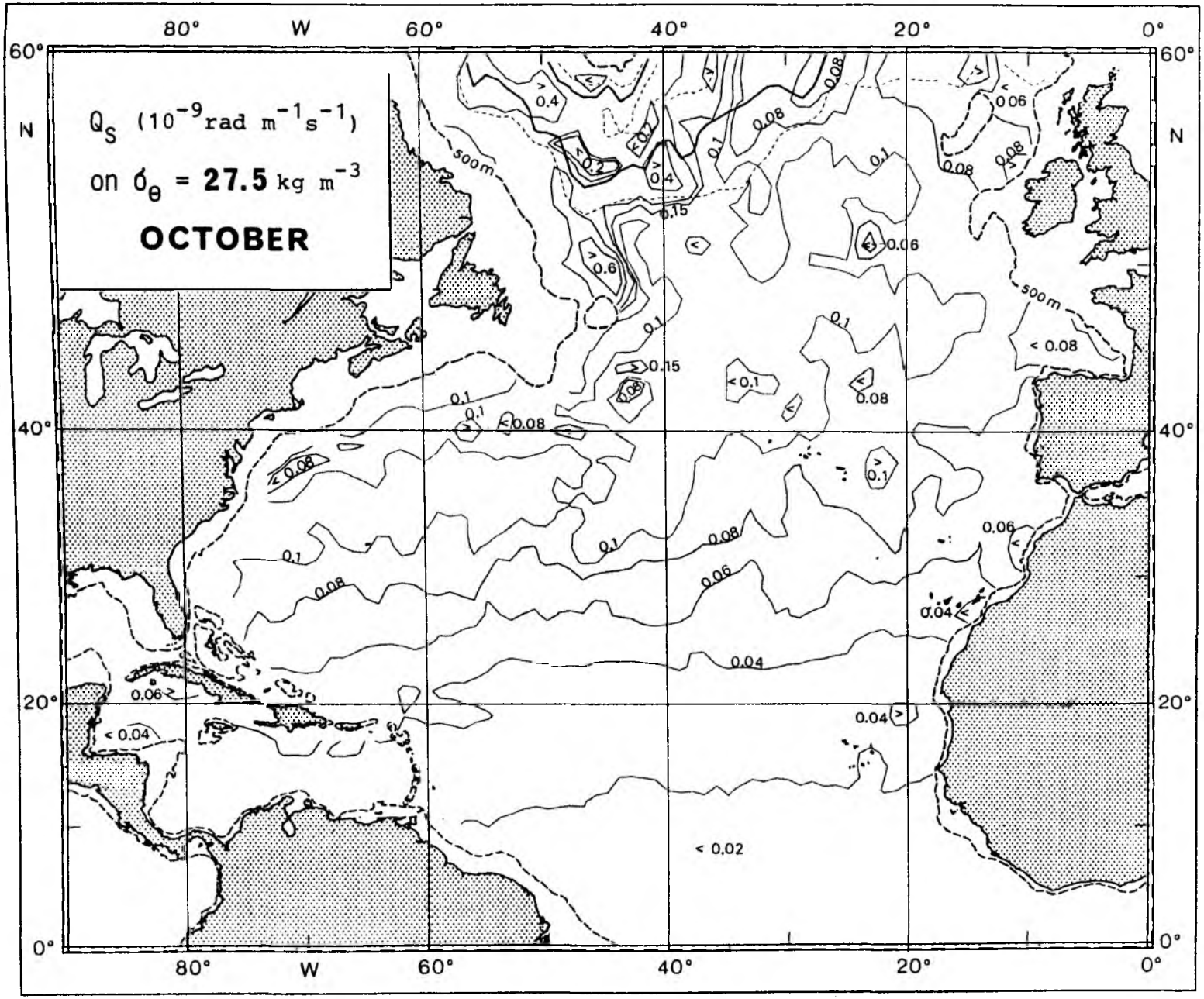
Q_S (10^{-9} rad $m^{-1}s^{-1}$)
on σ_θ = 27.5 kg m^{-3}
OCTOBER
80° W
60°
40°
20°
0°
60° N
40°
20°
0°
500m
< 0.08
< 0.1
< 0.02
< 0.04
0.06
0.08
0.1
0.15
0.4
0.6

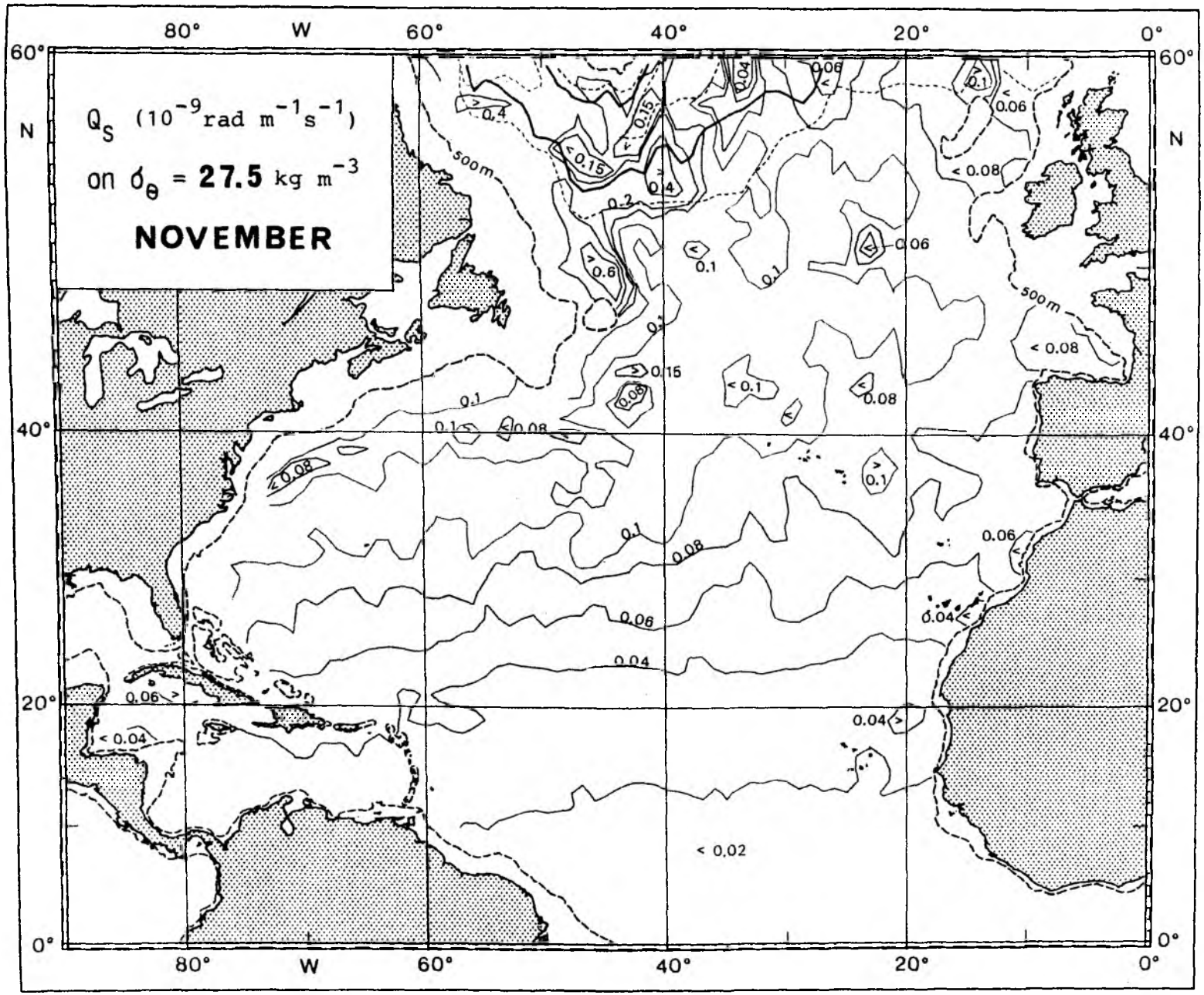
Q_S (10^{-9}rad $m^{-1}s^{-1}$)
on σ_θ = 27.5 kg m^{-3}
NOVEMBER
80° W
60°
40°
20°
0°
60° N
40°
20°
0°
500m
< 0.02

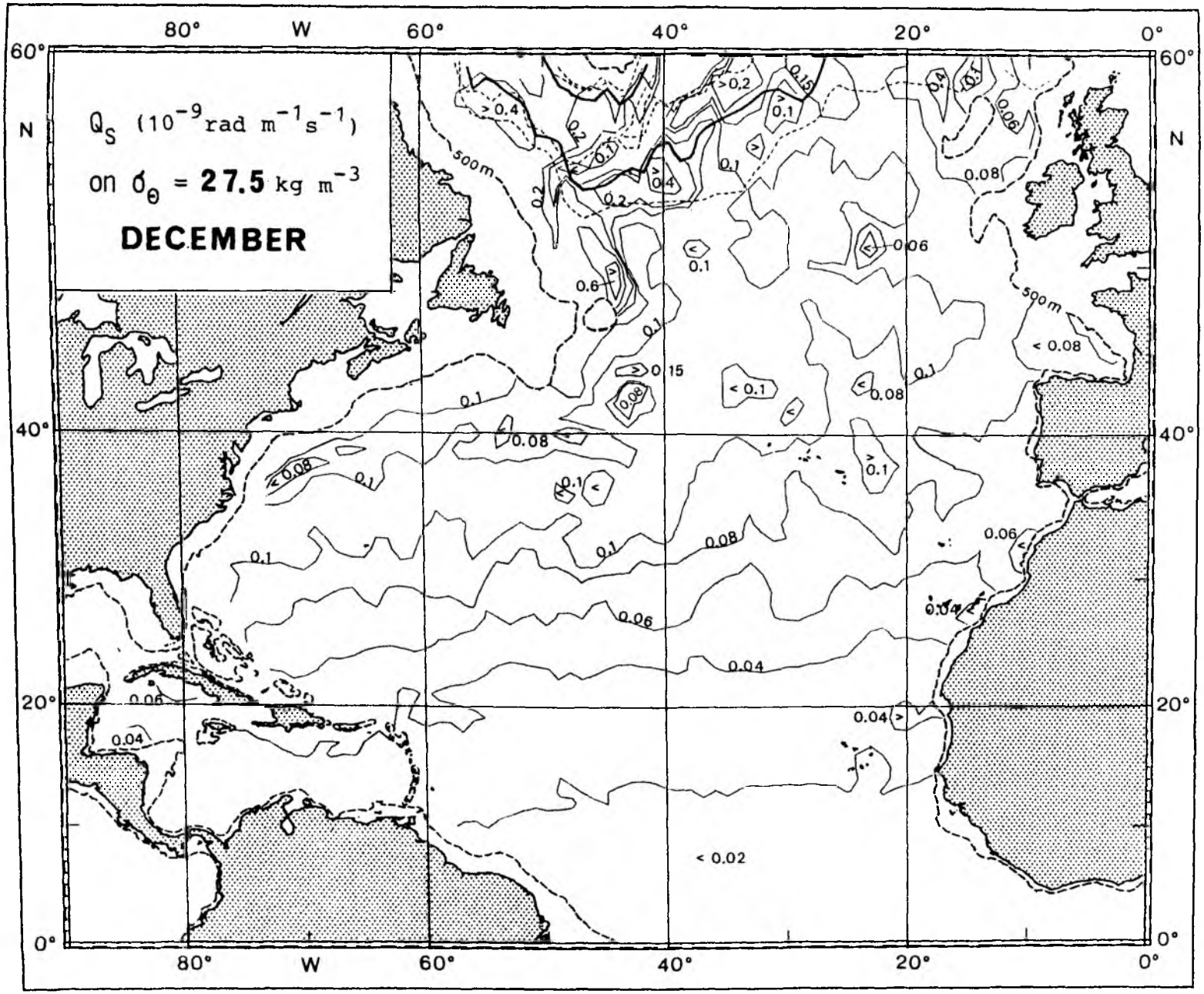
Q_S (10^{-9} rad $m^{-1}s^{-1}$)
on σ_Θ = 27.5 kg m^{-3}
DECEMBER
80° W
60°
40°
20°
0°
60° N
40°
20°
0°
500m
< 0.02
< 0.08
< 0.1
0.1
0.2
0.4
0.6
0.08
0.06
0.04
0.15

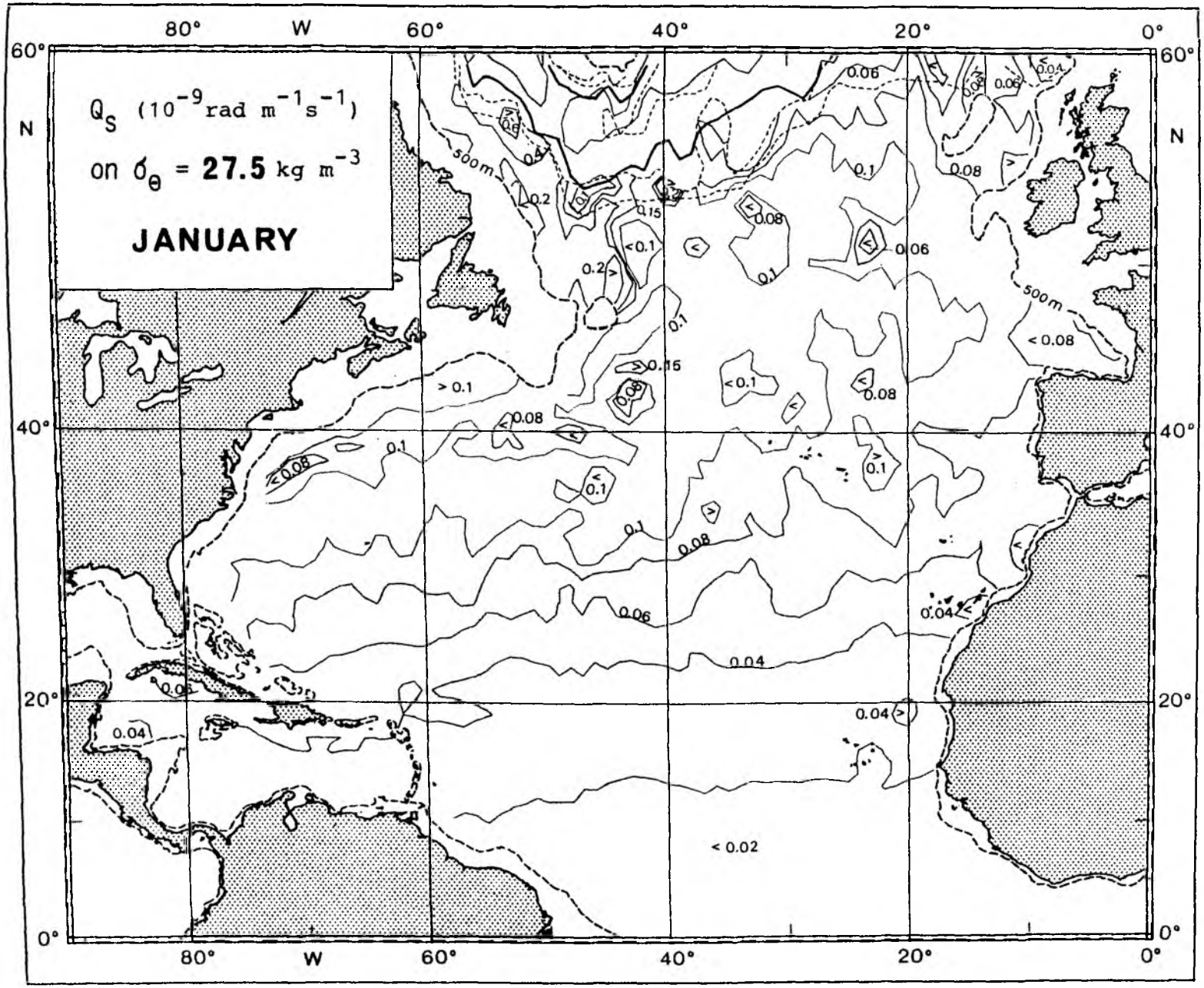
Q_S (10^{-9} rad $m^{-1}s^{-1}$)
on σ_θ = 27.5 kg m^{-3}
JANUARY
80° W
60°
40°
20°
0°
60° N
40°
20°
0°
500m
0.06
0.08
0.1
0.2
0.15
0.04
0.02
< 0.1
> 0.1
< 0.08
< 0.02

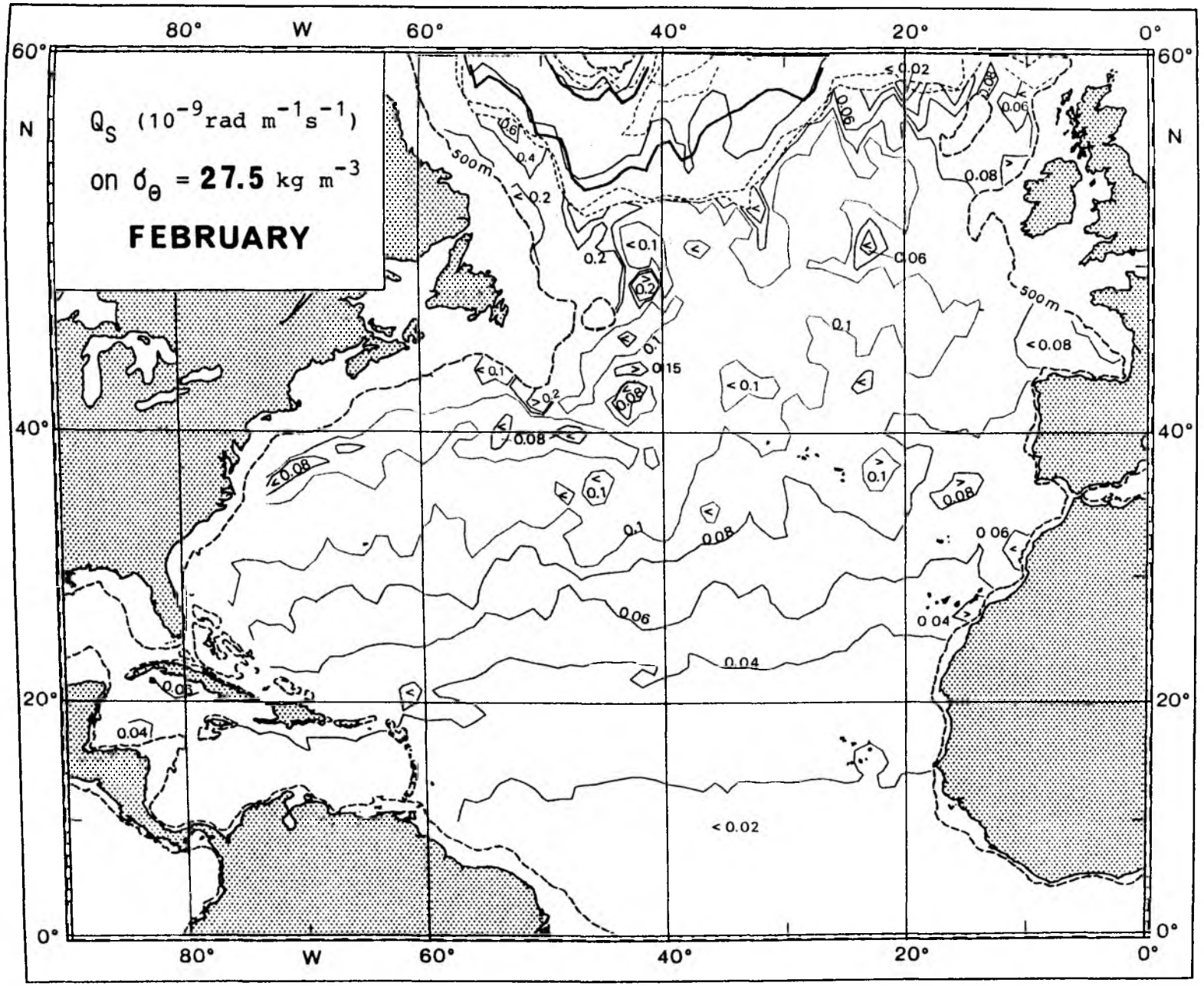
Q_S (10^{-9}rad $m^{-1}s^{-1}$)
on σ_θ = 27.5 kg m^{-3}
FEBRUARY
80° W
60°
40°
20°
0°
60° N
40°
20°
0°
500m
< 0.02
0.4
0.2
< 0.1
0.1
0.15
0.08
0.06
0.04

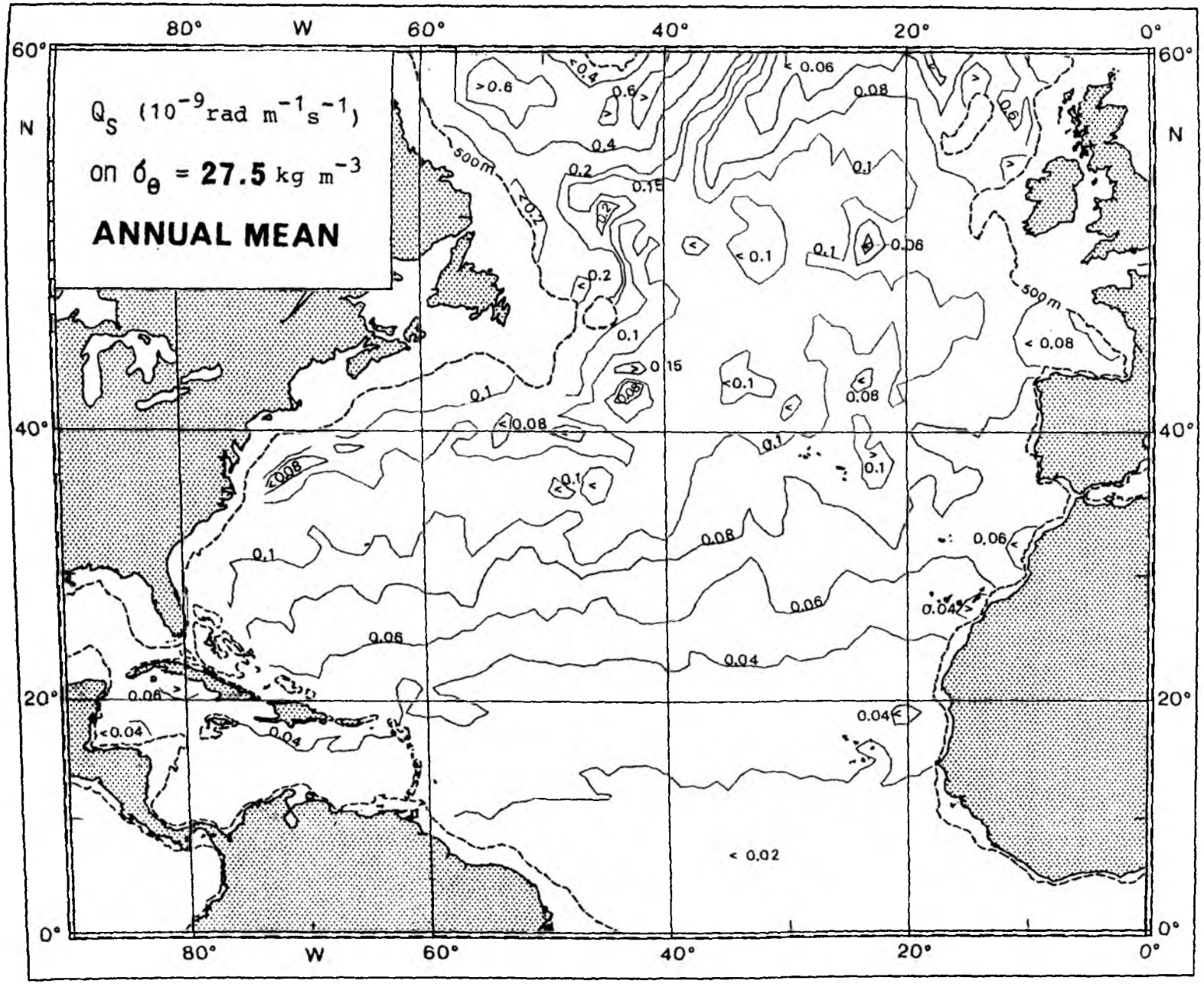
Q_S (10^{-9}rad $m^{-1}s^{-1}$)
on σ_θ = 27.5 kg m^{-3}
ANNUAL MEAN
80° W
60°
40°
20°
0°
60° N
40°
20°
0°
500m
> 0.6
0.6 >
0.4
0.2
0.15
0.1
< 0.1
0.1
0.06
< 0.06
0.08
0.6
0.2
0.1
0.15
0.08
< 0.08
0.1
< 0.08
0.1
0.1
0.08
0.1
0.06
0.06
0.04
0.04
0.06
0.04
< 0.04
0.04
< 0.02